Title
Analysis, Design, And Evaluation Of Avcs For Heavy-duty Vehicles With Actuator Delays

Authors
Yanakiev, Diana
Eyre, Jennifer
Kanellakopoulos, Ioannis

Publication Date
1998

CALIFORNIA PATH PROGRAM
INSTITUTE OF TRANSPORTATION STUDIES
UNIVERSITY OF CALIFORNIA, BERKELEY

Analysis, Design, and Evaluation of AVCS for Heavy-Duty Vehicles with Actuator Delays

Diana Yanakiev, Jennifer Eyre,
Ioannis Kanellakopoulos
University of California, Los Angeles

California PATH Research Report
UCB-ITS-PRR-98-18

This work was performed as part of the California PATH Program of the University of California, in cooperation with the State of California Business, Transportation, and Housing Agency, Department of Transportation; and the United States Department of Transportation, Federal Highway Administration.

Report for MOU 240

April 1998

ISSN 1055-1425

Analysis, Design, and Evaluation of AVCS for Heavy-Duty Vehicles with Actuator Delays

Diana Yanakiev
Jennifer Eyre
Ioannis Kanellakopoulos

UCLA Electrical Engineering
Los Angeles, CA 90095-1594

Analysis, Design, and Evaluation of AVCS for Heavy-Duty Vehicles with Actuator Delays

Diana Yanakiev, Jennifer Eyre, and Ioannis Kanellakopoulos

Abstract

This report describes the results of the project that was funded first under MOU 124 and then under MOU 240.

The main result is a new generation of longitudinal controllers for commercial heavy vehicles with and without intervehicle communication. These algorithms use nonlinear spacing policies, backstepping control design, and aggressive prediction schemes to deal with the presence of significant delays and saturations in the fuel and brake actuators. As a result, their performance in the absence of delays is far superior to that of any algorithm "ported" from passenger cars, and, furthermore, this performance can be preserved even in the presence of significant delays. This is the first class of algorithms which can deal with delays both in the presence and in the absence of intervehicle communication, a property that was heretofore believed impossible to achieve. The significance of these results in terms of ITS deployment is that we have removed several major obstacles to the implementation of many different ITS scenarios to commercial heavy vehicles (CHVs), ranging from adaptive cruise control to fully automated operation. It also means that we can implement adaptive cruise control and autonomous vehicle following in trucks and buses that are not equipped with expensive brake-by-wire systems usually referred to as EBS (Electronic Brake Systems); this includes virtually every CHV on the road today, since EBS is only now starting to appear as an option on new trucks.

As a by-product of our research on longitudinal control of CHVs, we have developed two software packages for simulation and animation of CHV platoons. These packages, called *Platoon-Builder* and *TruckVis*, include graphical user interfaces for automated construction of simulation models and automated data generation, and are available for downloading on the project Website (http://ansl.ee.ucla.edu/ahv).

Another important result of this project is a new simplified framework for evaluating the longitudinal string stability properties of platoons of automated vehicles. In this framework, the platoon is considered to be a mass-spring-damper system with linear characteristics. We were able to represent a large number of different controller configurations into this framework and produce several new analysis results.

Keywords

Adaptive Cruise Control
Advanced Vehicle Control Systems
Automated Highway Systems Control
Autonomous Intelligent Cruise Control
Buses
Commercial Vehicle Operations
Control Algorithms
Control Systems
Intelligent Vehicle Highway Systems
Longitudinal Control
Public Transit
Speed Control
Trucking
Vehicle Follower Control

Executive Summary

This project is concerned with the design of longitudinal control algorithms for commercial heavy vehicles (CHVs). This report gives a comprehensive account of all the results that were produced under this project, first under MOU 124 and then (primarily) under MOU 240.

One of the main requirements we imposed on our designs was that they should be useful in *all* stages of ITS deployment, from adaptive cruise control to fully automated highway systems. To satisfy this requirement, a controller must be able to perform well both in existing vehicles retrofitted with ITS equipment, and in vehicles which will be produced in the near future. It must also be able to function both in the presence and in the absence of communication with other vehicles and with the roadway. A key property that must be achieved under all these different scenarios is *string stability*, which ensures that errors decrease as they propagate upstream the vehicle formation (string). The fact that string stability cannot be achieved for platoons with *constant intervehicle spacing* under autonomous operation has been known for more than twenty years (Garrard et al. 1978, Shladover 1978). String stability can be guaranteed if the lead vehicle is transmitting its velocity (Shladover 1978) or velocity and acceleration (Sheikholeslam and Desoer 1990) to all other vehicles in the platoon. This approach yields stable platoons with small intervehicle spacings at the cost of introducing and maintaining continuous intervehicle communication with high reliability and small delays. String stability can also be recovered in autonomous operation if a *speed-dependent* spacing policy is adopted, which incorporates a *fixed time headway* term in addition to the constant distance (Chien and Ioannou 1992, Garrard et al. 1978). This approach avoids the communication overhead, but results in larger spacings between adjacent vehicles and thus in longer platoons, thereby yielding smaller increases in traffic throughput.

This problem is much more serious in the case of CHV platoons, primarily due to their low actuation-to-weight ratio: the levels of acceleration and deceleration achievable by CHVs are almost an order of magnitude lower than for passenger cars. As we will see, this makes string stability a much more elusive goal for CHVs; in the absence of intervehicle communication, the fixed time headway necessary for string stability is significantly larger, hence the reduction in traffic throughput is much more pronounced. This necessitates the design of new longitudinal control algorithms, which are the focus of this report: we design several new spacing policies and control schemes which use *nonlinearity* to endow the vehicles in the platoon with a "group conscience" and occasionally even sacrifice the individual performance of some vehicles in order to improve the performance of the whole platoon. We propose two new nonlinear spacing policies which achieve this goal. First, we introduce the notion of *variable time headway*, i.e., a headway which, instead of being constant varies with the relative speed between adjacent vehicles. The effect of introducing the variable time headway h is quite dramatic, as seen in our results from the simulation of a ten-truck platoon. They reveal an impressive reduction of errors and a considerably smoother control activity without any increase in steady-state intervehicle spacing. Another "upgrade" is the introduction of a *variable separation error gain* k. Our simulation results illustrate that the use of variable instead of constant k yields significantly improved platoon performance: it makes the control effort noticeably smoother and all but eliminates amplification of errors as they propagate upstream the platoon. The proposed form of this nonlinear spacing policy is suitable for CHVs since it alleviates the effect of their low actuation-to-weight ratio. The individual performance of the first few vehicles in the platoon may be compromised, but the improvement in the performance of the remaining vehicles results in a better overall tradeoff.

Another one of the most critical obstacles in the automated operation of CHVs is the presence of significant delays in the fuel and brake actuators. These delays are especially important in longitudinal control of vehicle platoons which do not employ intervehicle communication, because their effect becomes cumulative as it propagates upstream, resulting in considerably degraded performance.

Until last year, there were only two ways one could deal with the actuator delay problem:

1. Use intervehicle communication with preview: if the leading vehicle transmits its desired speed profile to the followers a little bit ahead of time, then every vehicle can start the corresponding maneuver at the right moment, thus compensating for the presence of the delays.

2. Ensure that all the automated CHVs have brake-by-wire capabilities, often referred to as Electronic Brake Systems (EBS). These systems transmit brake commands via electronic signals instead of the usual air pressure signals which are transmitted through the brake lines, thus resulting in a very significant reduction of the brake actuator delays, which are usually much more severe than fuel actuator delays.

Clearly , both of these solutions have some drawbacks. Intervehicle communication comes at a considerable additional cost of installation and maintenance, and it assumes that the other vehicles will be equipped with it as well. EBS systems are even more expensive; they are only now starting to appear as an OEM option on new trucks, so existing CHVs would have to be retrofitted with them, a process which further increases the associated cost.

Therefore, in this project (and the companion project under MOU 293), we set out to find an alternative solution to the actuator delay problem. We design novel nonlinear algorithms for longitudinal control of CHVs without intervehicle communication. We use two different approaches which are tailored to different performance requirements and computational resources. First, we design algorithms that use nonlinear spacing policies, backstepping control design, and aggressive prediction schemes; their performance in the presence of large delays is almost identical to the performance achieved when the delays are negligible. This is the first class of algorithms which can deal with delays without relying on intervehicle communication, a property that was heretofore believed impossible to achieve. However, this desirable property comes at the expense of significant additional controller complexity. Therefore, we also design much simpler PID-like controllers which use nonlinear spacing policies and a filtered estimate of the preceding vehicle's acceleration; their performance is only slightly lower than that of the backstepping-predictive schemes, but their computational requirements are much lower.

To assist the reader in evaluating the relative merits of all these different control schemes, we provide qualitative comparison charts, which should be used as "visual aids" in determining the most appropriate longitudinal control scheme for a CHV platoon. Each choice involves a tradeoff between control smoothness, platoon performance, robustness to different maneuvers and actuator delays, and controller complexity. From these charts, it is easy to see that in autonomous operation it is always worth using either variable time headway or variable separation error gain. With either of these modifications, both control smoothness and platoon performance are much better than without any of the two, and this benefit justifies the additional control complexity. If platoon performance is the primary consideration, then variable time headway is the modification of choice,

while variable separation error gain should be preferred when control smoothness is more important. It is also clear that if any of these two is used, the additional complexity of a nonlinear Q term may not be justified, since the resulting change is barely noticeable. Finally, the schemes with intervehicle communication appear to have a distinct advantage over the autonomous schemes. However, this must be weighed against the considerable additional complexity of establishing and maintaining reliable communication between the vehicles in the platoon.

The situation changes if we consider *robustness* with respect to actuator delays and also with respect to a large variety of scenarios as an additional criterion. If we expect our controller to perform safely even when faced with abrupt merge commands followed by significant decelerations of the lead platoon, without relying on the usually considered additional layer of "nonlinear path planning", our options are somewhat limited. The conclusion that it is always worth using either variable time headway or variable separation error gain is still valid. However, the variable separation error gain contributes much more to the robustness of the controller. Now it becomes clear that even when platoon performance is more important than control smoothness, it is advisable to tolerate the additional complexity of a variable separation error gain term with a small value of its design parameter σ, since that yields a very significant robustness enhancement to merge maneuvers. Again, when either variable h or k is used, the additional complexity of a nonlinear Q term may not be justified, since the resulting change is barely noticeable. Taking into consideration all of the above, the scheme which utilizes both variable h and variable k with $\sigma = 0.1$ appears to have the clear advantage over all other autonomous controllers.

Furthermore, if we expect our controller to perform just as well in the presence of large actuator delays as it does when these delays are negligible, then we have to accommodate the significant additional complexity of both nonlinear spacing policies combined with backstepping control design and an aggressive predictor. On the other hand, if simplicity and ease of implementation are more important, one can still achieve very good performance in the presence of delays by using the simpler PID-based scheme with nonlinear spacing policies. What may seem surprising at first in these comparison charts is the worse overall robustness of schemes with predictive action compared to the ones without. This is due to the fact that the schemes with predictor perform poorer in extremely challenging maneuvers as the merge/brake considered here. This makes sense intuitively: The predictor attempts to "figure out" ahead of time what is going to happen in τ s and when something totally unexpected happens, the predictor is misleading rather than helping.

It is important to note that we do not assume perfect knowledge of the plant model; our results incorporate a great deal of modeling uncertainty due to the fact that the models we use for control design are only crude approximations of our complex simulation models. The only parameter which is assumed to be very well known is the actuator delay used in the design of our predictor. However, further simulations have indicated that the performance is not affected by small errors in this assumed value. Nevertheless, in real applications it is nearly impossible to measure this value with high accuracy, primarily because these delays change significantly with temperature and operating conditions. Hence, if the performance requirements dictate that these delays be fairly well known, it may be necessary to install torque sensors on the wheels in order to perform on-line measurements of the time it takes for a fuel or brake command to affect vehicle acceleration.

The significance of these results in terms of ITS deployment is that now we have removed many of the major obstacles to autonomous vehicle following for CHVs. It also means that we can implement adaptive cruise control in trucks and buses that are not equipped with EBS. The

significance of these results in terms of ITS deployment is that we have removed several major obstacles to the implementation of many different ITS scenarios to CHVs, ranging from adaptive cruise control to fully automated operation. It also means that we can implement adaptive cruise control and autonomous vehicle following in trucks and buses that are not equipped with EBS.

As a by-product of our research on longitudinal control of CHVs, we have developed two software packages for simulation and animation of CHV platoons. *Platoon Builder* is a MATLAB/SIMULINK based graphical user interface program. Through the graphical interface, the user can select platoon parameters such as number of vehicles in the platoon, control algorithm, and controller parameters, and the program automatically generates a SIMULINK model of the platoon for the chosen parameters. The simulation results can be plotted or used for the animation of the platoon (on some hardware platforms) using the *TruckVis* (Truck Visualization) software, which allows the animation of longitudinal and lateral control simulations of automated heavy-duty vehicles. These packages are available for downloading on the project Website (http://ansl.ee.ucla.edu/ahv).

Another important result of this project is a new simplified framework for evaluating the longitudinal string stability properties of platoons of automated vehicles. In this framework, the platoon is considered to be a mass-spring-damper system with linear characteristics. We were able to represent a large number of different controller configurations into this framework and produce several new analysis results for the delay-free case. Due to the fact that local linearization is used in this analysis, the corresponding results must be viewed not as definitive answers, but rather as reasonably valid in the case of negative results and as simple guidelines in the case of positive results: if a specific controller does not possess a desirable property in this simplified linearized setting, it will certainly not possess it in the real world, when nonlinearities and delays are present. For example, from our analysis we can confirm that a longitudinal controller which relies only on relative distance and velocity measurements with respect to both the vehicle in front and the vehicle in back (bidirectional and autonomous) and uses a constant spacing policy, can not achieve string stability without overshoot under any circumstances; thus if our requirements include string stability without overshoot, we need not bother with such a controller. On the other hand, our analysis shows that the same controller can achieve string stability with overshoot, provided its gains satisfy certain inequalities; since this is a positive result based on our simplified framework, it means that in the real world this property may or may not be achievable, and further analysis, simulation, and experimentation is needed to either confirm or deny it.

Contents

List of Figures

1 Introduction

1.1 Motivation and background

Advanced Vehicle Control System (AVCS) design is an integral part of the rapidly growing national and international initiatives on Intelligent Transportation Systems (ITS) and Automated Highway Systems (AHS), which aim at significantly increasing the traffic capacity of existing highways through vehicle and roadway automation. In the past few years, AVCS research and development has been primarily focused on passenger vehicles, while commercial heavy vehicles (CHVs) such as heavy-duty freight trucks (including tractor-trailer combinations) and commuter buses have been largely ignored. The obvious justification is that there are many more passenger vehicles on the road, and thus their automation will have the largest possible impact on the desired increase of highway traffic flow.

However, this argument does not take into account the many differences in the operational modes between commercial and passenger vehicles, which render the relative impact of CHVs on traffic congestion and economic growth much larger than their numbers suggest. In fact, the motivation for automating CHVs goes far beyond the need to include these vehicles in the automated highways of the future; it is often argued that CHVs have the potential of becoming the flagships of AHS efforts, due to several economic and policy issues.

To justify this position, let us consider one of the most visible proposed strategies for highway automation, which is to group automatically controlled vehicles in *platoons* (Hedrick et al. 1991, Ioannou and Xu 1994, Sheikholeslam and Desoer 1990, Shladover 1978, Varaiya 1993), i.e., tightly spaced vehicle group formations. Since platooning is likely to improve fuel consumption, we can see why the most important reason that CHVs, and in particular heavy-duty freight trucks, are likely to be the first semi- or fully-automated vehicles is *profit-driven operation*: The average truck travels *six times the miles* and consumes *twenty-seven times the fuel* of the average passenger car, and these numbers are even higher if restricted to heavy commercial trucks, rated at 40,000 lbs or more. Thus, even a small improvement in fuel efficiency can be incentive enough for truck fleet operators to invest in AVCS equipment. Moreover, truck traffic follows much more regular patterns than passenger car traffic; trucks usually travel on well-established commercial routes, mostly between major cities. Thus, fleet operators can easily compose platoons of trucks with the same origination and destination points which will travel together for the entire trip. Under this scenario, in the first stages of AHS deployment, freight transport companies will operate departure/arrival stations in major cities. Individual trucks will be driven manually from all over the city to the station, where they will join the platoon departing for their destination city. Each platoon will consist of several trucks, with only two drivers in the lead vehicle who can take turns driving, while the following vehicles will be driverless. In the mean time, the drivers who are not on the departing platoons will manually drive the trucks from arriving platoons to their individual points destination points within the city. This reduction in the number of drivers will yield significant savings (25% or more) in operating costs, thereby reducing the time to recovery of the initial investment and increasing the profit margin. The effect of these savings through platooning is further compounded by the fact that the ratio of intercity to intracity miles traveled by freight trucks is much higher than for passenger cars. Hence, CHVs will utilize their automation capabilities much more than passenger cars, since they spend most of their travel time on interstate highways, where they will

be able to travel in platoons.

The longitudinal control problem for this type of "intercity platooning" is significantly simplified by the absence of split/merge maneuvers. However, to obtain significantly higher traffic throughput in urban freeways, platoons must operate with small intervehicle spacings and many vehicles in each group. Therefore, the longitudinal control design for platoons of automated vehicles has to guarantee the desired performance not only for each individual vehicle, but also for the whole formation. A key property is *string stability*, which ensures that errors decrease as they propagate upstream through the platoon. The fact that string stability cannot be achieved for platoons with *constant intervehicle spacing* under autonomous operation has been known for more than twenty years (Garrard et al. 1978, Shladover 1978) String stability can be guaranteed if the lead vehicle is transmitting its velocity (Shladover 1978) or velocity and acceleration (Sheikholeslam and Desoer 1990) to all other vehicles in the platoon. This approach yields stable platoons with small intervehicle spacings at the cost of introducing and maintaining continuous intervehicle communication with high reliability and small delays. String stability can also be recovered in autonomous operation if a *speed-dependent* spacing policy is adopted, which incorporates a *fixed time headway* term in addition to the constant distance (Chien and Ioannou 1992, Garrard et al. 1978). This approach avoids the communication overhead, but results in larger spacings between adjacent vehicles and thus in longer platoons, thereby yielding smaller increases in traffic throughput.

This problem is much more serious in the case of CHV platoons, primarily due to their low actuation-to-weight ratio: the levels of acceleration and deceleration achievable by CHVs are almost an order of magnitude lower than for passenger cars. As we will see in section 2.2.5, this makes string stability a much more elusive goal for CHVs; in the absence of intervehicle communication, the fixed time headway necessary for string stability is significantly larger, hence the reduction in traffic throughput is much more pronounced. This necessitates the design of new longitudinal control algorithms, which are the focus of section 3: we design several new spacing policies and control schemes which use *nonlinearity* to endow the vehicles in the platoon with a "group conscience" and occasionally even sacrifice the individual performance of some vehicles in order to improve the performance of the whole platoon.

1.2 Results

A necessary prelude to our control design efforts was the development of realistic models which capture all the important characteristics of the longitudinal vehicle dynamics. Our first modeling task was the development of a turbocharged (TC) diesel engine model suitable for vehicle control which is briefly presented in section 2.1. The engine model is then combined with the automatic transmission, drivetrain and brake models to obtain a longitudinal heavy-duty vehicle model. Section 2.1 also contains a linearization-based analysis of the longitudinal vehicle model, which provides useful information regarding the significance of each state for the longitudinal behavior of the vehicle. We first developed two nonlinear control schemes for speed tracking (Yanakiev and Kanellakopoulos 1996). The performance of the designed fixed-gain PIQD and adaptive PIQ controllers was evaluated on the basis of simulation results and compared to the performance of existing PID and adaptive PI speed controllers applied to our longitudinal truck model. Then, in section 2.2, we design an adaptive nonlinear controller for vehicle following which can operate in both autonomous mode (AICC) and cooperative mode with intervehicle communication (platoon-

ing). The single-vehicle stability properties of this controller are proven via Lyapunov analysis, while its string stability and transient performance properties under several scenarios are evaluated through simulation.

In section 3, we design several new spacing policies and control schemes which use *nonlinearity* to endow the vehicles in the platoon with a "group conscience" and occasionally even sacrifice the individual performance of some vehicles in order to improve the performance of the whole platoon. The longitudinal control design is presented in the modular framework of section 3.1: we start with a PI scheme based on the linearized vehicle model and develop independent "upgrades" in the subsequent sections. This format has been chosen to emphasize the fact that the modifications of the original scheme can be applied either separately or in combination. In this section we also investigate the string stability properties of the resulting control schemes through analysis and numerical simulations of a single platoon, while in section 3.2 we test their robustness in a more challenging scenario involving the merger of two platoons. In the concluding section of this section, 3.3, we give a graphical qualitative comparison of the new control schemes, which not only summarizes the results presented in the former sections, but also allows designers to better negotiate the trade-offs between platoon performance, control smoothness, robustness, and controller complexity in the choice of a scheme which best fits the needs of a particular implementation.

When evaluating platoon performance the key criteria are: (i) the magnitude of the errors and (ii) their propagation properties through the platoon. String stability analysis for each particular scheme proves to be a tedious procedure thus motivating the search for a systematic approach, which can be successfully applied to various scenarios. The analogy between a platoon of vehicles and a mass-spring-damper system has been suggested before (Chien et al. 1995, Yang and Tongue 1996). In section 4, we explore the idea of developing a simplified framework for string stability analysis in AHS based on a mass-spring-damper system. This approach has a dual effect: it facilitates the investigation of string stability properties of existing longitudinal control schemes and, in addition, it suggests new possible scenarios which can result in stable platoon behavior.

While full automation is the long-term goal, AHS deployment is likely to proceed in incremental stages, thus utilizing available results as early as possible. In the first stage, for example, vehicles would have only longitudinal control capabilities for vehicle following without intervehicle communication, with the driver assuming responsibility for steering and emergency situations. It is worth noting that commercial vehicles will benefit from automation in all intermediate stages, both in terms of safety and traffic throughput. Of course, the reverse is true as well: AHS research will benefit from advances made in the design of heavy vehicles. In fact, the problem of slow brake response is already being addressed in the commercial trucking industry, albeit for safety reasons rather than as a consideration for AHS. CHV manufacturers are beginning to equip their vehicles with brake-by-wire systems, commonly referred to as Electronic Braking Systems (EBS), which significantly reduce brake actuator delays in order to meet ever-stricter government regulations on braking distances. While these developments justify our effort on controller design for vehicles with very small actuator delays, presented in section 3, their widespread implementation is still far enough into the future. Furthermore, one has to remember that EBS is even farther away when it comes to trailer brakes, where the largest delays occur. And even if we assume that all future trailers will be equipped with EBS, controller design must still allow for large delays: Since tractor/trailer combinations are mixed and matched, a tractor modified for automated operation must also be able to pull a trailer without EBS.

In light of these short-term objectives, it becomes imperative to design controllers which will require only minimal modifications to vehicles currently in operation and production. Our previous controller designs (sections 2 and 3) were based on the fact that for the purpose of AHS participation, CHVs will be equipped with actuators which feature considerably reduced delays. In simulations where delays were assumed to be small, our adaptive nonlinear controllers and nonlinear spacing policies demonstrated robust behavior in demanding merge-and-brake inter-platoon maneuvers, in addition to the objective for which they were they designed: maintaining small intra-platoon spacing errors. However, the nonlinear spacing policies which have proven so beneficial in vehicles with negligible actuator delays are not entirely able to cope with the effect of large delays. Inclusion of a realistic model of air brake response behavior has presented a formidable challenge for longitudinal control design in the vehicle following scenario.

This was the motivation for the new design presented in section 5. In the original design we used a detailed nonlinear vehicle model for simulations, but the controller design was based on a simplified first-order representation of a truck. The idea was to introduce complexity only when necessary to improve performance. Now, in the case of significant delays, we use a second-order model in which actuator dynamics are included. Starting from our original controller and using a backstepping procedure, we derive a new control law which demonstrates significantly improved performance in the presence of large actuator delays.

A traditional approach to systems with known delays and available plant models is the use of prediction. While beneficiary for the stability of an individual vehicle, a predictive approach is not expected to achieve a lot in our case of cumulative effect of the delay in the platoon scenario. Nevertheless, the inclusion of a particular kind of predictor in the control loop demonstrates a positive impact on the control smoothness and hence on safety and fuel consumption improvement.

2 Vehicle Follower Control Design

2.1 Longitudinal truck model

The longitudinal model of a truck is shown in Fig. 1. The Engine module contains the TC diesel engine model. The four gear automatic transmission model is included in the Transmission block. The longitudinal dynamics equations are in the Chassis module.

Turbocharged (TC) diesel engine model

The vast majority of existing internal combustion engine models serve purposes such as engine performance improvement or diagnostics. Engine models suitable for vehicle control have been developed only for normally aspirated spark ignition (SI) engines. Unfortunately, they cannot be adapted to describe the compression ignition (CI) of the diesel engine and to capture the effect of the turbocharger.

Using several TC diesel engine modeling techniques available in the literature (Hendricks 1989, Horlock and Winterbone 1986, Jennings et al. 1986, Jensen et al. 1991, Ledger et al. 1971, Winterbone et al. 1977), we have compiled a model consisting of three differential and several algebraic equations, as well as four 2-D maps, which are compiled from experimental data available in the literature. Our model is based on the *mean torque production* model developed by Kao

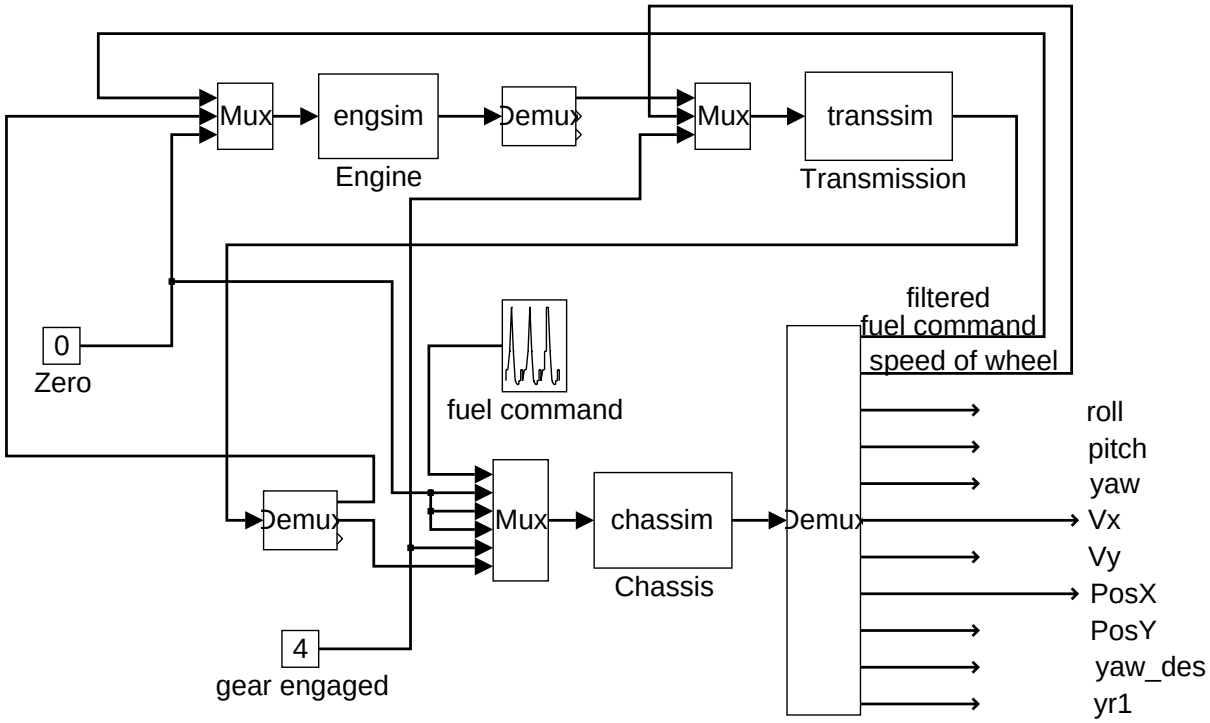

Input to Engine:	fuel command load torque unused	Output From Engine:	rpm net torque unused
Input to Trans:	rpm speed of wheel gear engaged	Ouput from Trans:	load torque driving torque unused
Input to Chassis:	commanded fuel commanded steering commanded brake road curvature gear engaged driving torque		

Figure 1: Truck longitudinal model.

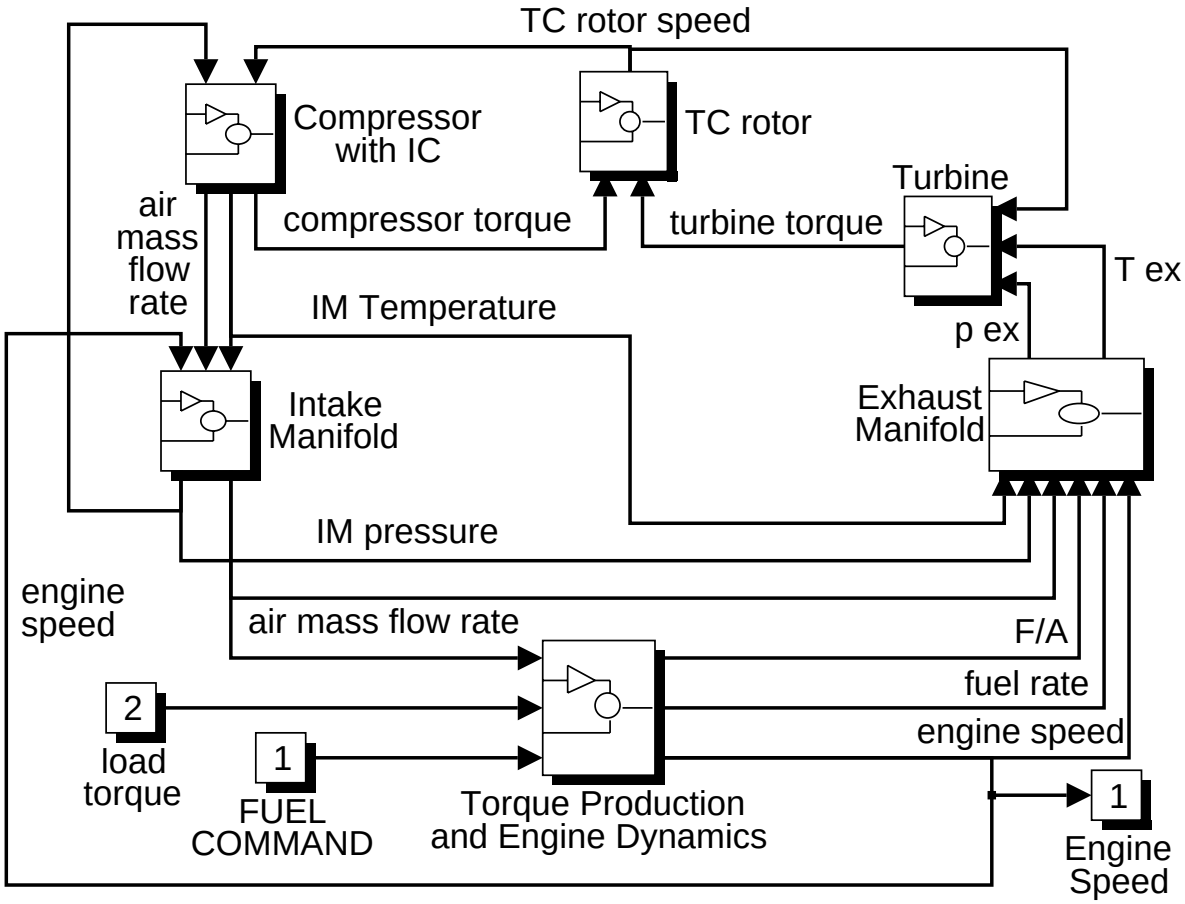

Figure 2: TC diesel engine model representation.

and Moskwa (1993). The modeled engine is turbocharged and intercooled, has six cylinders and $0.014\,\mathrm{m}^3$ (14 liters) displacement volume. The block diagram in Fig. 2 gives an overview of the model structure.

As in the SI engine model developed by Cho and Hedrick (Cho and Hedrick 1989, McMahon et al. 1990) two of the states are the *intake manifold (IM) pressure* and the *engine speed*. However, due to the different fueling method, the fueling lag is not considered here. In the diesel engine, the fuel is injected directly into the cylinder immediately before the combustion takes place. This eliminates the need to account for the fueling dynamics. The *TC rotor speed* is another state which needs to be introduced due to the presence of the turbocharger.

The equation for the IM pressure p_{im} has been derived by differentiating the ideal gas law:

$$\dot{p}_{\mathrm{im}} + \frac{\eta_{\mathrm{v}} V_{\mathrm{d}} N_{\mathrm{e}}}{120 V_{\mathrm{im}}} p_{\mathrm{im}} = \dot{m}_{\mathrm{c}} \frac{R T_{\mathrm{im}}}{V_{\mathrm{im}}} \,, \tag{2.1}$$

where T_{im} and V_{im} are respectively the IM temperature and volume, η_{v} is the volumetric efficiency, V_{d} is the displacement volume of the engine, N_{e} is the engine speed in revolutions per minute (rpm)—so that $N_{\mathrm{e}} = \omega_{\mathrm{e}} \frac{60}{2\pi}$, where ω_{e} is the engine speed in rad/s—and $\dot{m}_{\mathrm{c}}$ is the compressor air mass flow rate.

The engine speed ω_e is obtained by integrating the angular acceleration of the crankshaft, which is determined from Newton's second law:

$$M_{\rm ind}(t-\tau_{\rm i}) - M_{\rm f}(t) - M_{\rm load}(t) = J_{\rm e}\,\dot{\omega}_{\rm e}(t)\,. \tag{2.2}$$

In the above equation, $M_{\rm ind}$ is the indicated torque and $M_{\rm f}$ the friction torque of the engine, $M_{\rm load}$ is the load torque which is determined by the transmission and the drivetrain subsystems of the vehicle model, and $J_{\rm e}$ is the effective inertia of the engine. The *production delay* $\tau_{\rm i}$ represents the average difference between the time of issuing a command to change the indicated engine torque and the time when the injection valve can be operated. These events are determined by the position of the crankshaft angle. Therefore, the production delay and all other delays associated with this model have constant values measured in crankshaft angle. Converted in seconds, they become inversely proportional to the engine speed.

The TC dynamic equation is also derived using Newton's second law:

$$M_{\rm t} - M_{\rm c} = J_{\rm tc}\,\dot{\omega}_{\rm tc}\,, \tag{2.3}$$

where $M_{\rm t}$ is the torque provided by the turbine, $M_{\rm c}$ is the torque absorbed by the compressor, and $J_{\rm tc}$ is the effective inertia of the turbocharger. Integration of the TC angular acceleration $\dot{\omega}_{\rm tc}$ yields the TC rotor speed $\omega_{\rm tc}$.

Some intermediate computations are necessary to determine the other variables participating in the state equations. Steady-state empirical characteristics and experimental data in the form of 2-D maps, as well as algebraic relations are used, in addition to the state equations, to obtain a complete mathematical description of the system.[1]

Torque converter

Our automatic transmission model is based on the assumptions that gear shifting is instantaneous and that there is no torsion in the driveline. The static nonlinear torque converter model derived by Kotwicki (1982) has been employed. This model is well suited for vehicle modeling because it provides explicit terminal relations between torques and speeds. Experimentally justified approximation of the exact detailed expressions yields the following representation of the pump torque $M_{\rm P}$ and the turbine torque $M_{\rm T}$ as functions of the pump speed $\omega_{\rm P} = \omega_{\rm e}$ and the turbine speed $\omega_{\rm T}$:

$$M_{\rm P} = \alpha_0\omega_{\rm P}^2 + \alpha_1\omega_{\rm P}\omega_{\rm T} + \alpha_2\omega_{\rm T}^2 \tag{2.4}$$

$$M_{\rm T} = \beta_0\omega_{\rm P}^2 + \beta_1\omega_{\rm P}\omega_{\rm T} + \beta_2\omega_{\rm T}^2. \tag{2.5}$$

The coefficients $\alpha_0, \alpha_1, \alpha_2, \beta_0, \beta_1, \beta_2$ are obtained by regression from experimental data. Although the form of the equations is preserved in both modes of operation, different coefficients have to be determined for the regions when the engine is driving the vehicle and vice versa. The pump and turbine angular velocities are compared to determine the current operating region. The respective coefficients are then used to compute the pump torque, which is the load torque applied to the engine, and the turbine torque, which is the shaft torque transmitted to the drivetrain.

[1] For a detailed description of our engine and transmission model, the reader is referred to the report by Yanakiev and Kanellakopoulos (1995).

Transmission mechanicals

The assumption that there is no torsion in the driveline establishes a direct relationship between the angular velocity of the torque converter turbine ω_{t} and that of the vehicle's driving wheels ω_{w}:

$$\omega_{\mathrm{w}} = R_{\mathrm{total}}\,\omega_{\mathrm{T}} = R_i\,R_{\mathrm{d}}\,\omega_{\mathrm{T}}\,, \tag{2.6}$$

where R_i is the reduction ratio of the ith gear range and R_{d} is the final drive reduction ratio. The model is further simplified by the instantaneous gear shifting assumption, eliminating the need for an additional state which appears during shifting.

Longitudinal drivetrain equations

The angular velocity of the driving wheels is determined by the torque converter turbine torque M_{T}, the tractive tire torque $F_{\mathrm{t}}h_{\mathrm{w}}$, where F_{t} is the tractive tire force and h_{w} is the static ground-to-axle height of the driving wheels, and the braking torque M_{b}:

$$J_{\mathrm{w}}\,\dot{\omega}_{\mathrm{w}} = \frac{M_{\mathrm{T}}}{R_{\mathrm{total}}} - F_{\mathrm{t}}h_{\mathrm{w}} - M_{\mathrm{b}}\,, \tag{2.7}$$

where J_{w} is the lumped inertia of the wheels.

Currently, the brake actuating system is represented via a first-order linear system with a time constant τ_{b}, i.e., the braking torque M_{b} is obtained from

$$\dot{M}_{\mathrm{b}} = \frac{M_{\mathrm{bc}} - M_{\mathrm{b}}}{\tau_{\mathrm{b}}}\,, \tag{2.8}$$

where M_{bc} is the commanded braking torque. This is only a crude approximation of the complicated brake dynamics present in heavy-duty vehicles, but it is fairly reasonable for longitudinal control. A more detailed brake model is currently under development.

The tractive force F_{t} depends linearly on the tire slip up to approximately 15% slip. Since the tire slip is always positive, it is defined as:

$$i_{\mathrm{d}} = 1 - \frac{v}{h_{\mathrm{w}}\,\omega_{\mathrm{w}}} \quad \text{or} \quad i_{\mathrm{b}} = 1 - \frac{h_{\mathrm{w}}\,\omega_{\mathrm{w}}}{v}\,, \tag{2.9}$$

where v is the vehicle velocity, depending on whether the tire is under driving torque ($F_{\mathrm{t}} = k_i\,i_{\mathrm{d}}$) or under braking torque ($F_{\mathrm{t}} = -k_i\,i_{\mathrm{b}}$).

The aerodynamic drag force F_{a} and the force generated by the rolling resistance of the tires ($F_{\mathrm{r}} = \frac{M_{\mathrm{r}}}{h_{\mathrm{w}}}$) have to be subtracted from the tractive force to yield the force that accelerates or decelerates the vehicle. The state equation for the truck velocity becomes:

$$\dot{v} = \frac{F_{\mathrm{t}} - F_{\mathrm{a}} - F_{\mathrm{r}}}{m}\,, \tag{2.10}$$

where the vehicle mass is denoted by m. The force F_{a} is determined from the aerodynamic drag coefficient c_{a} and the vehicle speed:

$$F_{\mathrm{a}} = c_{\mathrm{a}}\,v^2\,. \tag{2.11}$$

The rolling resistance torque $M_{\rm r} = F_{\rm r}\, h_{\rm w}$ is a linear function of the vehicle mass:

$$M_{\rm r} = c_{\rm r}\, m\, g\,. \tag{2.12}$$

Substituting (2.11) and (2.12) into (2.10), we obtain:

$$\dot{v} = \frac{F_{\rm t} - c_{\rm a}\, v^2}{m} - \frac{c_{\rm r}\, g}{h_{\rm w}}\,. \tag{2.13}$$

Finally, a first-order filter with a time constant $\tau_{\rm f}$ is also included in the vehicle model to account for the dynamics of the fuel pump and the actuators which transmit the fuel command u to the injectors:

$$\dot{u}_{\rm f} = \frac{1}{\tau_{\rm f}}\left(-u_{\rm f} + u\right). \tag{2.14}$$

The variable $u_{\rm f}$ is a scaled version of the index[2] Y. The minimum index necessary to maintain idle speed corresponds to $u_{\rm f}^{\rm min} = 0$ and the maximum index corresponds to $u_{\rm f}^{\rm max} = 100$.

Linearization of the longitudinal model

The resulting longitudinal vehicle model described so far is highly nonlinear and detailed enough to capture all the important characteristics of the dynamic behavior of a heavy-duty vehicle. However, it is far too complex to be used as the basis for control design. Due to the presence of several implicit algebraic relations and empirical 2-D maps, it is virtually impossible to obtain a state-space model in a form that is useful for control design. Instead, the model was linearized around several operating points determined by different fuel command/vehicle mass combinations. The results showed that the sixth-order linearized model has the same number of dominant modes throughout the examined range, albeit with significant variations in individual parameter values. The modes associated with the angular velocity of the wheel and the fuel system (cf. (2.14)) are always very fast compared to the remaining ones, and can thus be ignored. Of the remaining four modes, those associated with the IM pressure, the engine speed and the TC rotor speed are much faster than the mode corresponding to the vehicle velocity.

Thus, the longitudinal truck model relating the vehicle speed to the fuel command input can be reduced to a first-order linear model:

$$\frac{\delta v}{\delta u} = \frac{b}{s + a}\,, \tag{2.15}$$

where the values of b and a depend on the operating point, i.e., on the steady state values of the vehicle speed and the load torque. This reduced-order linearized model is the starting point for the design of our control schemes. However, this does not imply that our modeling effort was wasted, since our simulations are always carried out using the full nonlinear model. What this order reduction and linearization do imply is that our controllers do not rely on the particular details of the vehicle model and are thus inherently robust to modeling uncertainties. They are also

[2]The index Y is defined as the position of the fuel pump rack, which determines the amount of fuel provided for combustion.

easier to implement, since they do not contain highly complicated algebraic or dynamic equations. The price paid for this simplicity and robustness is that we can only achieve good performance if the required maneuvers are slower than the slowest neglected modes. But since here we are only interested in maneuvers with time constants of several seconds, this limitation does not play a significant role.

2.2 Control design for vehicle following

In this section we design an adaptive nonlinear controller which can operate both autonomously as well as with intervehicle communication. To illustrate the various features of our control design framework, we use simulations of a platoon comprising ten (10) tractor-semitrailer combination vehicles. Each vehicle weighs 20,000 kg (44,000 lbs) and is powered by a 14-liter turbocharged diesel engine capable of producing approximately 1,000 Nm (740 ft-lbs) in peak torque and 300 kW (400 hp) in peak power. The platoon starts out at an initial speed of 22 m/s (49.10 mph). At $t = 10$ s the platoon leader decides to reduce his speed by 10 m/s (22.32 mph) and then, at $t = 80$ s, to increase it by 5 m/s (11.16 mph). The minimum desired separation between vehicles is $s_0 = 3$ m. This demanding scenario is representative of the difficulties the system might have maintaining string stability when trying to meet a challenging acceleration/deceleration objective. In all our simulation plots, different vehicles are represented by lines of different styles: Vehicle 1 is shown with a solid line, while following vehicles cycle through dash-dotted, dashed, dotted, and solid lines (so that, for example, Vehicles 5 and 9 are shown with solid lines).

2.2.1 Control objective

The parameters relevant to any two adjacent vehicles in a platoon are illustrated in Fig. 3. In the platoon scenario, the controller has to regulate to zero both the relative velocity $v_{\rm r}$ and the separation error δ,

$$v_{\rm r} = v_{\rm l} - v_{\rm f}\,, \quad \delta = x_{\rm r} - s_{\rm d}\,, \tag{2.16}$$

where $v_{\rm l}$ and $v_{\rm f}$ are the velocities of the leading and following vehicle, while $x_{\rm r}$ is the actual and $s_{\rm d}$ the desired separation between vehicles. The desired separation may be constant (fixed spacing policy) or a function of the follower's velocity:

$$s_{\rm d} = s_0 + hv_{\rm f} \tag{2.17}$$

as shown in Fig. 3. The parameter h is called *time headway* and its effect is to introduce more spacing at higher velocity in addition to the *constant spacing* s_0.

The tasks of regulating the relative velocity and the separation error can be combined into the control objective $v_{\rm r} + k\delta = 0$, where k is a positive design constant. This control objective makes sense intuitively: If two vehicles are closer than desired ($\delta < 0$) but the leader's speed is larger than the follower's ($v_{\rm r} > 0$), then the controller in the follower does not need to take drastic action. The same can be said if the vehicles are farther apart than desired ($\delta > 0$) but the leader's speed is lower than the follower's ($v_{\rm r} < 0$). The selection of the coefficient k influences the response of the controller, and can be changed depending on the performance requirements. In fact, as we will see

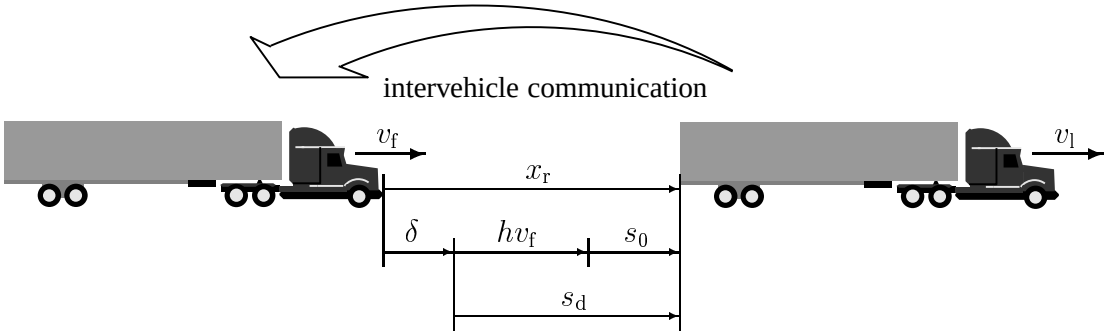

s_0 : minimum distance between vehicles
h : time headway (for speed-dependent spacing)
x_r : vehicle separation
$s_\mathrm{d} = s_0 + hv_\mathrm{f}$: desired vehicle separation
v_l : velocity of leading vehicle
v_f : velocity of following vehicle
$v_\mathrm{r} = v_\mathrm{l} - v_\mathrm{f}$: relative vehicle velocity
$\delta = x_\mathrm{r} - s_\mathrm{d}$: separation error

Figure 3: Parameters of a truck platoon.

beginning with section 3.1.2, making this coefficient a nonlinear function of the separation error δ can significantly enhance platoon performance as well as control smoothness.

Let us now show that when our control objective is achieved, i.e., when $v_\mathrm{r} + k\delta \equiv 0$, both the relative velocity and the separation error are regulated: $v_\mathrm{r} \to 0$ and $\delta \to 0$. When the velocity of the lead vehicle is constant ($\dot{v}_\mathrm{l} = 0$), we have

$$\delta = x_\mathrm{r} - s_\mathrm{d} = x_\mathrm{r} - hv_\mathrm{f} - s_0 \quad \Rightarrow \quad \dot{\delta} = v_\mathrm{r} - h\dot{v}_\mathrm{f} \tag{2.18}$$

$$v_\mathrm{r} = v_\mathrm{l} - v_\mathrm{f} \quad \Rightarrow \quad \dot{v}_\mathrm{r} = -\dot{v}_\mathrm{f} \,. \tag{2.19}$$

But $v_\mathrm{r} + k\delta \equiv 0$ implies that

$$\dot{v}_\mathrm{r} + k\dot{\delta} \equiv 0. \tag{2.20}$$

Combining this with (2.18) and (2.19), we obtain

$$\dot{v}_\mathrm{r} + k\left(v_\mathrm{r} + h\dot{v}_\mathrm{r}\right) \equiv 0 \;\Rightarrow\; (1+kh)\dot{v}_\mathrm{r} + kv_\mathrm{r} \equiv 0\,, \tag{2.21}$$

which shows that $v_\mathrm{r} \to 0$ (since $k > 0$ and $h > 0$). From $v_\mathrm{r} + k\delta \equiv 0$ and $v_\mathrm{r} \to 0$ we conclude that $\delta \to 0$.

In general, for variable h or k, the above is not necessarily true and has to be shown for the particular form of h or k respectively.

Since the control objective is to maintain $v_\mathrm{r} + k\delta = 0$, we linearize the model around the corresponding trajectory and obtain:

$$\dot{v}_\mathrm{f} = a(v_\mathrm{r} + k\delta) + bu + d\,, \tag{2.22}$$

where d again incorporates external disturbances and modeling errors, as well as the unknown nominal value of the control.

2.2.2 PI controller

Since our simplified longitudinal model is a first-order linear system, the Proportional-Integral (PI) controller is the simplest controller which can achieve regulation of both v_r and δ with some robustness with respect to disturbances and unmodeled effects. Hence, the PI controller is the starting point of our control design. The control law is

$$u = k_\mathrm{p}(v_\mathrm{r} + k\delta) + k_\mathrm{i}\frac{1}{s}(v_\mathrm{r} + k\delta)\,, \tag{2.23}$$

where k_p is the proportional and k_i is the integral gain.

However, in the demanding scenario of the presented simulations, a simple PI controller is not adequate. Therefore, we introduce several modifications in order to improve platoon performance and smoothness of control effort. These modifications of the control law can be viewed as independent modules which may be used separately or combined. By qualitatively evaluating the contribution of each module, we can add complexity to the control design only as needed to meet the given performance specifications.

2.2.3 Signed-quadratic (Q) term

The lower actuation-to-weight ratio of heavy-duty vehicles requires a controller which is more aggressive at large errors but does not have the undesirable side-effect of overshoot. This is achieved by adding a signed quadratic (Q) term of the form $(v_\mathrm{r} + k\delta)|v_\mathrm{r} + k\delta|$ to the PI controller, which thus becomes a nonlinear PIQ controller:

$$u = k_\mathrm{p}(v_\mathrm{r} + k\delta) + k_\mathrm{i}\frac{1}{s}(v_\mathrm{r} + k\delta) + k_\mathrm{q}(v_\mathrm{r} + k\delta)|v_\mathrm{r} + k\delta|\,. \tag{2.24}$$

This Q term was used successfully in the speed control problem of heavy-duty vehicles, (Yanakiev and Kanellakopoulos 1996), where it proved to be more efficient in avoiding overshoot than an anti-windup term and provided faster attenuation of errors compared to linear controllers. It also performed well in the platoon scenario, where overshoot is even less desirable.

2.2.4 Adaptive gains

Even if a controller is perfectly tuned for some operating region, it is likely to demonstrate inferior performance in other conditions due to the severe nonlinearities present in the system. A gain scheduling approach could be successful in overcoming the disadvantages of a fixed gain controller, but it would require extensive a priori information. Moreover, due to large variations in the mass of heavy duty vehicles (the change in mass between a lightly loaded and heavily loaded truck can be as much as 300%), such a priori information may even be impossible to obtain. Adaptation of the control gains is the natural solution, since it makes the closed-loop system response much less dependent on the current operating region and on the specific vehicle characteristics. The latter consideration becomes more significant in the platoon scenario where even if the grouped vehicles are not identical, they are expected to respond uniformly to different commands or disturbances.

The adaptive PI control law is:

$$u = \hat{k}_\mathrm{p}(v_\mathrm{r} + k\delta) + \hat{k}_\mathrm{i} \tag{2.25}$$

and the adaptive PIQ is:

$$u = \hat{k}_{\rm p}(v_{\rm r} + k\delta) + \hat{k}_{\rm i} + \hat{k}_{\rm q}(v_{\rm r} + k\delta)|v_{\rm r} + k\delta| \,, \tag{2.26}$$

where $\hat{k}_{\rm p}$, $\hat{k}_{\rm i}$, and $\hat{k}_{\rm q}$ are time-varying parameters which are being updated by an adaptive law. We are going to derive the parameter update laws only for the adaptive PIQ controller, and then show the modification necessary to obtain the adaptive PI control law.

Substituting (2.26) into (2.22) yields:

$$\dot{v}_{\rm f} = (a + b\hat{k}_{\rm p})(v_{\rm r} + k\delta) + b\hat{k}_{\rm i} + b\hat{k}_{\rm q}\,(v_{\rm r} + k\delta)\,|v_{\rm r} + k\delta| + d \,. \tag{2.27}$$

To design update laws for the parameter estimates, we consider a nonlinear reference model:

$$\dot{v}_{\rm m} = a_{\rm m}(v_{\rm l} - v_{\rm m} + k\delta) + q_{\rm m}(v_{\rm l} - v_{\rm m} + k\delta)|v_{\rm r} + k\delta| \,. \tag{2.28}$$

where $a_{\rm m} > 0$ and $q_{\rm m} \geq 0$. If a, b, and d were known, the coefficients of the controller could be chosen so that the plant and the reference model would respond identically to the same input signal. The corresponding values $k_{\rm p}$, $k_{\rm i}$, and $k_{\rm q}$ are computed from the following equations:

$$\begin{aligned} a + bk_{\rm p} &= a_{\rm m} \\ bk_{\rm i} &= -d \\ bk_{\rm q} &= q_{\rm m} \,. \end{aligned} \tag{2.29}$$

Since the parameters of the plant are unknown, we replace $k_{\rm p}$, $k_{\rm i}$, and $k_{\rm q}$ by their estimates in the control law (2.26). To design update laws for these estimates, we use the tracking error $e_{\rm r} = v_{\rm f} - v_{\rm m}$ computed from (2.27)–(2.29) as:

$$\begin{aligned} \dot{e}_{\rm r} = \dot{v}_{\rm f} - \dot{v}_{\rm m} \;\; = \;\; & -a_{\rm m}e_{\rm r} - q_{\rm m}e_{\rm r}|v_{\rm r} + k\delta| \\ & -b[\tilde{k}_{\rm p}(v_{\rm r} + k\delta) + \tilde{k}_{\rm i} + \tilde{k}_{\rm q}(v_{\rm r} + k\delta)|v_{\rm r} + k\delta|] \,. \end{aligned} \tag{2.30}$$

where $\tilde{k}_{\rm p} = k_{\rm p} - \hat{k}_{\rm p}$, $\tilde{k}_{\rm i} = k_{\rm i} - \hat{k}_{\rm i}$, $\tilde{k}_{\rm q} = k_{\rm q} - \hat{k}_{\rm q}$ are the parameter errors.

Then

$$\begin{aligned} \dot{v}_{\rm r} \;\; &= \;\; \dot{v}_{\rm l} - \dot{v}_{\rm f} \;\; = \;\; \dot{v}_{\rm l} - \dot{e}_{\rm r} - \dot{v}_{\rm m} \\ &= \;\; \dot{v}_{\rm l} - a_{\rm m}(v_{\rm r} + k\delta) - q_{\rm m}(v_{\rm r} + k\delta)|v_{\rm r} + k\delta| \\ &\quad\; + b\left[\tilde{k}_{\rm p}(v_{\rm r} + k\delta) + \tilde{k}_{\rm i} + \tilde{k}_{\rm q}(v_{\rm r} + k\delta)|v_{\rm r} + k\delta|\right] . \end{aligned} \tag{2.31}$$

Recall that

$$v_{\rm r} + k\delta = v_{\rm l} - v_{\rm f} + kx_{\rm r} - khv_{\rm f} - ks_0 \,, \tag{2.32}$$

which yields

$$\dot{v}_{\rm r} + k\dot{\delta} = \dot{v}_{\rm r}(1 + kh) + kv_{\rm r} - kh\dot{v}_{\rm l} \,. \tag{2.33}$$

Let us now define the variables $x_1 = v_{\rm r}$ and $x_2 = v_{\rm r} + k\delta$. We can rewrite equations (2.31) and (2.33) and obtain the state space representation:

$$\begin{aligned} \dot{x}_1 &= -(a_{\rm m} + q_{\rm m}|x_2|)x_2 + b(\tilde{k}_{\rm p}x_2 + \tilde{k}_{\rm i} + \tilde{k}_{\rm q}x_2|x_2|) + u_1 \\ \dot{x}_2 &= kx_1 - (a_{\rm m} + q_{\rm m}|x_2|)(1+kh)x_2 \\ &\quad + b(\tilde{k}_{\rm p}x_2 + \tilde{k}_{\rm i} + \tilde{k}_{\rm q}x_2|x_2|)(1+kh) + u_2\,, \end{aligned} \tag{2.34}$$

where $u_1 = \dot{v}_{\rm l}$ is the leading vehicle's acceleration and $u_2 = -kh\dot{v}_{\rm l}$.

Consider the Lyapunov function:

$$V = \frac{1}{2}x^T P x + \frac{e_{\rm r}^2}{2} + b\frac{\tilde{k}_{\rm p}^2}{2\gamma_1} + b\frac{\tilde{k}_{\rm i}^2}{2\gamma_2} + b\frac{\tilde{k}_{\rm q}^2}{2\gamma_3}\,, \tag{2.35}$$

where $P = \begin{bmatrix} p_1 & p_2 \\ p_2 & p_3 \end{bmatrix}$ is a positive definite symmetric matrix. This is a complete Lyapunov function for our closed-loop system. To see this, note that it includes the variables $v_{\rm r}$, $v_{\rm r} + k\delta$, $v_{\rm f} - v_{\rm m}$, $\tilde{k}_{\rm p}$, $\tilde{k}_{\rm i}$, and $\tilde{k}_{\rm q}$. Since $v_{\rm l}$, $k_{\rm p}$, $k_{\rm i}$, and $k_{\rm q}$ are bounded external signals, the variables in (2.35) are related via a nonsingular transformation to $v_{\rm f}$, $v_{\rm m}$, δ, $\hat{k}_{\rm p}$, $\hat{k}_{\rm i}$, and $\hat{k}_{\rm q}$, which are all the variables of our system.

The derivative of (2.35) is

$$\begin{aligned} \dot{V} &= p_1x_1\dot{x}_1 + p_2x_1\dot{x}_2 + p_2\dot{x}_1x_2 + p_3x_2\dot{x}_2 \\ &\quad -\frac{b}{\gamma_1}\tilde{k}_{\rm p}\dot{\hat{k}}_{\rm p} - \frac{b}{\gamma_2}\tilde{k}_{\rm i}\dot{\hat{k}}_{\rm i} - \frac{b}{\gamma_3}\tilde{k}_{\rm q}\dot{\hat{k}}_{\rm q} + e_{\rm r}\dot{e}_{\rm r}\,. \end{aligned} \tag{2.36}$$

The choices $p_2 < 0$ and $p_1 = -(1+kh)p_2$ cancel several cross-terms in (2.36). With these choices, we need $p_3 > \frac{-p_2}{1+kh}$ to guarantee the positive definiteness of P. The update laws:

$$\begin{aligned} \dot{\hat{k}}_{\rm p} &= \text{Proj}\left[\gamma_1\left\{[p_2 + p_3(1+kh)]x_2^2 - e_{\rm r}x_2\right\}\right] \\ \dot{\hat{k}}_{\rm i} &= \text{Proj}\left[\gamma_2\left\{[p_2 + p_3(1+kh)]x_2 - e_{\rm r}\right\}\right] \\ \dot{\hat{k}}_{\rm q} &= \text{Proj}\left[\gamma_3\left\{[p_2 + p_3(1+kh)]x_2^2|x_2| - e_{\rm r}x_2|x_2|\right\}\right] \end{aligned} \tag{2.37}$$

yield

$$\begin{aligned} \dot{V} &\le p_2kx_1^2 + p_3kx_1x_2 - [p_2 + p_3(1+kh)](a_{\rm m} + q_{\rm m}|x_2|)x_2^2 \\ &\quad -(a_{\rm m} + q_{\rm m}|x_2|)e_{\rm r}^2 + p_2x_1[u_2 - (1+kh)u_1] + x_2(p_2u_1 + p_3u_2)\,, \end{aligned} \tag{2.38}$$

Adding and subtracting $\frac{k\lambda p_3^2}{-4p_2}x_2^2$, where $\lambda > 1$ is a constant, and regrouping terms, we obtain:

$$\begin{aligned} \dot{V} &\le -\frac{\lambda-1}{\lambda}(-p_2k)x_1^2 - \left(\sqrt{\frac{-p_2k}{\lambda}}x_1 - \frac{p_3}{2}\sqrt{\frac{k\lambda}{-p_2}}x_2\right)^2 \\ &\quad -\left\{[p_2 + p_3(1+kh)](a_{\rm m} + q_{\rm m}|x_2|) - \frac{k\lambda p_3^2}{-4p_2}\right\}x_2^2 \\ &\quad -(a_{\rm m} + q_{\rm m}|x_2|)e_{\rm r}^2 + p_2x_1[u_2 - (1+kh)u_1] + x_2(p_2u_1 + p_3u_2)\,, \end{aligned} \tag{2.39}$$

hence

$$\begin{aligned}\dot{V} \;\leq\; & -\frac{\lambda-1}{\lambda}(-p_2 k)x_1^2 \\ & -\left\{[p_2+p_3(1+kh)](a_{\rm m}+q_{\rm m}|x_2|)-\frac{k\lambda p_3^2}{-4p_2}\right\}x_2^2 \\ & -(a_{\rm m}+q_{\rm m}|x_2|)e_{\rm r}^2+p_2x_1[u_2-(1+kh)u_1]+x_2(p_2u_1+p_3u_2)\,. \end{aligned} \tag{2.40}$$

To guarantee that $\dot{V}\leq 0$ when $u_1=u_2=0$, we need

$$[p_2+p_3(1+kh)](a_{\rm m}+q_{\rm m}|x_2|)-\frac{k\lambda p_3^2}{-4p_2}>0\,. \tag{2.41}$$

Since we already have the constraint $p_3>\frac{-p_2}{1+kh}$ for the positive definiteness of P, the inequality (2.41) can be satisfied for all values of x_2 if and only if

$$a_{\rm m}>\frac{\lambda k}{(1+kh)^2}\,. \tag{2.42}$$

Returning to (2.40), we use the notation

$$c_1=\frac{\lambda-1}{\lambda}(-p_2k)\,,\;\; c_2=[p_2+p_3(1+kh)]a_{\rm m}-\frac{k\lambda p_3^2}{-4p_2}\,,\;\; c_3=[p_2+p_3(1+kh)]q_{\rm m}\,, \tag{2.43}$$

and completion of squares to account for the last two cross-terms:

$$\begin{aligned}\dot{V} \;\leq\; & -c_1x_1^2-c_2x_2^2-c_3|x_2|^3-(a_{\rm m}+q_{\rm m}|x_2|)e_{\rm r}^2 \\ & +p_2x_1[u_2-(1+kh)u_1]+x_2(p_2u_1+p_3u_2) \\ \leq\; & -\frac{c_1}{2}x_1^2-\frac{c_2}{2}x_2^2-c_3|x_2|^3-(a_{\rm m}+q_{\rm m}|x_2|)e_{\rm r}^2 \\ & +\frac{p_2^2}{2c_1}[u_2-(1+kh)u_1]^2+\frac{1}{2c_2}(p_2u_1+p_3u_2)^2\,. \end{aligned} \tag{2.44}$$

Coupled with the boundedness of $\tilde{k}_{\rm p}$, $\tilde{k}_{\rm i}$ and $\tilde{k}_{\rm q}$, which is guaranteed by the projection in (2.37), and with the fact that $u_1=\dot{v}_{\rm l}$ and $u_2=-kh\dot{v}_{\rm l}$ are bounded and converge to zero, the inequality (2.44) proves the boundedness and regulation of x_1, x_2 and $e_{\rm r}$. Hence, the variables $v_{\rm f}$, $v_{\rm m}$ and δ are bounded and the vehicle following objective is achieved: $v_{\rm r}\to 0$, $\delta\to 0$ as $t\to\infty$.

2.2.5 Autonomous operation

As shown in the previous section, the presented adaptive PIQ control law guarantees individual stability of the vehicles in the platoon. Now we also need to ensure string stability, i.e., attenuation of errors as they propagate upstream.

In the case of autonomous operation, the information available to each vehicle is its own velocity and the relative velocity and separation from the preceding one. If the desired intervehicle spacing is constant, i.e., $h=0$, string stability cannot be achieved. This result is not specific to

truck platoons; similar results are available for passenger cars (Garrard et al. 1978, Sheikholeslam and Desoer 1990, Hedrick et al. 1991, Chien and Ioannou 1992, Ioannou and Xu 1994). This lack of stability is caused by the nature of propagating information in the platoon rather than by the particular vehicle dynamics.

A simple way to circumvent this problem without providing any additional information to the vehicles is to introduce a fixed time headway, i.e., $h > 0$ (Garrard et al. 1978, Chien and Ioannou 1992), thus adding time-dependent spacing to the constant spacing. This strategy is successful in achieving string stability (Garrard et al. 1978, Ioannou and Xu 1994) but due to the lower actuation-to-weight ratio of heavy vehicles compared to the passenger cars, the necessary minimum value of h is significantly higher and yields large intervehicle spacings at higher speeds, thereby reducing the traffic throughput.

We obtained the update law for the adaptive parameters of the PIQ controller in the previous section via the complete Lyapunov function of our closed-loop system. Here we use a simplified design which works just as well; we obtain the update law via the partial Lyapunov function:[3]

$$V = \frac{e_{\rm r}^2}{2} + b\frac{\tilde{k}_{\rm p}^2}{2\gamma_{\rm p}} + b\frac{\tilde{k}_{\rm i}^2}{2\gamma_{\rm i}} + b\frac{\tilde{k}_{\rm q}^2}{2\gamma_{\rm q}}\,, \tag{2.45}$$

where $\gamma_{\rm p}$, $\gamma_{\rm i}$, $\gamma_{\rm q}$ are positive design constants and b is unknown but positive. With the choices:

$$\begin{aligned} \dot{\hat{k}}_{\rm p} &= \mathrm{Proj}[-\gamma_{\rm p} e_{\rm r}(v_{\rm r} + k\delta)] \\ \dot{\hat{k}}_{\rm i} &= \mathrm{Proj}[-\gamma_{\rm i} e_{\rm r}] \\ \dot{\hat{k}}_{\rm q} &= \mathrm{Proj}[-\gamma_{\rm q} e_{\rm r}(v_{\rm r} + k\delta)|v_{\rm r} + k\delta|]\,, \end{aligned} \tag{2.46}$$

where $\mathrm{Proj}\,[\cdot]$ is the projection operator to a compact interval containing the true value of the parameter, we obtain for $\dot{V}$:

$$\dot{V} = -a_{\rm m} e_{\rm r}^2 - q_{\rm m}|v_{\rm r} + k\delta|e_{\rm r}^2 \;\leq\; 0\,. \tag{2.47}$$

This guarantees the boundedness of $e_{\rm r}$, $\hat{k}_{\rm p}$, $\hat{k}_{\rm i}$, $\hat{k}_{\rm q}$ and the regulation of $e_{\rm r}$.

The derivation of the parameter update laws for the adaptive PI controller is obtained by setting $q_{\rm m} = 0$ in the reference model (2.28) which yields the same update laws for $\hat{k}_{\rm p}$ and $\hat{k}_{\rm i}$. From (2.46) we see that the $\hat{k}_{\rm i}$-term in (2.25) and (2.26) is indeed an "integral" term, since it is the integral of the error $e_{\rm r}$. This term attenuates the effects of external disturbances such as road grades and headwinds, and it also provides the nominal control value necessary to maintain a constant speed with zero steady-state error.

The resulting adaptive PIQ controller can operate autonomously using a speed-dependent spacing policy. However, the fixed time headway has to be significantly larger than for passenger cars in order to guarantee good CHV platoon performance. This is illustrated in Fig. 4, which shows that with time headway $h = 0.1$ s the errors are significantly amplified as they propagate upstream through the platoon (from Vehicle 1 to Vehicle 10). As can be seen from the "vehicle separation" plot, there are even several collisions between Vehicles 7, 8, and 9 (a collision is indicated by a

[3]This Lyapunov function is called partial because it does not include the states $v_{\rm r}$ and δ which are part of our controller dynamics.

"vehicle separation" curve which becomes negative). In order to get acceptable performance and avoid collisions, one must increase the headway to $h = 0.5\,\mathrm{s}$. Then, as seen in Fig. 5, errors become much smaller and the fuel/brake activity much smoother (implying better fuel efficiency), but the intervehicle spacing grows significantly from about 4–5 m to 10–14 m. The value of 0.5 s for the constant time headway is substantially larger than the 0.1-0.2 s which yields good results for passenger cars. This increase is mainly due to the typically 5-10 times smaller actuation-to-weight ratio of CHVs.

2.2.6 Intervehicle communication

If the larger separation between adjacent vehicles resulting from the use of constant time headway is not acceptable, intervehicle communication can be introduced to obtain string stability with tighter spacing.

In this report we consider the case where the lead vehicle transmits to all following vehicles in the platoon its desired speed v_{d}. This is a relatively simple scheme, which requires distinguishing only between the leader and the followers, who need not be aware of their sequential number in the platoon. Such a scheme was first proposed by Shladover (1978), where it was shown to yield string stability for automated vehicle platoons.

In order to incorporate the new information, the difference between the platoon leader's desired speed and the current speed of the follower is defined as $v_{\mathrm{df}} = v_{\mathrm{d}} - v_{\mathrm{f}}$. The control objective is modified to $v_{\mathrm{r}} + k\delta + k_{\mathrm{df}} v_{\mathrm{df}} = 0$, where k_{df} is a tunable parameter. If we choose $k_{\mathrm{df}} = 0$, we recover the control objective used in the autonomous operation case.

The control law is changed to reflect the new control objective:

$$u = \hat{k}_{\mathrm{p}}(v_{\mathrm{r}} + k\delta + k_{\mathrm{df}} v_{\mathrm{df}}) + \hat{k}_{\mathrm{i}} + \hat{k}_{\mathrm{q}} \left(v_{\mathrm{r}} + k\delta + k_{\mathrm{df}} v_{\mathrm{df}}\right) \left|v_{\mathrm{r}} + k\delta + k_{\mathrm{df}} v_{\mathrm{df}}\right| . \tag{2.48}$$

Similarly, the term $v_{\mathrm{r}} + k\delta$ is replaced by $v_{\mathrm{r}} + k\delta + k_{\mathrm{df}} v_{\mathrm{df}}$ in (2.26)–(2.31). Equations (2.34)–(2.42) still hold if we replace $v_{\mathrm{r}} + k\delta$ by $v_{\mathrm{r}} + k\delta + k_{\mathrm{df}} v_{\mathrm{df}}$, kh by $kh + k_{\mathrm{df}}$, and set $u_2 = -kh\dot{v}_{\mathrm{l}} + k_{\mathrm{df}} \dot{v}_{\mathrm{d}}$. As in the autonomous operation scenario, one can show that this control law guarantees $v_{\mathrm{r}} \to 0$ and $\delta \to 0$.

The performed simulations confirm that using the above communication scheme guarantees string stability even for constant intervehicle spacing, i.e., for $h = 0$, as demonstrated in Fig. 6.

It is worth noting that our notion of intervehicle communication includes only transmission of the *desired* speed v_{d} of the platoon leader, and can be viewed as a variation of the approach proposed by Shladover, (1978). In terms of bandwidth and reliability, this is a much less demanding (and hence more robust) scheme than the usually considered ones, which require transmission of the leader's *current speed and acceleration*.

2.3 Conclusions

Linear controller creates a large overshoot, which is very undesirable in vehicle following. To allow fast compensation of large errors without excessive overshoot, we include nonlinear terms in our controllers, which thus outperform conventional linear controllers. We also include adaptation to make our controller response less dependent on the specific vehicle characteristics. This results

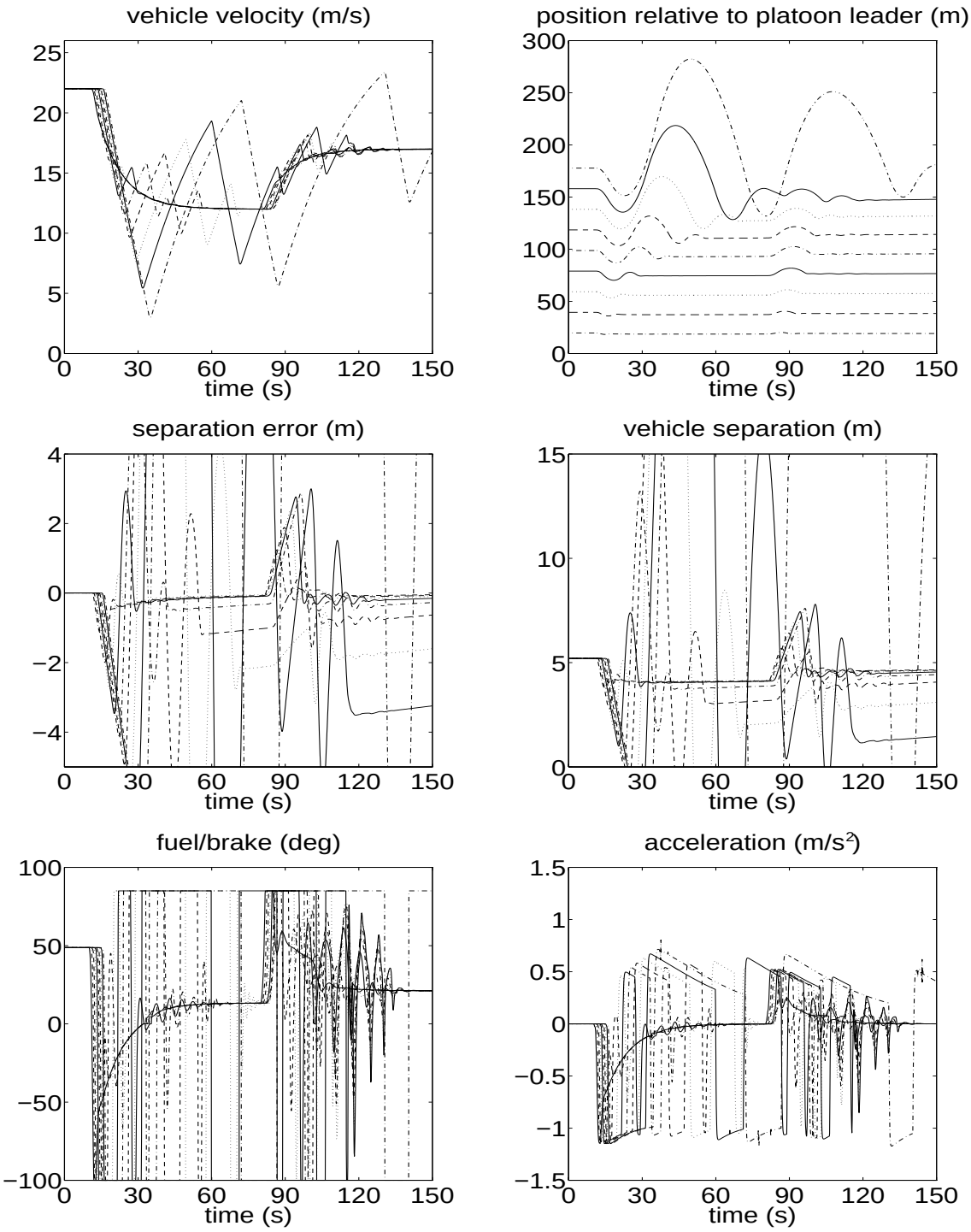

Figure 4: Ten autonomous vehicles, constant $h = 0.1\,\mathrm{s}$.

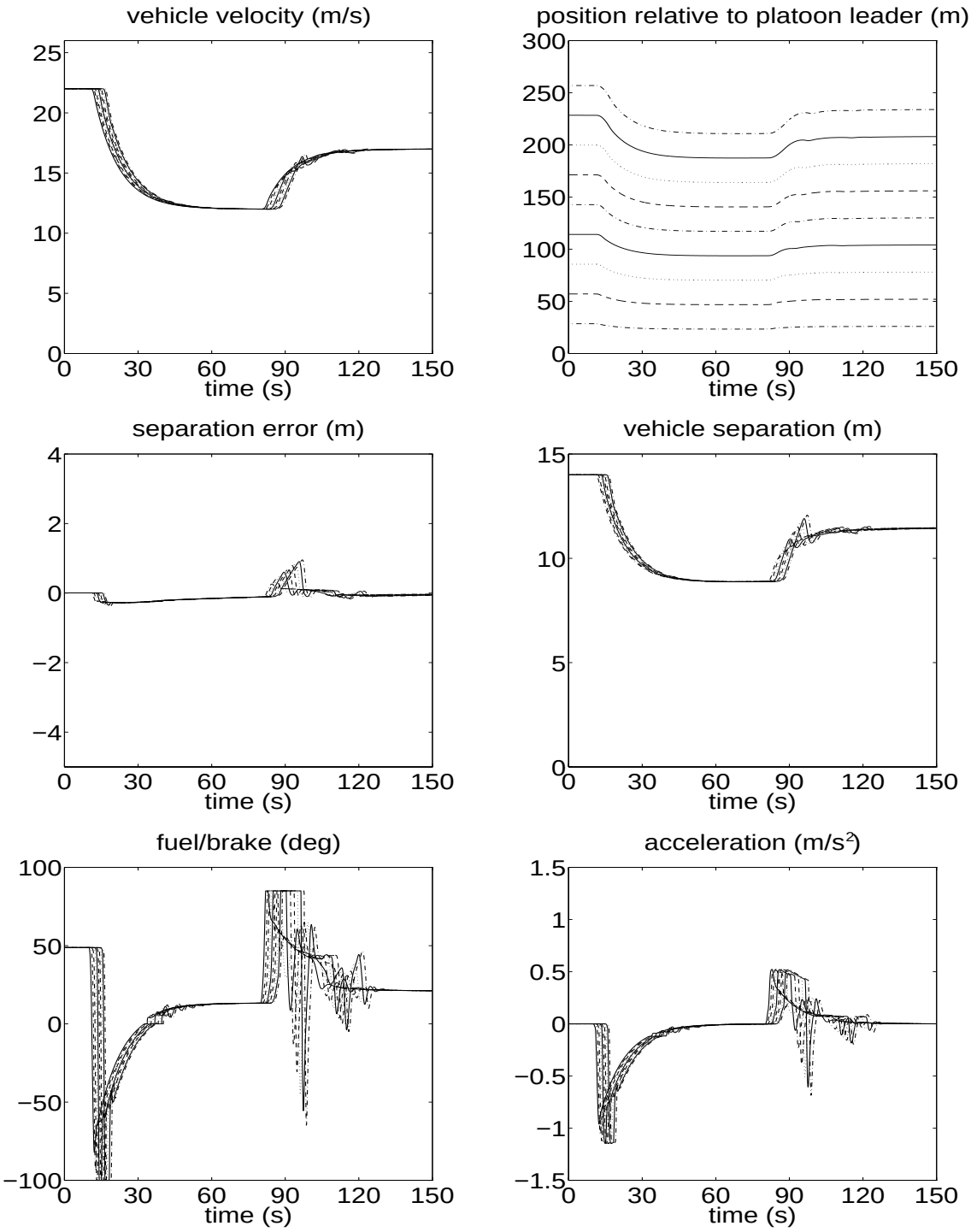

Figure 5: Ten autonomous vehicles, constant $h = 0.5\,\mathrm{s}$.

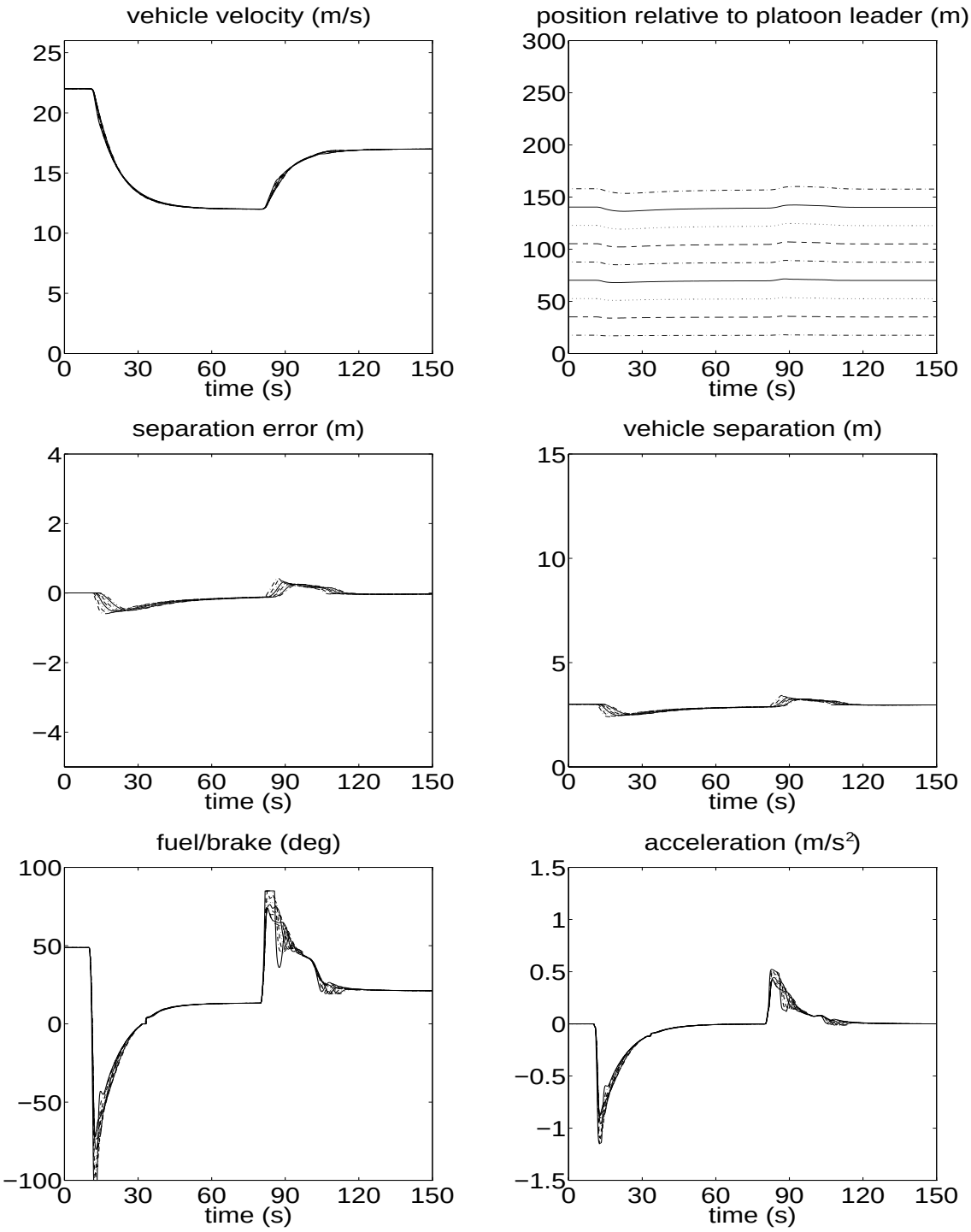

Figure 6: Ten vehicles with intervehicle communication, $h = 0$.

in more uniform performance over a wide operating region and across non-identical vehicles, a very desirable property in platoons.

The adaptive nonlinear controller we design commands both fuel and brake, thus eliminating the need for separate fuel and brake controllers with ad hoc switching logic. Moreover, it can operate both autonomously as well as with intervehicle communication. This flexibility is desirable for two reasons:

- A vehicle equipped with this controller can take full advantage of future automated lanes, but it can also be operated in Autonomous Intelligent Cruise Control (AICC) mode in non-automated lanes.
- The AICC capability can act as a fail-safe in automated lanes, in case there is a breakdown in intervehicle communication. In the event of such a failure, the controller can simply increase the time headway and continue to operate with guaranteed string stability, albeit with lower traffic throughput.

Our results also indicate that, in the case of autonomous operation, much larger time headways are required to achieve string stability in truck platoons—at least 0.7 s, compared to 0.25 s for cars. Finally, it is worth noting that our notion of intervehicle communication includes only transmission of the *desired* speed of the leading vehicle, and can be viewed as a variation on the approach proposed by Shladover (1978). In terms of bandwidth and reliability, this is a much less demanding scheme than the recently developed ones, which require transmission of the leader's *current speed and acceleration* in order to guarantee good performance even during very fast and demanding maneuvers.

3 Nonlinear Spacing Policies

Intervehicle communication may not be implemented in the beginning stages of truck automation, and even if it is implemented it may sometimes fail. Therefore, it is desirable to develop control algorithms which yield small separation errors without increased intervehicle spacing under autonomous vehicle operation. Such algorithms could be used not only under autonomous operation, but also in the intervehicle communication scenario as "backups" for the case of communication malfunctions or even failures. In this section, we will focus on the development of new nonlinear spacing policies which achieve this goal.

3.1 Variable time headway (variable h)

First, we introduce the notion of *variable time headway*, i.e., a headway which, instead of being constant varies with the relative speed v_{r} between adjacent vehicles. The intuition behind this modification, which was first presented by Yanakiev and Kanellakopoulos (1995), is as follows: Suppose that a vehicle wants to maintain a 0.1 s time headway from the preceding vehicle, when both of them are traveling at the same speed. If the relative speed between the two vehicles is positive, that is, if the preceding vehicle is moving faster, then it is safe to reduce this headway,

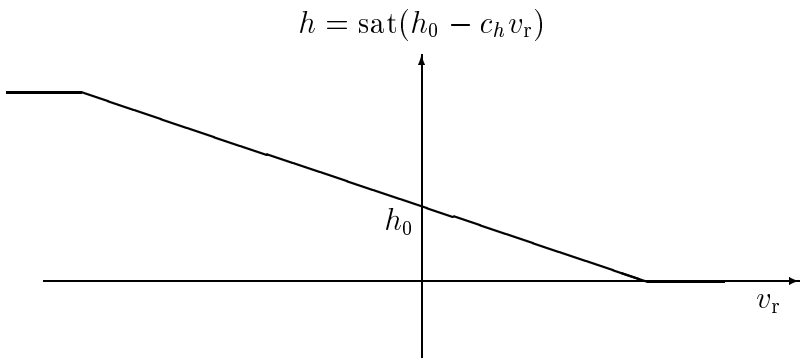

Figure 7: Variable time headway $h = \mathrm{sat}(h_0 - c_h v_\mathrm{r})$.

while if the preceding vehicle is moving slower then it would be advisable to increase the headway. This leads to the following choice for h as a function of the relative velocity v_r:

$$h = h_0 - c_h v_\mathrm{r} \,, \tag{3.1}$$

where $h_0 > 0, c_h > 0$ are constant. For safety reasons, the headway h cannot be allowed to become negative, while very large headways are undesirable as has been shown by Yanakiev and Kanellakopoulos (1996). Thus, we limit the headway in the interval $[0, 1]$ and arrive at the form of h shown in Fig. 7:

$$h = \mathrm{sat}(h_0 - c_h v_\mathrm{r}) = \begin{cases} 1 & \text{if } h_0 - c_h v_\mathrm{r} \geq 1, \\ h_0 - c_h v_\mathrm{r} & \text{if } 0 < h_0 - c_h v_\mathrm{r} < 1, \\ 0 & \text{otherwise.} \end{cases} \tag{3.2}$$

The effect of introducing the variable time headway $h = \mathrm{sat}(0.1 - 0.2 v_\mathrm{r})$ in our ten-truck platoon is quite dramatic, as seen in Fig. 8. Comparing Fig. 8 with Fig. 4 reveals an impressive reduction of errors and a considerably smoother control activity without any increase in steady-state intervehicle spacing. In fact, the response is quite similar to that obtained with $h = 0.5\,\mathrm{s}$ in Fig. 5, but with much smaller intervehicle spacing.

3.2 Variable separation error gain (variable *k*)

Another simple modification is the introduction of a *variable separation error gain* k. Recall that the intuition behind choosing the control objective as regulation of $v_\mathrm{r} + k\delta$ was as follows: If two vehicles are closer than desired ($\delta < 0$) but the preceding vehicle's speed is larger than the follower's ($v_\mathrm{r} > 0$), then the controller in the following vehicle does not need to take drastic action, and the same is true if the vehicles are farther apart than desired ($\delta > 0$) but the preceding vehicle's speed is lower than the follower's ($v_\mathrm{r} < 0$). However, when the separation error gain k is constant, the controller will try to reduce a very large spacing error δ through a very large relative velocity

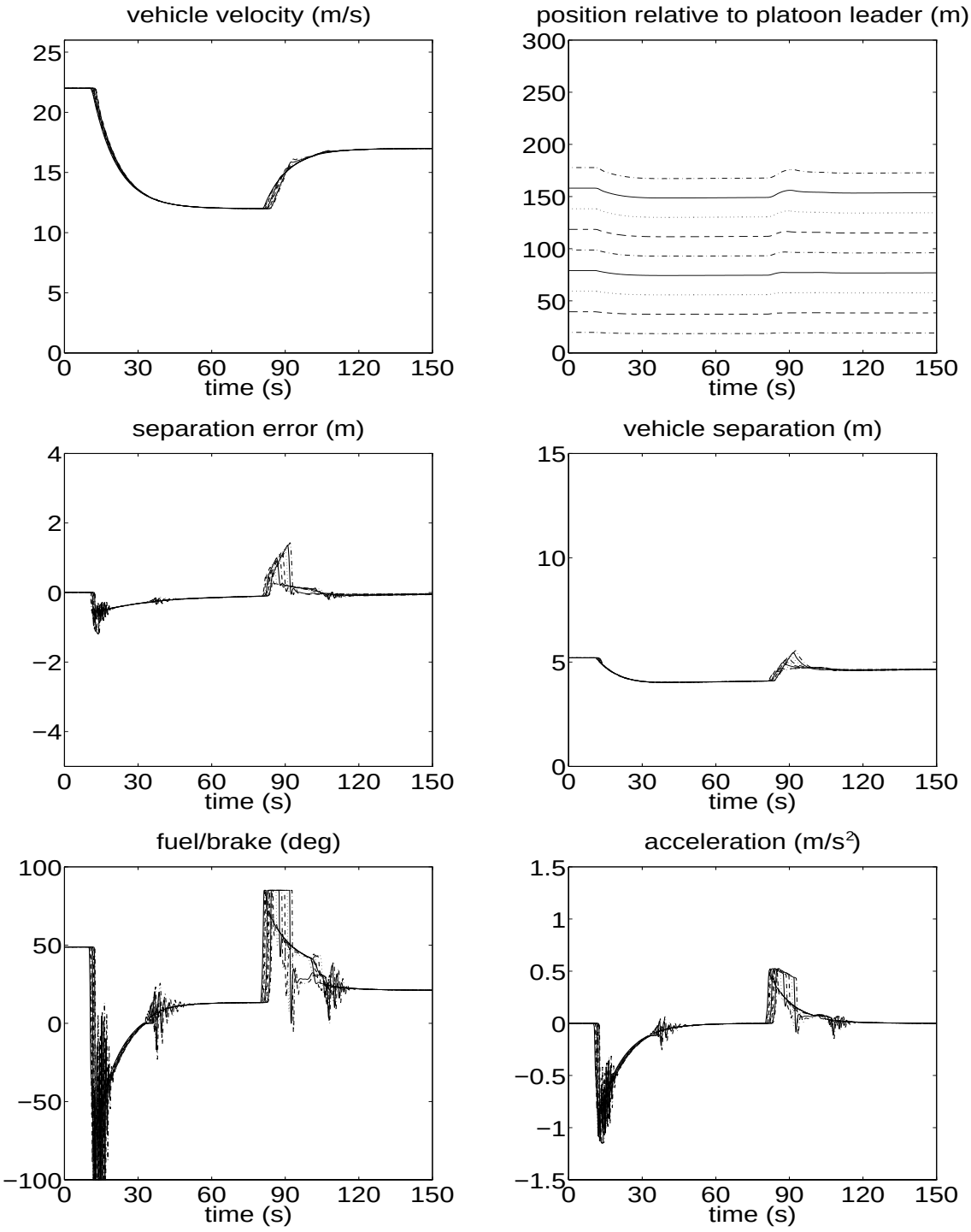

Figure 8: Ten autonomous vehicles, $h = \mathrm{sat}(0.1 - 0.2v_{\mathrm{r}})$.

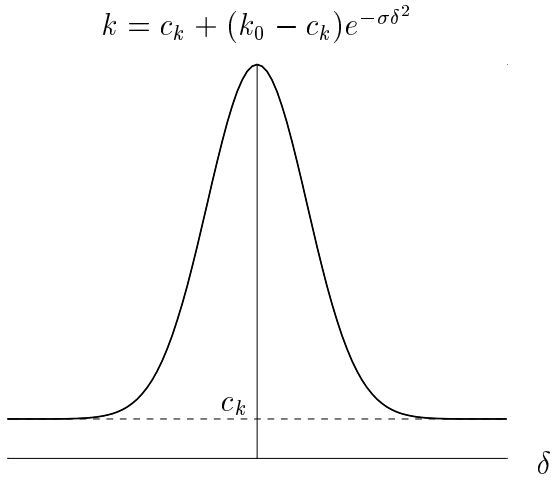

Figure 9: Variable k choice.

$v_{\rm r}$ of opposite sign. Hence, if a vehicle falls far behind the preceding vehicle, its controller will react aggressively by accelerating to a very high speed. This behavior is not only undesirable, since it increases fuel consumption and can even lead to collisions in extreme situations, but is also counter-intuitive. It would be much more natural for the controller to accelerate to a speed somewhat higher than that of the preceding vehicle's, and reduce the spacing error smoothly and progressively. To achieve such a response, we need to decrease the gain k as δ becomes large and positive, making sure that it remains above some reasonable positive lower bound. The choice of k

$$k = c_k + (k_0 - c_k)e^{-\sigma\delta^2}\ , \tag{3.3}$$

where $0 < c_k < k_0$ and $\sigma \geq 0$ are design constants, satisfies this requirement. This choice of k, shown in Fig. 9, makes the control objective $v_{\rm r} + k\delta = 0$ nonlinear in δ. It also has another feature which at first glance may seem counter-intuitive: The gain k is reduced even when δ becomes negative. A careful examination of the truck platoon characteristics and of the simulation results yields the following explanation for this choice: In autonomous operation, each vehicle relies only on its own measurements of relative speed and distance from the preceding vehicle. This means that if the preceding vehicle suddenly decelerates, then the following vehicle will have to decelerate even more to maintain the desired spacing. Hence, to maintain string stability, aggressive control actions must be amplified as they propagate upstream through the platoon. While this may not be a big problem for passenger cars, it becomes crucial for CHVs due to their low actuation-to-weight ratio which severely limits the accelerations and decelerations they are capable of achieving. During a sudden braking maneuver, only the first few vehicles in the platoon will be able to achieve the necessary decelerations; the controllers of the next vehicles will quickly saturate, and collisions may occur. In fact, the likelihood of a collision increases with the number of vehicles in the platoon. On the other hand, if the reaction of the first few vehicles is not as aggressive, then the decelerations are not amplified as much, and hence the remaining vehicles can achieve the necessary profiles. In a sense, reducing the gain k for negative δ endows the controller with a "platoon conscience", which sacrifices the individual performance of the first few vehicles in order to improve the overall behavior of the platoon. This is clearly illustrated in Fig. 10, which uses $k_0 = 1$, $c_k = 0.1$, and the

same fixed headway $h = 0.1$ s as Fig. 4. Comparing the two figures we see that the use of variable k yields significantly improved platoon performance: The errors are not amplified as they propagate upstream through the platoon, there are no collisions, and the control effort is noticeably smoother. However, the errors of the first five vehicles are larger than in Fig. 4, because their controllers did not react as aggressively. The individual performance of these vehicles has been compromised, but the improvement in the performance of the remaining vehicles results in a better overall tradeoff.

3.3 Variable h and variable k

As mentioned previously, the "modules" described so far in this section can be used in the controller separately or in combination. Hence, we now set out to examine the asymptotic convergence and string stability properties of the resulting closed-loop system, in the case where both k and h are variable.

3.3.1 Asymptotic convergence.

First we need to verify that when the control objective $v_{\rm r} + k\delta \equiv 0$ is achieved, both the relative velocity $v_{\rm r}$ and the separation error δ converge to zero. When $v_{\rm r} + k\delta \equiv 0$ we have:

$$\dot{v}_{\rm r} + \dot{k}\delta + k\dot{\delta} \equiv 0\,. \tag{3.4}$$

For variable h, equation (2.18) becomes:

$$\delta = x_{\rm r} - hv_{\rm f} - s_0 \Rightarrow \dot{\delta} = v_{\rm r} - h\dot{v}_{\rm f} - \dot{h}v_{\rm f}\,. \tag{3.5}$$

Combining this with (2.19), (3.2), and (3.4), we obtain:

$$\dot{\delta} = -k\delta + (h + \alpha(h)c_h v_{\rm f})\left(-k\dot{\delta} - \dot{k}\delta\right)\,,\;\; \alpha(h) = \begin{cases} 1 & 0 < h < 1, \\ 0 & \text{otherwise.} \end{cases} \tag{3.6}$$

With our particular choice of k, given in (3.3), this expression becomes:

$$\dot{\delta}\left\{1 + (h + \alpha(h)c_h v_{\rm f})\left[c_k + (k_0 - c_k)\,e^{-\sigma\delta^2}\left(1 - 2\sigma\delta^2\right)\right]\right\} + k\delta \equiv 0\,. \tag{3.7}$$

The term in the square brackets, $\phi(\delta) = c_k + (k_0 - c_k)\,e^{-\sigma\delta^2}\,(1 - 2\sigma\delta^2)$, achieves its minimum value of $c_k - 2\,(k_0 - c_k)\,e^{-3/2}$ at $\delta = \pm\sqrt{3/2\sigma}$. Therefore, the condition

$$h \;<\; \frac{1}{2\,(k_0 - c_k)\,e^{-3/2} - c_k} \tag{3.8}$$

gives $1 + h\phi(\delta) > 0$ and (since $v_{\rm f} > 0$) $1 + (h + \alpha(h)c_h v_{\rm f})\,\phi(\delta) > 0$ for all values of δ. Combined with (3.7) and the boundedness of $v_{\rm f}$ and $\phi(\delta)$, this guarantees that $\delta \to 0$. From $v_{\rm r} + k\delta \equiv 0$ and $\delta \to 0$ we conclude that $v_{\rm r} \to 0$. We have to note that the condition (3.8) is a conservative one since it is computed using the worst case value $\delta = \pm\sqrt{3/2\sigma}$. Thus, it is sufficient but not necessary for the convergence of δ to zero. Nevertheless, this condition is automatically satisfied with our choices: substituting $k_0 = 1$ and $c_k = 0.1$ into (3.8) yields the condition $h < 3.3$, while (3.2) guarantees that our variable h satisfies $0 \le h \le 1$.

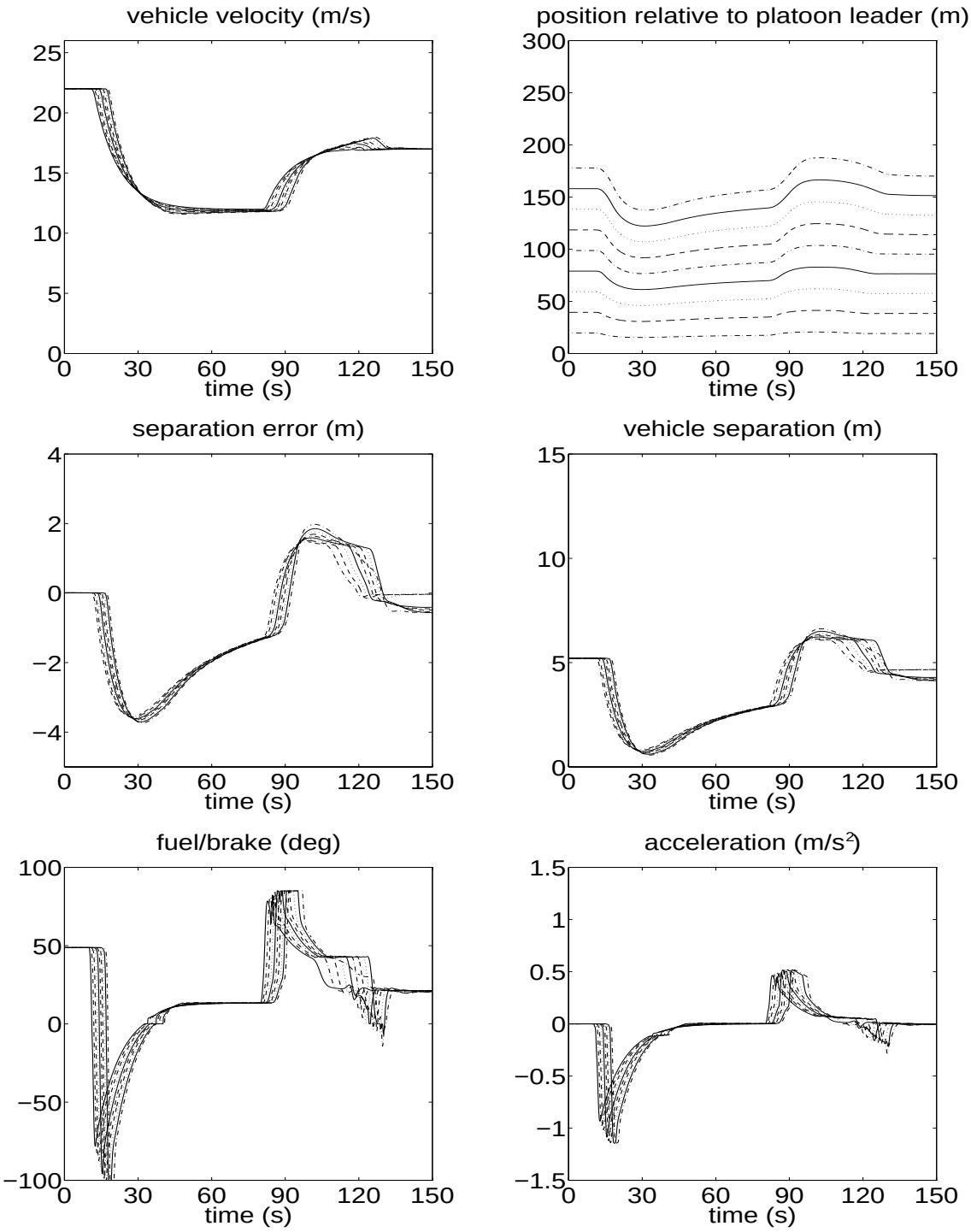

Figure 10: Ten autonomous vehicles, $h = 0.1$ s, variable k, $\sigma = 50$.

Simulation results for the case when both the time headway and the vehicle separation gain are variable are shown in Figs. 11 and 12. Comparing these two figures with Figs. 10 and 8, we see that the value of the constant σ determines whether the variable separation error gain or the variable time headway is the dominating factor in dictating platoon performance. For large values of σ the variable k dominates; the response in Fig. 11, where $\sigma = 50$ is used, is very similar to that in Fig. 10. On the other hand, for small σ it is the variable h that takes precedence; Fig. 12, with $\sigma = 0.1$, is almost identical to Fig. 8.

3.3.2 String stability.

One way to investigate string stability, i.e., to see how the separation errors propagate upstream through the platoon, is to consider the transfer function $G(s) = \frac{\delta_i(s)}{\delta_{i-1}(s)}$, where i is the vehicle number in the platoon. The requirement for upstream attenuation of errors will be satisfied when:

$$|G(j\omega)| = \left| \frac{\delta_i(j\omega)}{\delta_{i-1}(j\omega)} \right| < 1\,, \quad \forall\, \omega > 0\,. \tag{3.9}$$

Even though transfer function analysis does not take into account the effect of the initial conditions, it provides considerable insight and a firm basis for comparison between the different spacing policies. We emphasize that (3.9) is necessary but not sufficient for string stability: It is not sufficient because it is based on linearization analysis, and hence will not apply to large errors resulting from challenging maneuvers. However, since our controllers are supposed to keep the errors small, this analysis is useful for many practical cases. On the other hand, it is necessary: if $|G(j\omega_0)| > 1$ for some frequency ω_0, one can generate errors that increase upstream by using a small sinusoidal reference input of frequency ω_0 for the platoon leader.

The adaptation of the controller parameters is assumed to be fast enough so that v_i can be approximated by $v_{\rm m}$: $e_{\rm r} \to 0$ for constant v_{i-1}. Then, setting $q_{\rm m} = 0$ in (2.28) to obtain a PI controller, we have:

$$\dot{v}_i = a_{\rm m}\left(v_{{\rm r},i} + k_i\delta_i\right) \tag{3.10}$$

and

$$\dot{v}_{{\rm r},i} = \dot{v}_{i-1} - \dot{v}_i = a_{\rm m}\left(v_{{\rm r},i-1} + k_{i-1}\delta_{i-1}\right) - a_{\rm m}\left(v_{{\rm r},i} + k_i\delta_i\right). \tag{3.11}$$

Recall that $\delta_i = x_{{\rm r},i} - h_i v_i - s_0$, where h_i denotes the current value of the variable time headway used by vehicle i. Using (3.2) for the choice of variable h and assuming small enough variations to avoid the saturation regions of h, we obtain:

$$\dot{\delta}_i = v_{{\rm r},i} - h_i\dot{v}_i - \dot{h}_i v_i = v_{{\rm r},i} - h_0\dot{v}_i + c_h\dot{v}_{{\rm r},i}v_i + c_h v_{{\rm r},i}\dot{v}_i\,, \tag{3.12}$$

or

$$v_{{\rm r},i} = \dot{\delta}_i + h_0\dot{v}_i - c_h\dot{v}_{{\rm r},i}v_i - c_h v_{{\rm r},i}\dot{v}_i\,. \tag{3.13}$$

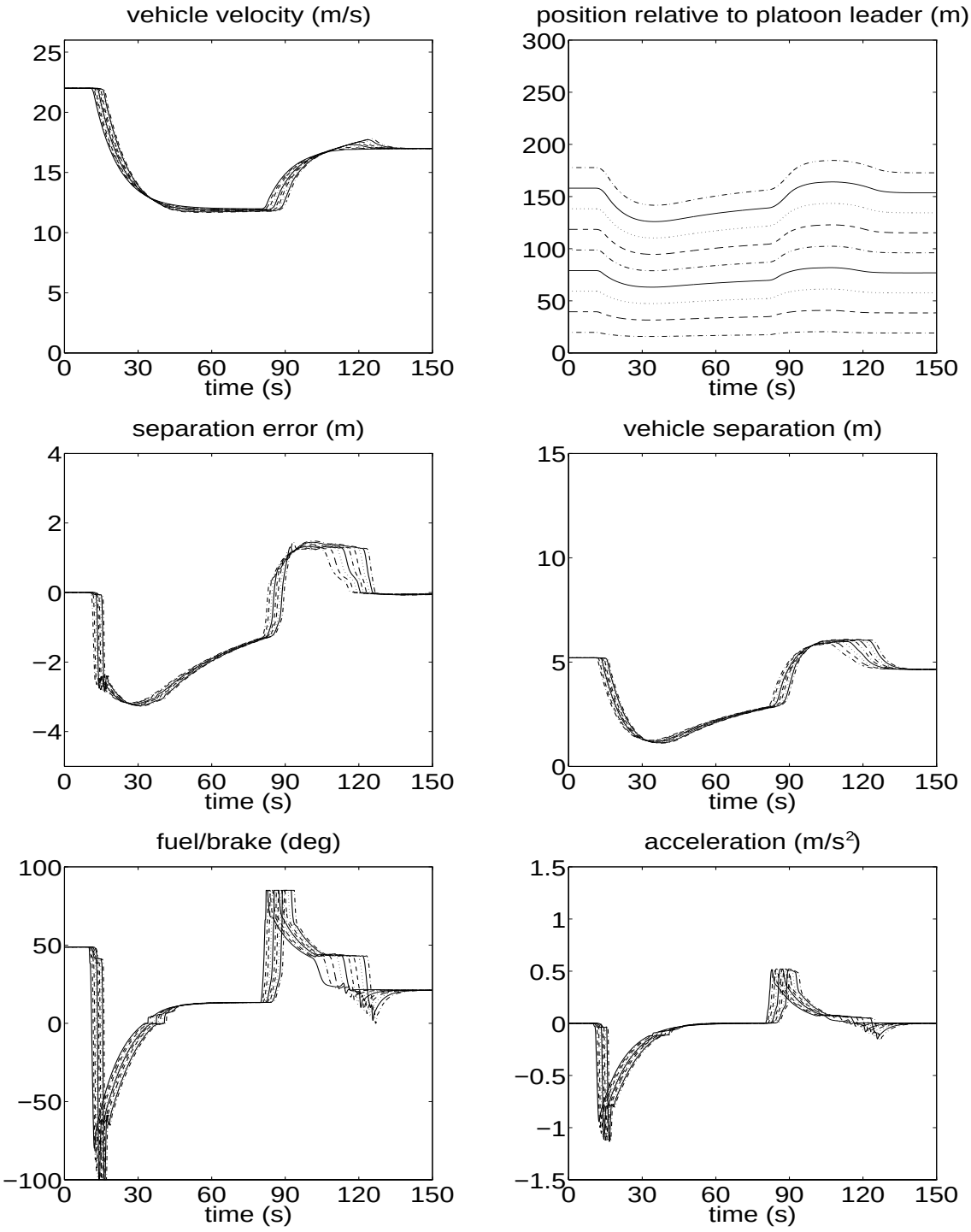

Figure 11: Ten autonomous vehicles, $h = \mathrm{sat}(0.1 - 0.2v_{\mathrm{r}})$, variable k, $\sigma = 50$.

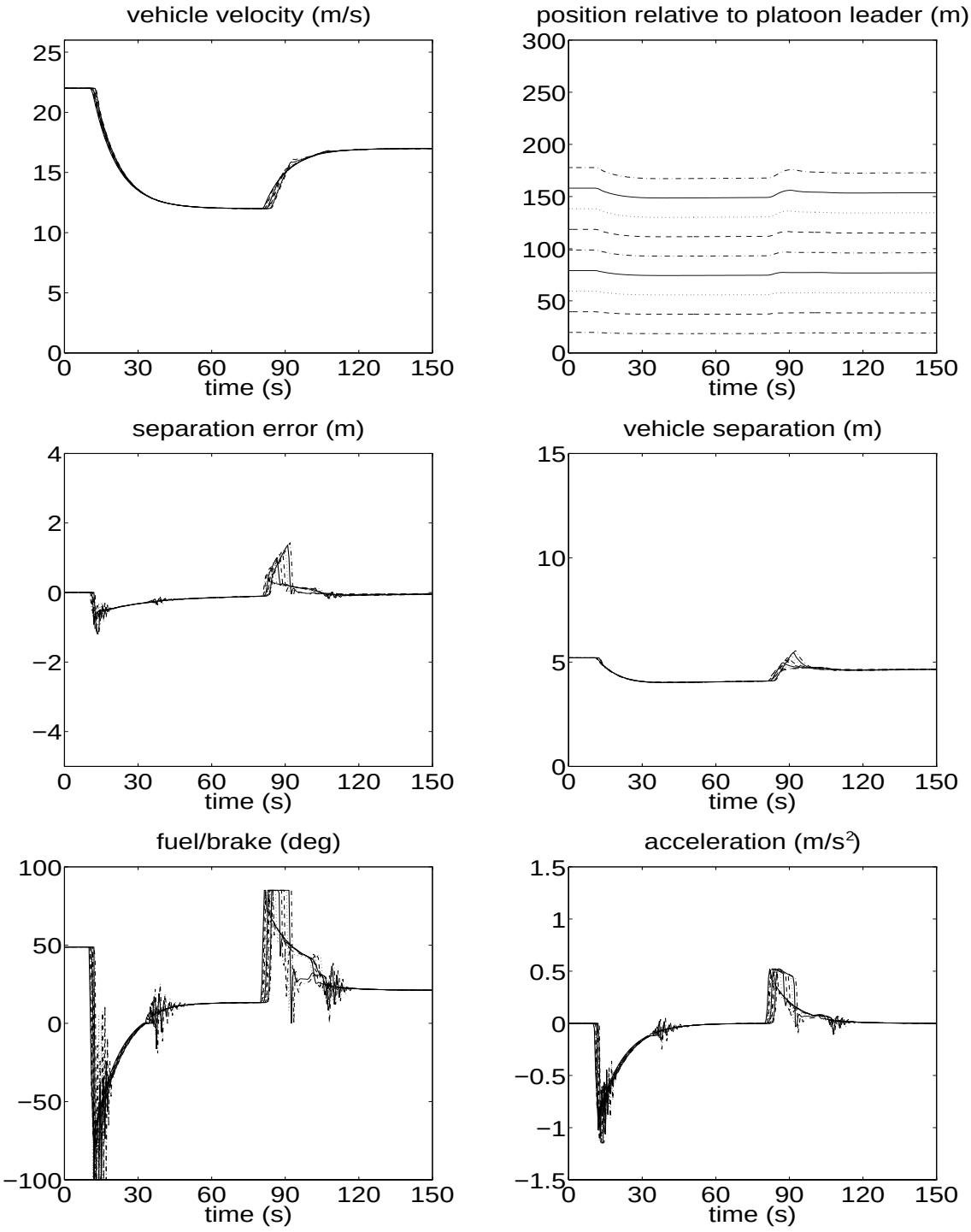

Figure 12: Ten autonomous vehicles, $h = \mathrm{sat}(0.1 - 0.2v_{\mathrm{r}})$, variable k, $\sigma = 0.1$.

Differentiation of (3.12) yields

$$\begin{aligned}
\ddot{\delta}_i &= \dot{v}_{\mathrm{r},i} - h_0\ddot{v}_i + c_h\ddot{v}_{\mathrm{r},i}v_i + 2c_h\dot{v}_{\mathrm{r},i}\dot{v}_i + c_h v_{\mathrm{r},i}\ddot{v}_i \\
&= a_{\mathrm{m}}\left(v_{\mathrm{r},i-1} + k_{i-1}\delta_{i-1} - v_{\mathrm{r},i} - k_i\delta_i\right) - h_0 a_{\mathrm{m}}\left(\dot{v}_{\mathrm{r},i} + k_i\dot{\delta}_i + \dot{k}_i\delta_i\right) \\
&\quad + c_h a_{\mathrm{m}}\left(\dot{v}_{\mathrm{r},i-1} + k_{i-1}\dot{\delta}_{i-1} + \dot{k}_{i-1}\delta_{i-1} - \dot{v}_{\mathrm{r},i} - k_i\dot{\delta}_i - \dot{k}_i\delta_i\right) v_i \\
&\quad + c_h a_{\mathrm{m}}\left(2\dot{v}_{\mathrm{r},i}v_{\mathrm{r},i} + 2\dot{v}_{\mathrm{r},i}k_i\delta_i + v_{\mathrm{r},i}\dot{v}_{\mathrm{r},i} + v_{\mathrm{r},i}k_i\dot{\delta}_i + v_{\mathrm{r},i}\dot{k}_i\delta_i\right). \qquad (3.14)
\end{aligned}$$

Using (3.13) twice, first with i replaced by $i-1$ and then with i, to expand the first term in (3.14), results in:

$$\begin{aligned}
\ddot{\delta}_i &= a_{\mathrm{m}}\Big(\dot{\delta}_{i-1} + h_0\dot{v}_{i-1} - c_h\dot{v}_{\mathrm{r},i-1}v_{i-1} - c_h v_{\mathrm{r},i-1}\dot{v}_{i-1} + k_{i-1}\delta_{i-1} \\
&\quad -\dot{\delta}_i - h_0\dot{v}_i + c_h\dot{v}_{\mathrm{r},i}v_i + c_h v_{\mathrm{r},i}\dot{v}_i - k_i\delta_i\Big) \\
&\quad -h_0 a_{\mathrm{m}}\left(\dot{v}_{i-1} - \dot{v}_i\right) - h_0 a_{\mathrm{m}}\left(k_i\dot{\delta}_i + \dot{k}_i\delta_i\right) \\
&\quad + c_h a_{\mathrm{m}}\left(\dot{v}_{\mathrm{r},i-1} - \dot{v}_{\mathrm{r},i}\right) v_i + c_h a_{\mathrm{m}}\left(k_{i-1}\dot{\delta}_{i-1} + \dot{k}_{i-1}\delta_{i-1} - k_i\dot{\delta}_i - \dot{k}_i\delta_i\right)\left(v_{i-1} - v_{\mathrm{r},i}\right) \\
&\quad + c_h a_{\mathrm{m}}\left(3\dot{v}_{\mathrm{r},i}v_{\mathrm{r},i} + 2\dot{v}_{\mathrm{r},i}k_i\delta_i + v_{\mathrm{r},i}k_i\dot{\delta}_i + v_{\mathrm{r},i}\dot{k}_i\delta_i\right) \\
&= a_{\mathrm{m}}\dot{\delta}_{i-1} + a_{\mathrm{m}}k_{i-1}\delta_{i-1} - a_{\mathrm{m}}\left(1 + h_0k_i\right)\dot{\delta}_i - a_{\mathrm{m}}k_i\delta_i + c_h a_{\mathrm{m}}k_{i-1}\dot{\delta}_{i-1}v_{i-1} - c_h a_{\mathrm{m}}k_i\dot{\delta}_i v_{i-1} \\
&\quad -c_h a_{\mathrm{m}}\dot{v}_{\mathrm{r},i-1}v_{\mathrm{r},i} - c_h a_{\mathrm{m}}v_{\mathrm{r},i-1}\dot{v}_{\mathrm{r},i} + c_h a_{\mathrm{m}}v_{\mathrm{r},i}\dot{v}_i - c_h a_{\mathrm{m}}k_{i-1}\dot{\delta}_{i-1}v_{\mathrm{r},i} + c_h a_{\mathrm{m}}k_i\dot{\delta}_i v_{\mathrm{r},i} \\
&\quad +c_h a_{\mathrm{m}}\dot{v}_{\mathrm{r},i}\left(3v_{\mathrm{r},i} + 2k_i\delta_i\right) + c_h a_{\mathrm{m}}v_{\mathrm{r},i}k_i\dot{\delta}_i \\
&\quad -a_{\mathrm{m}}\left[h_0 + c_h\left(v_i - v_{\mathrm{r},i}\right)\right]\dot{k}_i\delta_i + c_h a_{\mathrm{m}}\dot{k}_{i-1}\delta_{i-1}v_i\,. \qquad (3.15)
\end{aligned}$$

For our choice of k we denote

$$\dot{k} = -2\sigma\delta(k_0 - c_k)e^{-\sigma\delta^2}\dot{\delta} \stackrel{\triangle}{=} \psi(\delta)\delta\dot{\delta}\,. \qquad (3.16)$$

Substitution of (3.10–3.12) and (3.16) into (3.15) results in:

$$\begin{aligned}
\ddot{\delta}_i &= a_{\mathrm{m}}\left(1 + c_h k_{i-1}v_{i-1}\right)\dot{\delta}_{i-1} + a_{\mathrm{m}}k_{i-1}\delta_{i-1} - a_{\mathrm{m}}\left(1 + h_0k_i + c_h k_i v_{i-1}\right)\dot{\delta}_i - a_{\mathrm{m}}k_i\delta_i \\
&\quad +c_h a_{\mathrm{m}}^2\left(v_{\mathrm{r},i-2} + k_{i-2}\delta_{i-2} - v_{\mathrm{r},i-1} - k_{i-1}\delta_{i-1}\right)v_{\mathrm{r},i} \\
&\quad -c_h a_{\mathrm{m}}^2 v_{\mathrm{r},i-1}\left(v_{\mathrm{r},i-1} + k_{i-1}\delta_{i-1}\right) + c_h a_{\mathrm{m}}^2 v_{\mathrm{r},i}\left(v_{\mathrm{r},i} + k_{i-1}\delta_i\right) \\
&\quad -c_h a_{\mathrm{m}}k_{i-1}v_{\mathrm{r},i}\left[v_{\mathrm{r},i-1} - h_0 a_{\mathrm{m}}\left(v_{\mathrm{r},i-1} + k_{i-1}\delta_{i-1}\right)\right. \\
&\quad \left.+c_h a_{\mathrm{m}}\left(v_{\mathrm{r},i-2} + k_{i-2}\delta_{i-2} - v_{\mathrm{r},i-1} - k_{i-1}\delta_{i-1}\right)v_{i-1} + c_h a_{\mathrm{m}}v_{\mathrm{r},i-1}\left(v_{\mathrm{r},i-1} + k_{i-1}\delta_{i-1}\right)\right] \\
&\quad +2c_h a_{\mathrm{m}}k_i v_{\mathrm{r},i}\left[v_{\mathrm{r},i} - h_0 a_{\mathrm{m}}\left(v_{\mathrm{r},i} + k_i\delta_i\right)\right. \\
&\quad \left.+c_h a_{\mathrm{m}}\left(v_{\mathrm{r},i-1} + k_{i-1}\delta_{i-1} - v_{\mathrm{r},i} - k_i\delta_i\right)v_i + c_h a_{\mathrm{m}}v_{\mathrm{r},i}\left(v_{\mathrm{r},i} + k_i\delta_i\right)\right] \\
&\quad +c_h a_{\mathrm{m}}^2\left(v_{\mathrm{r},i-1} + k_{i-1}\delta_{i-1} - v_{\mathrm{r},i} - k_i\delta_i\right)\left(3v_{\mathrm{r},i} + 2k_i\delta_i\right) \\
&\quad -a_{\mathrm{m}}\left[h_0 + c_h\left(v_i - v_{\mathrm{r},i}\right)\right]\psi(\delta_i)\delta_i^2\left[v_{\mathrm{r},i} - h_0 a_{\mathrm{m}}\left(v_{\mathrm{r},i} + k_i\delta_i\right)\right. \\
&\quad \left.+c_h a_{\mathrm{m}}\left(v_{\mathrm{r},i-1} + k_{i-1}\delta_{i-1} - v_{\mathrm{r},i} - k_i\delta_i\right)v_i + c_h a_{\mathrm{m}}v_{\mathrm{r},i}\left(v_{\mathrm{r},i} + k_i\delta_i\right)\right] \\
&\quad +c_h a_{\mathrm{m}}v_i\psi(\delta_{i-1})\delta_{i-1}^2\left[v_{\mathrm{r},i-1} - h_0 a_{\mathrm{m}}\left(v_{\mathrm{r},i-1} + k_i\delta_{i-1}\right)\right. \\
&\quad +c_h a_{\mathrm{m}}\left(v_{\mathrm{r},i-2} + k_{i-2}\delta_{i-2} - v_{\mathrm{r},i-1} - k_{i-1}\delta_{i-1}\right)v_{i-1} \\
&\quad \left.+c_h a_{\mathrm{m}}v_{\mathrm{r},i-1}\left(v_{\mathrm{r},i-1} + k_{i-1}\delta_{i-1}\right)\right]. \qquad (3.17)
\end{aligned}$$

Linearizing (3.17) around $v_{\rm r} = 0$ and $\delta = 0$ yields:

$$\ddot{\delta}_i + a_{\rm m}\left(1 + h_0 k_0 + c_h k_0 v_{i-1}\right)\dot{\delta}_i + a_{\rm m} k_0 \delta_i = a_{\rm m}\left(1 + c_h k_0 v_{i-1}\right)\dot{\delta}_{i-1} + a_{\rm m} k_0 \delta_{i-1}\,, \tag{3.18}$$

and the transfer function becomes:

$$G_{\rm var}(s) = \frac{a_{\rm m}\left(1 + c_h k_0 v_{i-1}\right) s + a_{\rm m} k_0}{s^2 + a_{\rm m}\left(1 + h_0 k_0 + c_h k_0 v_{i-1}\right) s + a_{\rm m} k_0}\,. \tag{3.19}$$

In the case of constant separation error gain $k \equiv k_0$, i.e., when $\sigma = 0$, (3.17) reduces to:

$$\begin{aligned}
\ddot{\delta}_i \;=\;& a_{\rm m}\left(1 + c_h k_0 v_{i-1}\right)\dot{\delta}_{i-1} + a_{\rm m} k_0 \delta_{i-1} - a_{\rm m}\left(1 + h_0 k_0 + c_h k_0 v_{i-1}\right)\dot{\delta}_i - a_{\rm m} k_0 \delta_i \\
& + c_h a_{\rm m}^2 \left(v_{{\rm r},i-2} + k_0 \delta_{i-2} - v_{{\rm r},i-1} - k_0 \delta_{i-1}\right) v_{{\rm r},i} \\
& - c_h a_{\rm m}^2 v_{{\rm r},i-1}\left(v_{{\rm r},i-1} + k_0 \delta_{i-1}\right) + c_h a_{\rm m}^2 v_{{\rm r},i}\left(v_{{\rm r},i} + k_0 \delta_i\right) \\
& - c_h a_{\rm m} k_0 v_{{\rm r},i}\left[v_{{\rm r},i-1} - h_0 a_{\rm m}\left(v_{{\rm r},i-1} + k_0 \delta_{i-1}\right)\right. \\
& \left. + c_h a_{\rm m}\left(v_{{\rm r},i-2} + k_0 \delta_{i-2} - v_{{\rm r},i-1} - k_0 \delta_{i-1}\right) v_{i-1} + c_h a_{\rm m} v_{{\rm r},i-1}\left(v_{{\rm r},i-1} + k_0 \delta_{i-1}\right)\right] \\
& + 2 c_h a_{\rm m} k_0 v_{{\rm r},i}\left[v_{{\rm r},i} - h_0 a_{\rm m}\left(v_{{\rm r},i} + k_0 \delta_i\right)\right. \\
& \left. + c_h a_{\rm m}\left(v_{{\rm r},i-1} + k_0 \delta_{i-1} - v_{{\rm r},i} - k_0 \delta_i\right) v_i + c_h a_{\rm m} v_{{\rm r},i}\left(v_{{\rm r},i} + k_0 \delta_i\right)\right] \\
& + c_h a_{\rm m}^2 \left(v_{{\rm r},i-1} + k_0 \delta_{i-1} - v_{{\rm r},i} - k_0 \delta_i\right)\left(3 v_{{\rm r},i} + 2 k_0 \delta_i\right),
\end{aligned} \tag{3.20}$$

which after linearization leads to the same transfer function (3.19). It is now straightforward to show that $G_{\rm var}(s)$ given by (3.19) satisfies the magnitude requirement $|G_{\rm var}(j\omega) < 1 \;\forall\, \omega > 0$ if and only if

$$k_0 > \frac{2(1 - a_{\rm m} h_0)}{a_{\rm m} h_0 (h_0 + 2 c_h v_{i-1})}\,. \tag{3.21}$$

To compare this string stability condition with the one obtained by Garrard et al. (1978) and Ioannou and Xu (1994) for the case where both h and k are constant, we set $c_h = 0$ in (3.19) to obtain:

$$G(s) = \frac{a_{\rm m} s + a_{\rm m} k_0}{s^2 + a_{\rm m}\left(1 + h_0 k_0\right) s + a_{\rm m} k_0}\,. \tag{3.22}$$

This is the same transfer function obtained by Ioannou and Xu (1994), where it is shown that the corresponding string stability condition is

$$k_0 > \frac{2(1 - a_{\rm m} h_0)}{a_{\rm m} h_0^2}\,. \tag{3.23}$$

The comparison of (3.21) to (3.23) reveals that string stability is easier to achieve in the variable h case than in the fixed h case, due to the additional term $2 c_h v_{i-1}$ in the denominator of (3.21). Indeed, the Bode plots of $G(s)$ and $G_{\rm var}(s)$ presented in Fig. 13 show that the variable time headway reduces the magnitude peak of the transfer function. The price paid for this reduction is that $|G_{\rm var}(j\omega)|$ does not drop as fast as $|G(j\omega)|$ at higher frequencies. However this is a good tradeoff:

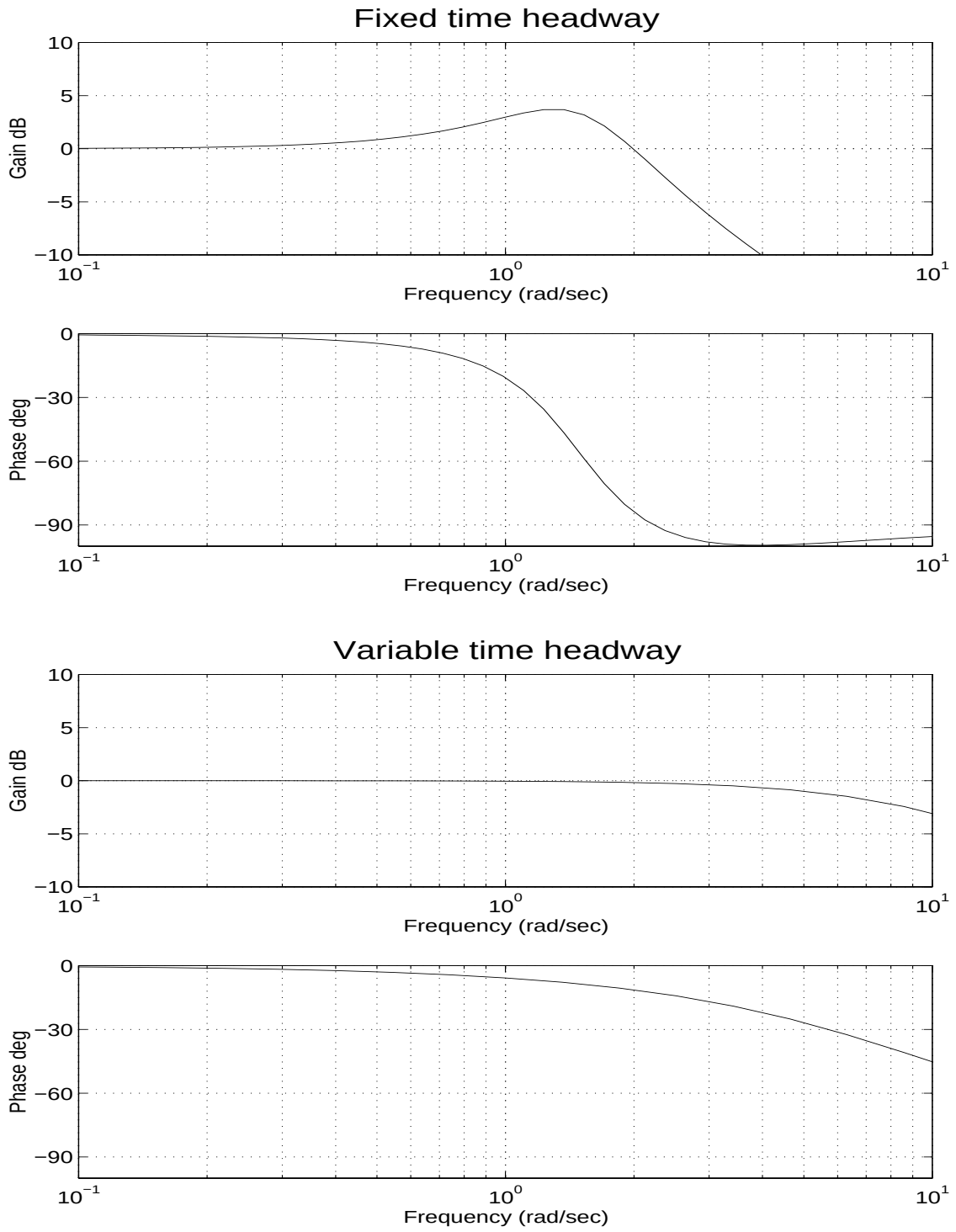

Figure 13: Typical Bode plots of $G(s)$ and $G_{\mathrm{var}}(s)$.

Since the natural dynamics of a CHV platoon act as a low-pass filter due to the low actuation-to-weight ratio, frequencies above 0.4 Hz are much less important than frequencies up to 0.4 Hz.

Finally, we should note that it is tedious but straightforward to extend all of the above analysis to the case $q_{\rm m} > 0$, since the linearization process eliminates the quadratic term and its derivatives. Therefore, the same conclusions drawn for the PI controller remain valid for the PIQ controller with variable h and k.

3.4 Merge maneuvers

The nonlinear spacing policies presented in the previous section have been designed to improve platoon performance and control smoothness during autonomous operation, i.e., in the absence of intervehicle communication. Since the focus was on the string stability properties of our controllers, we only considered a *single-platoon* scenario for our simulations. The basic advantage of the platoon structure is that its small intervehicle spacings guarantee that even if there are collisions, they will occur at small relative velocity, and thus will not be damaging. Things are much more complicated, however, when two platoons initially separated by a large distance merge to form a single platoon: the risk of collisions at high relative speed is significantly increased. Hence, a considerable amount of research effort is currently being devoted to developing robust and safe strategies for merging and splitting platoons. The most challenging scenario in this case is a merge/brake maneuver: after the merge maneuver has started and the following platoon has accelerated, the lead platoon decelerates hard.

It is then natural to ask whether the controllers developed in the previous section preserve their performance characteristics in merge/brake scenarios. This becomes then an issue of *robustness* with respect to a larger class of commanded maneuvers. To investigate whether our adaptive nonlinear controllers featuring variable time headway and/or variable separation error gain are robust enough to safely handle merge commands, we simulate their response under a challenging *merge-and-brake* maneuver: First, a five vehicle platoon is given a step command at $t = 20$ s to merge with a similar formation initially 87.75 m ahead. The leading platoon maintains a constant speed of 22 m/s. Then, 10 s after the merge has started, the leading platoon abruptly decreases its speed from 22 m/s to 12 m/s. The information available to the leader of the following platoon consists only of its relative position and velocity with respect to the last vehicle of the preceding platoon. The results obtained using variable h or variable k spacing policy are shown in Fig. 14 and Fig. 15 respectively. Fig. 16 illustrates the response of the controller used in Fig. 12, which combines the two terms with $\sigma = 0.1$.

Comparing Figs. 14 and 16 we see that the two controllers which behaved almost identically in the simpler deceleration/acceleration maneuver shown in Figs. 8 and 12 are anything but identical under this much more demanding merge/brake maneuver. In sharp contrast to the large errors and multiple collisions observed in Fig. 14 where only variable h is used, the addition of a seemingly mild nonlinearity in the separation error gain yields a nearly ideal response in Fig. 16. In reality, of course, this nonlinearity is not mild. As discussed in section 3.5, the benefits of variable separation error gain become significant as separation errors become large, which is certainly the case in this merge/brake scenario right after the merge command is issued. The role of the variable separation error gain for improving the robustness of the controller is further illustrated by comparing Figs. 10

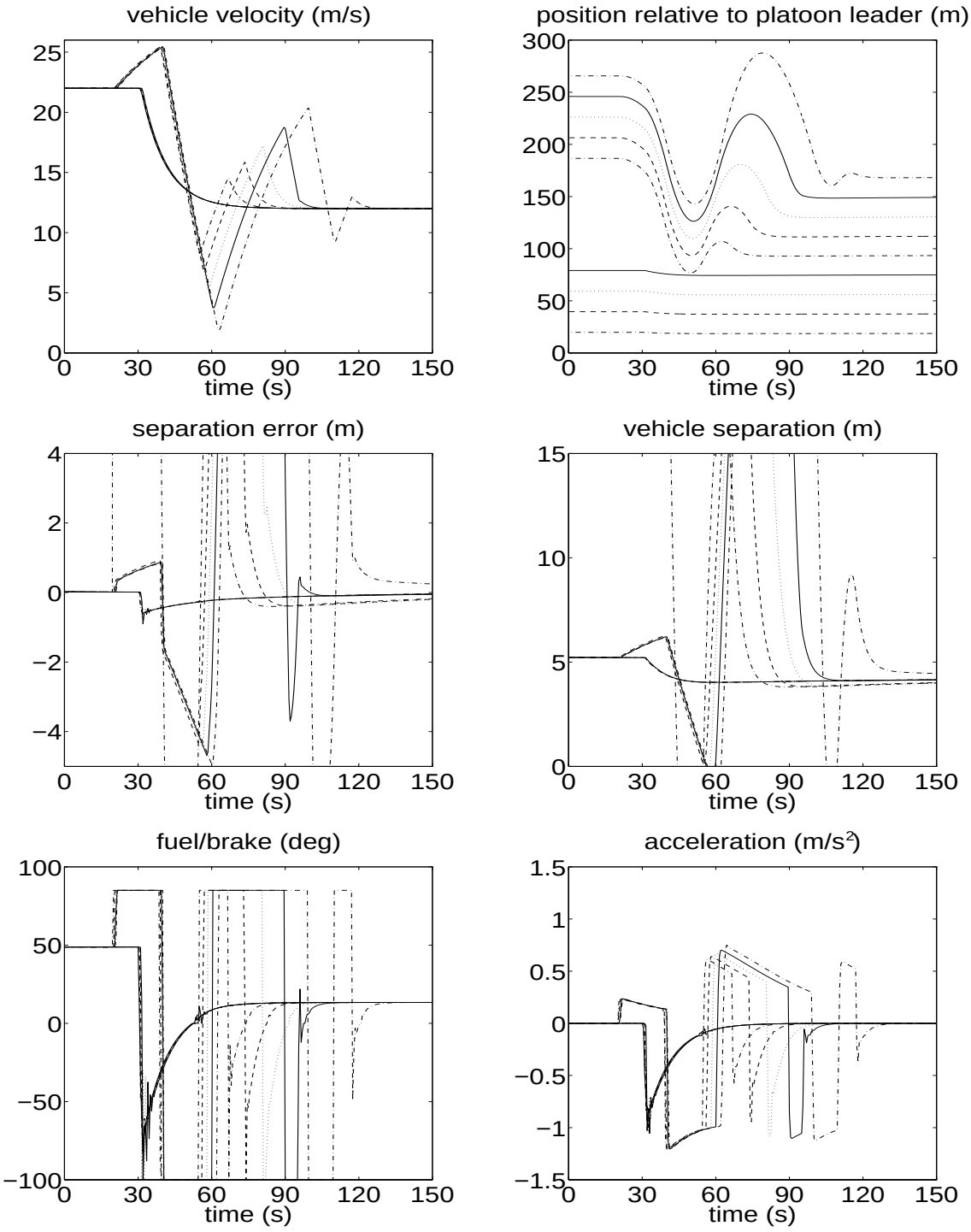

Figure 14: Merge and brake maneuver, $h = \mathrm{sat}(0.1 - 0.2v_{\mathrm{r}})$.

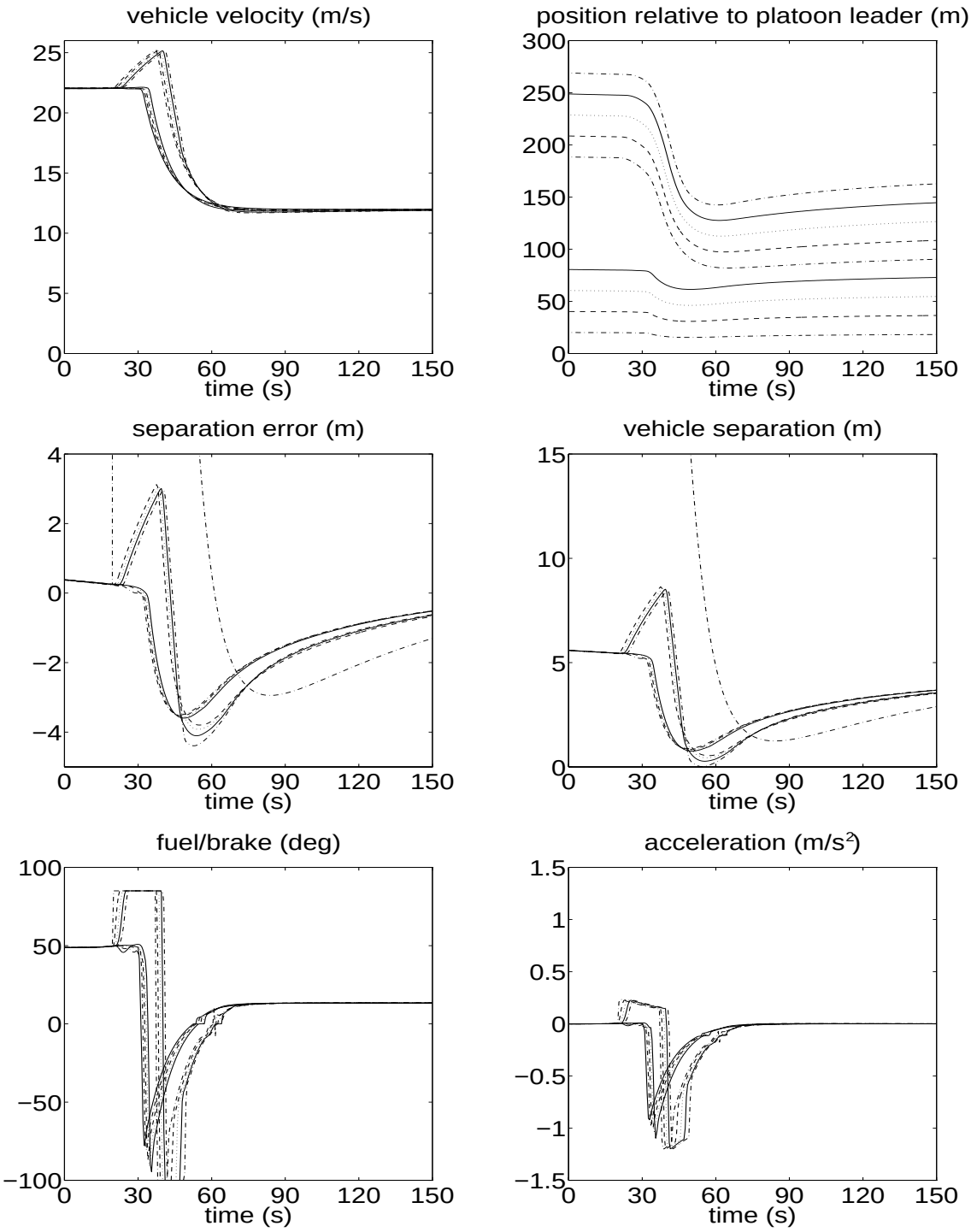

Figure 15: Merge and brake maneuver, variable k, $\sigma = 50$.

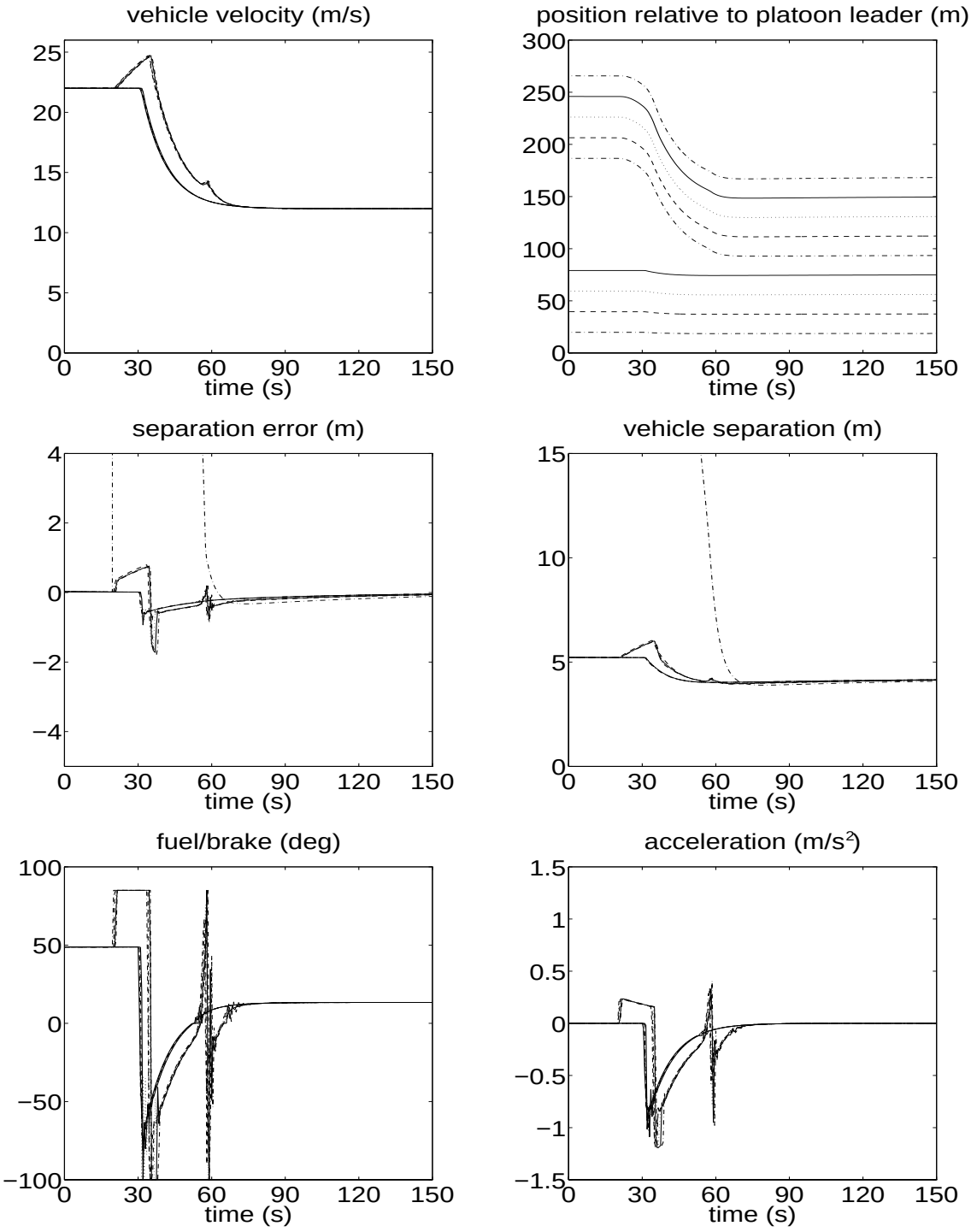

Figure 16: Merge and brake maneuver, $h = \mathrm{sat}(0.1 - 0.2v_{\mathrm{r}})$, variable k, $\sigma = 0.1$.

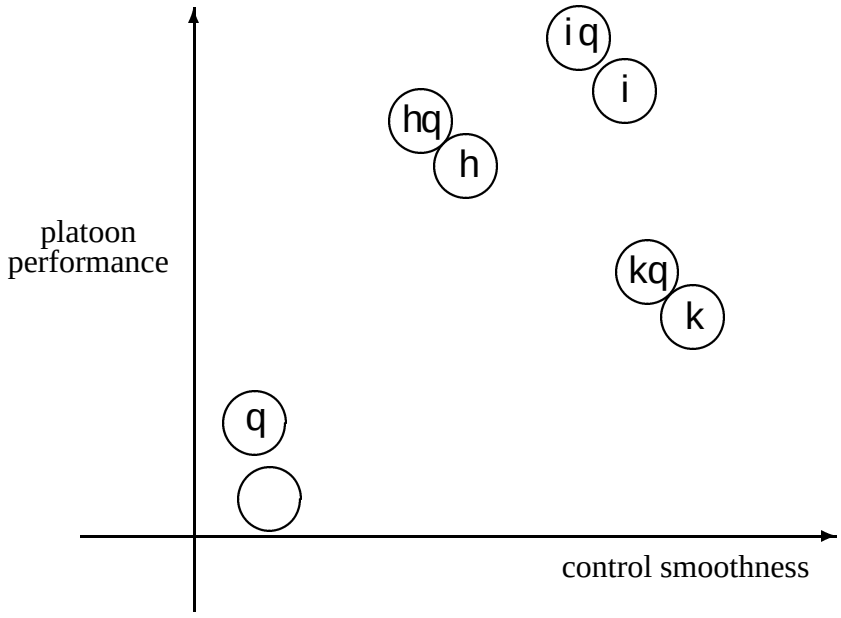

Figure 17: Qualitative comparison chart of CHV longitudinal control schemes.

and 15: the performance of the variable k controller is quite consistent under the two different scenarios. On the other hand, the variable h term alone does not provide enough robustness, as is evident from Figs. 8 and 14. Clearly, the added complexity of the variable separation error gain should be viewed as necessary for maneuvers involving more than one platoon.

3.5 Qualitative comparison

The control schemes examined in sections 2 and 3 are promising, but need to be tested in real experiments. Before that, however, their advantages and disadvantages must be clearly understood. Each of the above modifications adds some complexity to the control algorithm, making it more computationally demanding, but at the same time results in improved performance. Comparing all the presented simulation results is not enough to determine which modifications are worth implementing and which are not, since these simulations are by no means exhaustive. Furthermore, each modification has something different to offer, and no single criterion can be used to compare and rank them. Therefore, we have compiled two qualitative comparison charts, which are based on our analytic results and on our extensive simulations of several AHS scenarios. In the diagrams of Fig. 17 and Fig. 18, each circle represents a different controller configuration. All configurations consist of a proportional and an integral term with adaptive gain, and in addition may feature a Q term (denoted by q), variable time headway (denoted by h), variable separation error gain (denoted by k), or intervehicle communication (denoted by i).

We start with the results presented up to and including section 3.3 (single platoon scenarios). The two criteria selected for this comparison are the two most important ones from the AHS point of view: *control smoothness*, which is directly related to fuel efficiency and driver comfort, and *platoon performance*, which is related to safety and traffic throughput. Fig. 17 should be used as a "visual aid" in determining the most appropriate longitudinal control scheme for a CHV platoon.

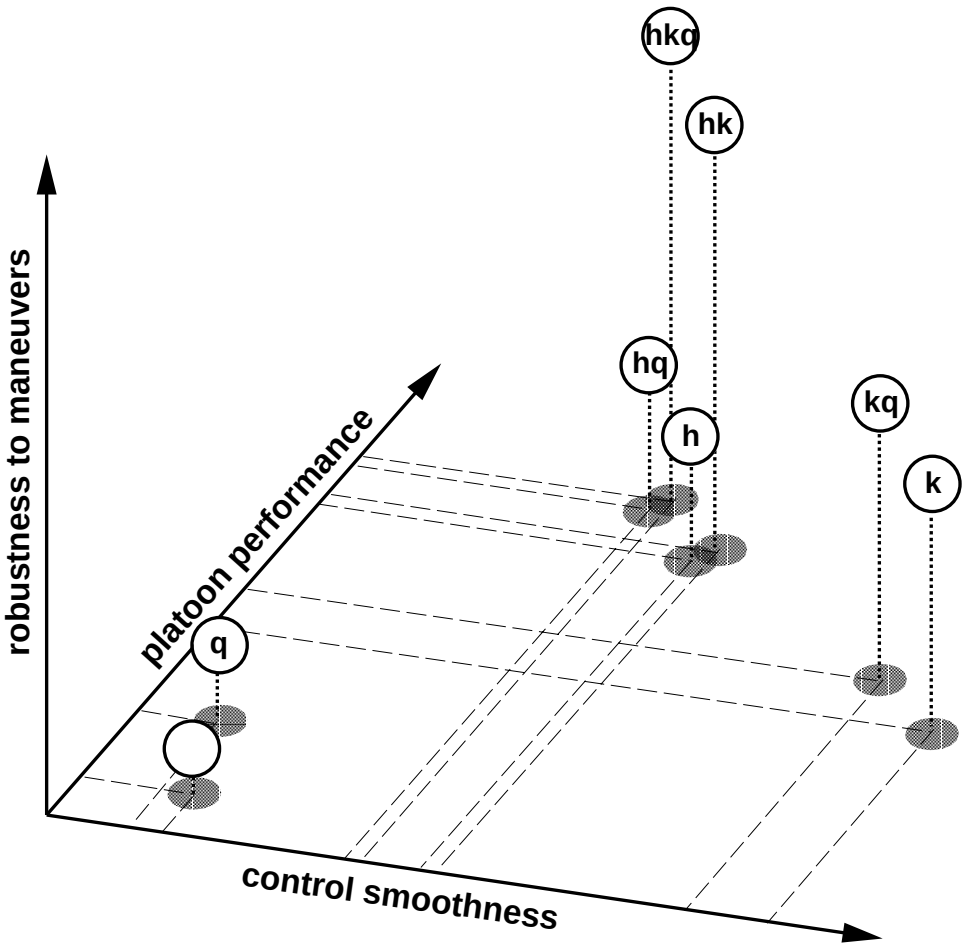

Figure 18: A more elaborate qualitative comparison.

Each choice involves a tradeoff between control smoothness, platoon performance, and controller complexity. In autonomous operation, for example, it is always worth using either variable time headway or variable separation error gain. With either of these modifications, both control smoothness and platoon performance are much better than without any of the two, and this benefit justifies the additional control complexity. If platoon performance is the primary consideration, then variable time headway is the modification of choice, while variable separation error gain should be preferred when control smoothness is more important. It is also clear that if any of these two is used, the additional complexity of a nonlinear Q term may not be justified, since the resulting change is barely noticeable. Finally, the schemes with intervehicle communication appear to have a distinct advantage over the autonomous schemes. However, this must be weighed against the considerable additional complexity of establishing and maintaining reliable communication between the vehicles in the platoon.

The situation changes if we consider *robustness* with respect to a large variety of scenarios as a third criterion, in addition to control smoothness and platoon performance. If we expect our controller to perform safely even when faced with abrupt merge commands followed by significant decelerations of the lead platoon, without relying on the usually considered additional layer of

"nonlinear path planning", then we must use the three-dimensional diagram of Fig. 18.[4] The conclusion that it is always worth using either variable time headway or variable separation error gain is still valid. However, the variable separation error gain contributes much more to the robustness of the controller. Now it becomes clear that even when platoon performance is more important than control smoothness, it is advisable to tolerate the additional complexity of a variable k term with a small value of σ, since that yields a very significant robustness enhancement to merge maneuvers. Again, when either variable h or k is used, the additional complexity of a nonlinear Q term may not be justified, since the resulting change is barely noticeable. Taking into consideration all of the above, the scheme which utilizes both variable h and variable k with $\sigma = 0.1$ appears to have the clear advantage over all other autonomous controllers.

4 String Stability

4.1 Introduction

Since string stability is one of the most important issues related to AHS safety and performance but its analysis can get complicated and tedious, as seen in the previous section. Therefore, it would be desirable to develop an efficient method for establishing the stability properties of different control approaches. As a first step in this search, we consider a simplified framework in which we view vehicles as masses and the "electronic connections" between them as springs and dampers.

A broad definition of string stability is that platoon members must not collide with each other; a slightly more rigorous definition is that spacing errors (the difference between the actual and desired inter-vehicle spacing) must be attenuated as they propagate through the platoon, thus eliminating the so-called "slinky effect." Unfortunately, string stability analysis is complicated by the presence of severe nonlinearities in realistic vehicle models. Linearized models are thus often used for this purpose, since for small deviations from the nominal operating conditions they retain much of the information contained in the nonlinear model.

There is a large body of work devoted to string stability in the literature; the reader is referred to the survey paper by Shladover (1995) and the references therein. In particular, there have been several definitions for string stability; some of the most notable are the one due to Chu (1974), which eliminates the spatial variable, and the one due to Swaroop (1997), which eliminates the temporal variable (see also Swaroop and Hedrick 1996, and Swaroop and Niemann 1996).

We propose a simplified framework in which the platoon is viewed as a (linear) mass-spring-damper system. This framework combines the tractability of linear analysis with the physical intuition of mechanical systems, and yields transfer functions which characterize the behavior of spacing errors as they propagate through the platoon. The transfer functions can be used to determine the string stability properties of a platoon operating under a given control scheme. Of course, the conclusions drawn from this linear approximation are to be used as guidelines, rather than rules, for longitudinal controller selection in Automated Highway System (AHS) applications.

[4]The intervehicle communication scheme is not included in this diagram because the form of communication we considered here, namely transmitting the desired speed of the platoon leader to all followers, is not well suited for the merge/brake scenario of section 3.4. Hence, including it would result in an unfair comparison, while more elaborate communication schemes are beyond our scope.

String stability analysis reveals how spacing errors are propagated through the platoon, but does not offer much insight into the behavior of the first spacing error (the spacing error between the first two vehicles) that is generated by acceleration of the lead vehicle. The framework for analysis used here lends itself to analyzing this spacing error by allowing computation of the transfer function relating the input force applied to the platoon leader to the spacing error between the first two vehicles. Again, it is desirable for this transfer function to have a corresponding impulse response that is positive to avoid position overshoot by the second vehicle. As will be shown, the relationship between the input force and the first spacing error may reveal important qualitative information about the platoon's performance that is not contained in the spacing error transfer function.

We use the mass-spring-damper framework to analyze a variety of longitudinal controllers. For each controller examined, we determine both its string stability properties and the behavior of the first spacing error.

4.2 Background

Spacing error attenuation is generally viewed as the only requirement for string stability. However, there is another issue to be addressed. Consider, for example, the following scenario: In a platoon with one meter (1 m) nominal intervehicle spacing, the lead vehicle accelerates and generates an 8 m positive spacing error between itself and its follower. This error is then propagated as a negative spacing error of 1.5 m between the second and third vehicles, and a collision occurs. This example of unacceptable platoon performance illustrates the fact that guaranteeing spacing error attenuation does not eliminate the possibility that a large positive spacing error may generate a smaller, but negative, error upstream. The issue here is not one of avoiding position overshoot during platoon braking maneuvers, which is impossible. Rather, it is one of avoiding overshoot in response to lead vehicle acceleration. To eliminate this possibility, the impulse response of the spacing error (the inverse Laplace transform of the spacing error transfer function) must remain positive. (Note that impulse response *undershoot* translates into vehicle position *overshoot*.) It is worth mentioning here that, although AHS-specific inputs do not take the form of impulse functions, position overshoot has been observed in systems that have impulse response undershoot, even during routine longitudinal maneuvers. This leads to the conclusion that requiring a positive impulse is not too stringent a constraint if the elimination of overshoot during acceleration maneuvers is desired.

Fig. 19 illustrates a typical spacing error in response to an acceleration by lead vehicle. As the lead vehicle accelerates away from its follower, the spacing error between the two vehicles becomes large. The second vehicle then accelerates and catches up to the leader, causing the spacing error to return to zero. As can be seen from the graph, the spacing error between the second and third vehicles does not become as large as that generated between the first two vehicles. This is what is meant by string stability; spacing errors generated between the first two vehicles should decrease monotonically as they propagate through the platoon. The important point to notice is that the spacing error between the second and third vehicles *does* become slightly negative, even though the initial spacing error was strictly positive. This behavior can be eliminated by requiring a positive impulse response. As shown by Swaroop and Niemann (1996), requiring a positive impulse response has an additional benefit: it makes possible the use of frequency-domain analysis for string stability. Some mathematical preliminaries are included here to provide the appropriate

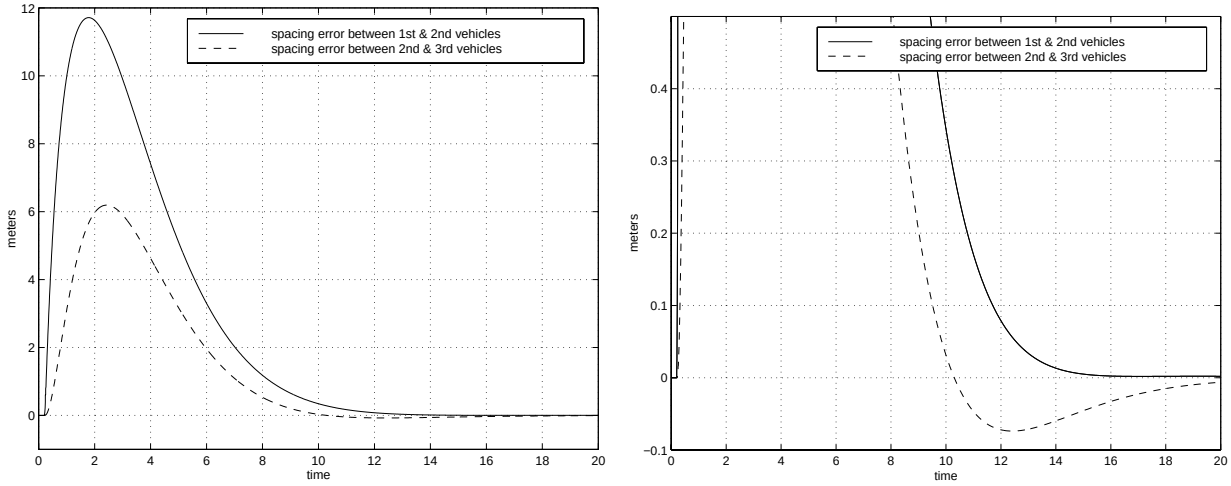

Figure 19: Typical spacing error (with close-up).

context in which to perform string stability analysis.

4.3 Mathematical preliminaries

In general, if $G(s)$ is a spacing error transfer function and $g(t)$ is its inverse Laplace transform, then

$$\|g * z\|_\infty \;\leq\; \|g\|_1 \, \|z\|_\infty \tag{4.1}$$

where $z(t)$ is the input spacing error and $(g * z)(t)$ is the output spacing error, and

$$\|g\|_1 \;=\; \int_0^\infty |g(t)| \, dt \, . \tag{4.2}$$

Equation (4.1) describes the relationship between the maximum input spacing error and the maximum output spacing error; they are related by the multiplicative factor of $\|g\|_1$. Therefore, the necessary and sufficient requirement for spacing error attenuation is

$$\|g\|_1 \;<\; 1 \, . \tag{4.3}$$

The disadvantage of working in the time domain is that $\|g\|_1$ can be quite difficult to analyze. The graphs of $\|g\|_1$ presented in this report were generated using numerical analysis; it was not possible to obtain analytical results even in cases with relatively simple transfer functions. It is desirable, therefore, to switch to the frequency domain for analysis.

From linear systems theory, it is known that

$$|G(0)| \;\leq\; \|G\|_\infty \;\leq\; \|g\|_1 \tag{4.4}$$

where

$$\|G\|_\infty \;=\; \max_\omega \, |G(j\omega)|. \tag{4.5}$$

Using the definition of the Laplace transform,

$$|G(0)| \;=\; |\int_0^\infty g(t)\,dt\,| \;\leq\; \int_0^\infty |g(t)|dt \;=\; \|g\|_1\,. \tag{4.6}$$

If the impulse response $g(t)$ remains positive, the inequality in equation (4.6) becomes an equality, and

$$\|G\|_\infty \;=\; \|g\|_1\,. \tag{4.7}$$

This is the only case in which the L_1 norm of $g(t)$ can be evaluated in the frequency domain. In this case, the condition $\|g\|_1 < 1$ is replaced by the equivalent condition

$$\|G\|_\infty < 1\,, \quad g(t) \geq 0\;\forall\, t\,. \tag{4.8}$$

Thus, we define three notions of string stability:

L_2 string stability: the energy (represented by the L_2 norm) of the output error is smaller than the energy of the input error (equivalent to $\|G\|_\infty < 1$).

L_∞ string stability: the maximum magnitude of the output error is smaller than the maximum magnitude of the input error (equivalent to $\|g\|_1 < 1$).

String stability without overshoot: the maximum magnitude of the output error is smaller than the maximum magnitude of the input error, and, in addition, if the input error does not change sign, then the output error always has the same sign as the input error (equivalent to $\|g\|_1 < 1$ and $g(t) \geq 0$).

It is important to note that, if the impulse response is not positive, frequency-domain analysis can guarantee only L_2 string stability, since $\|G\|_\infty$ is the frequency-domain equivalent of the L_2-induced norm. L_2 string stability can be viewed as a guarantee of energy attenuation, which is desirable but does not imply spacing error attenuation. In this case, ensuring L_∞ string stability requires analysis in the time domain. Frequency-domain analysis is still useful even when the impulse response is not positive, however, because the $\|G\|_\infty$ and $\|g\|_1$ norms are equivalent and will therefore exhibit the same trends in terms of attenuation versus control gains. If it is possible to achieve energy attenuation, then it is also possible to achieve magnitude attenuation with, perhaps, a more restricted set of control gains. In addition, frequency-domain analysis provides information about the effect of various controller characteristics on the ease with which one can obtain spacing error attenuation. As we will see, L_2 string stability and L_∞ string stability are "equivalent", in the sense that any controller configuration which can achieve one, can also achieve the other, possibly under more restrictive conditions on the controller gains. String stability without overshoot, on the other hand, imposes the additional requirement of positive impulse response, which is not always achievable, even in the presence of L_2 or L_∞ string stability.

4.4 Controller characteristics

We consider controllers that use various combinations of the following controller characteristics:

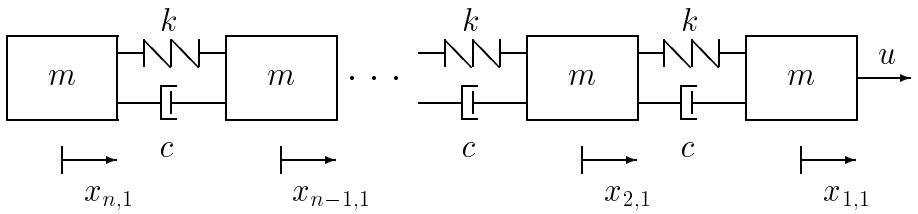

Figure 20: Mass-spring-damper system.

• **Unidirectional vs bidirectional** In the bidirectional control scheme, originally proposed as a means of improving platoon performance and safety (Peppard 1974, Yang and Tongue 1996), each mass is considered to be coupled by springs and dampers to both the preceding and following masses. This allows the controller to use information about the relative distance and velocity of both the immediately preceding and immediately following vehicles. In the unidirectional control scenario, each mass is considered to be connected only to its immediate predecessor without being affected by its follower. In the sense that unidirectional springs and dampers do not exist, this controller cannot be thought of as a physical system; however, we can still employ the mass-spring-damper framework for analysis and compare the results with those obtained in the bidirectional case.

• **Constant spacing vs time headway** If the controller uses a constant spacing policy, its objective is to maintain a constant distance (for example, three meters) between itself and its predecessor at all times. The time headway spacing policy, in contrast, allows the actual distance between vehicles to vary based on their velocities. Time headway is often referred to as speed-dependent spacing.

• **Autonomous vs non-autonomous** If the controller relies only on on-board sensors to determine the speeds and positions of other vehicles, we refer to the vehicle as being "autonomous." If some form of inter-vehicle communication is introduced, the vehicles are said to be operating non-autonomously.

4.5 Autonomous controllers

4.5.1 Mass-spring-damper framework

In the analysis presented here, the platoon is viewed as a mass-spring-damper (m-s-d) system. The stability of mass-spring-damper systems was examined by Barbieri (1993) as a special case of general interconnected systems. Here we apply this framework to the platoon string stability problem and develop equivalent m-s-d representations of all the configurations we consider.

As shown in Fig. 20, vehicles are represented as masses, and the electronic couplings between them are considered to be springs and dampers. The spring and damping constants represent the control gains on the relative position and velocity, respectively. Transfer functions describing the propagation of spacing errors are generated by deriving a state-space representation of the system using the position of each vehicle as a state, and then translating this representation into error coordinates. It should be noted that in this representation, the condition $x_{1,1} = x_{2,1} = \ldots = x_{n,1}$ is only satisfied when the platoon is in steady state; i.e., when all vehicles are separated by the

desired distance. The state-space representation of the bidirectional controller is

$$\begin{aligned}
\dot{x}_{1,1} &= x_{1,2} \\
\dot{x}_{1,2} &= -\frac{k}{m}x_{1,1} + \frac{k}{m}x_{2,1} - \frac{c}{m}x_{1,2} + \frac{c}{m}x_{2,2} + \frac{u}{m} \\
\dot{x}_{2,1} &= x_{2,2} \\
\dot{x}_{2,2} &= \frac{k}{m}x_{1,1} - \frac{2k}{m}x_{2,1} + \frac{k}{m}x_{3,1} + \frac{c}{m}x_{1,2} - \frac{2c}{m}x_{2,2} + \frac{c}{m}x_{3,2} \\
&\vdots \\
\dot{x}_{n-1,1} &= x_{n-1,2} \\
\dot{x}_{n-1,2} &= \frac{k}{m}x_{n-2,1} - \frac{2k}{m}x_{n-1,1} + \frac{k}{m}x_{n,1} + \frac{c}{m}x_{n-2,2} - \frac{2c}{m}x_{n-1,2} + \frac{c}{m}x_{n,2} \\
\dot{x}_{n,1} &= x_{n,2} \\
\dot{x}_{n,2} &= \frac{k}{m}x_{n-1,1} - \frac{k}{m}x_{n,1} + \frac{c}{m}x_{n-1,2} + \frac{c}{m}x_{n,2} \, .
\end{aligned} \tag{4.9}$$

The state-space representation of the unidirectional system is

$$\begin{aligned}
\dot{x}_{1,1} &= x_{1,2} \\
\dot{x}_{1,2} &= \frac{u}{m} \\
\dot{x}_{2,1} &= x_{2,2} \\
\dot{x}_{2,2} &= \frac{k}{m}x_{1,1} - \frac{k}{m}x_{2,1} + \frac{c}{m}x_{1,2} - \frac{c}{m}x_{2,2} \\
&\vdots \\
\dot{x}_{n-1,1} &= x_{n-1,2} \\
\dot{x}_{n-1,2} &= \frac{k}{m}x_{n-2,1} - \frac{k}{m}x_{n-1,1} + \frac{c}{m}x_{n-2,2} - \frac{c}{m}x_{n-1,2} \\
\dot{x}_{n,1} &= x_{n,2} \\
\dot{x}_{n,2} &= \frac{k}{m}x_{n-1,1} - \frac{k}{m}x_{n,1} + \frac{c}{m}x_{n-1,2} - \frac{c}{m}x_{n,2} \, .
\end{aligned} \tag{4.10}$$

In string stability analysis, the issue of interest is the behavior of the spacing error (the deviation from the desired inter-vehicle spacing). Therefore, we will convert our original state-space representation into "spacing error coordinates" using the following transformation:

$$\begin{aligned}
z_{1,1} &= x_{1,1} - x_{2,1} \\
z_{1,2} &= \dot{z}_{1,1} = x_{1,2} - x_{2,2} \\
z_{2,1} &= x_{2,1} - x_{3,1} \\
z_{2,2} &= \dot{z}_{2,1} = x_{2,2} - x_{3,2} \\
&\vdots \\
z_{n-1,1} &= x_{n-1,1} - x_{n,1} \\
z_{n-1,2} &= \dot{z}_{n-1,1} = x_{n-1,2} - x_{n,2} \, .
\end{aligned} \tag{4.11}$$

For the bidirectional mass-spring-damper system, the state-space representation in error coordinates is the following:

$$\begin{aligned}
\dot{z}_{1,1} &= z_{1,2} \\
\dot{z}_{1,2} &= -\frac{2k}{m}z_{1,1} + \frac{k}{m}z_{2,1} - \frac{2c}{m}z_{1,2} + \frac{c}{m}z_{2,2} + \frac{u}{m} \\
\dot{z}_{2,1} &= z_{2,2} \\
\dot{z}_{2,2} &= \frac{k}{m}z_{1,1} - \frac{2k}{m}z_{2,1} + \frac{k}{m}z_{3,1} + \frac{c}{m}z_{1,2} - \frac{2c}{m}z_{2,2} + \frac{c}{m}z_{3,2} \\
&\vdots \\
\dot{z}_{n-2,1} &= z_{n-2,2} \\
\dot{z}_{n-2,2} &= \frac{k}{m}z_{n-3,1} - \frac{2k}{m}z_{n-2,1} + \frac{k}{m}z_{n-1,1} + \frac{c}{m}z_{n-3,2} - \frac{2c}{m}z_{n-2,2} + \frac{c}{m}z_{n-1,2} \\
\dot{z}_{n-1,1} &= z_{n-1,2} \\
\dot{z}_{n-1,2} &= \frac{k}{m}z_{n-2,1} - \frac{2k}{m}z_{n-1,1} + \frac{c}{m}z_{n-2,2} - \frac{2c}{m}z_{n-1,2}\,.
\end{aligned} \tag{4.12}$$

The unidirectional system's representation in error coordinates can be derived using equations (4.10) and (4.11):

$$\begin{aligned}
\dot{z}_{1,1} &= z_{1,2} \\
\dot{z}_{1,2} &= -\frac{k}{m}z_{1,1} - \frac{c}{m}z_{1,2} + u \\
\dot{z}_{2,1} &= z_{2,2} \\
\dot{z}_{2,2} &= \frac{k}{m}z_{1,1} - \frac{k}{m}z_{2,1} + \frac{c}{m}z_{1,2} - \frac{c}{m}z_{2,2} \\
&\vdots \\
\dot{z}_{n-2,1} &= z_{n-2,2} \\
\dot{z}_{n-2,2} &= \frac{k}{m}z_{n-3,1} - \frac{k}{m}z_{n-2,1} + \frac{c}{m}z_{n-3,2} - \frac{c}{m}z_{n-2,2} \\
\dot{z}_{n-1,1} &= z_{n-1,2} \\
\dot{z}_{n-1,2} &= \frac{k}{m}z_{n-2,1} - \frac{k}{m}z_{n-1,1} + \frac{c}{m}z_{n-2,2} - \frac{c}{m}z_{n-1,2}\,.
\end{aligned} \tag{4.13}$$

Having reviewed the derivation of the basic state-space representation of these two types of controllers, we will now consider several intervehicle spacing policies, each of which has differing implications for string stability.

4.5.2 Unidirectional controller with constant spacing

The first controller we will consider employs constant inter-vehicle spacing. In the unidirectional case of (4.13), the magnitude of the transfer function that relates the output spacing error to the

input spacing error is

$$\left|\frac{z_{i,1}(j\omega)}{z_{i-1,1}(j\omega)}\right| = \left|\frac{\frac{c}{m}j\omega + \frac{k}{m}}{-\omega^2 + \frac{c}{m}j\omega + \frac{k}{m}}\right| \begin{cases} = 1 & \text{if } \omega = 0 \\ < 1 & \text{if } \omega^2 > \frac{2k}{m} \\ \geq 1 & \text{otherwise.} \end{cases} \tag{4.14}$$

For relatively high frequencies, the spacing error will be attenuated as it propagates through the platoon. For frequencies below $\sqrt{2k/m}$, however, the spacing errors are magnified. Unfortunately, low frequencies are the frequencies of interest in the platoon application, so this controller results in a platoon that does not meet the string stability requirement. The above analysis confirms (within the mass-spring-damper framework) the well-known result that it is impossible to achieve string stability in autonomous operation when the desired inter-vehicle spacing is constant and the controller receives relative distance and velocity information only with respect to the preceding vehicle. It is not necessary to evaluate the sign of the impulse response in this case, since we have already shown that all-frequency error attenuation is impossible.

Conclusion: The autonomous unidirectional constant spacing controller cannot achieve any of the three types of string stability.

4.5.3 Bidirectional controller with constant spacing

Using bidirectional control, the transfer function relating spacing errors between adjacent vehicles changes based on the position of the vehicle in the platoon. This is because, just as in the physical mass-spring-damper system, each vehicle "feels" the combined effects of all the preceding and following vehicles. Thus, string stability analysis of such a scenario is complicated by the fact that one has to consider disturbance propagation in both the forward and the backward directions. However, the symmetry of the system simplifies this task; it allows us to perform the analysis in only one direction by exploiting the fact that the last mass (for disturbance propagation front to back) and the first mass (for disturbance propagation back to front) are unique because they have only one neighboring mass which affects them. Thus, we analyze only front-to-back disturbances and use the results for general conclusions. To exploit the uniqueness of the last mass, we start our analysis at the back of the platoon:

$$|G_1(s)| \;=\; \left|\frac{z_{n-1,1}(s)}{z_{n-2,1}(s)}\right| \;=\; \left|\frac{\frac{c}{m}s + \frac{k}{m}}{s^2 + \frac{2c}{m}s + \frac{2k}{m}}\right| . \tag{4.15}$$

Going one step towards the platoon leader, we obtain

$$|G_2(s)| \;=\; \left|\frac{z_{n-2,1}(s)}{z_{n-3,1}(s)}\right| \;=\; \left|\frac{G_1(s)}{1 - G_1(s)G_1(s)}\right| . \tag{4.16}$$

As we proceed further, we arrive at the following iterative formula:

$$|G_i(s)| \;=\; \left|\frac{z_{n-i,1}(s)}{z_{n-i-1,1}(s)}\right| \;=\; \left|\frac{G_1(s)}{1 - G_1(s)G_{i-1}(s)}\right| . \tag{4.17}$$

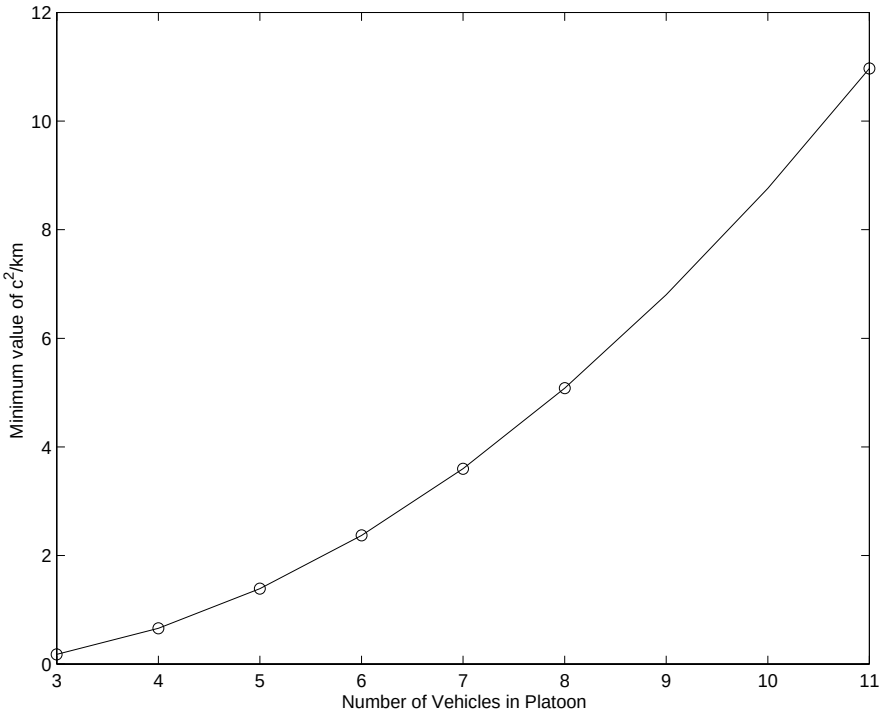

Figure 21: Minimum value of $\frac{c^2}{km}$ required for $||G(jw)||_\infty \leq 1$.

The computation of conditions which guarantee that $|G_i(j\omega)| < 1 \ \ \forall \omega > 0$ is now much more complicated than in (4.14, and requires the use of numerical methods. Analytical results can only be derived for the first transfer function, for which we find that

$$|G_1(j\omega)| < 1 \quad \forall\, \omega > 0 \text{ iff } \tfrac{c^2}{km} > 0.179\,. \tag{4.18}$$

It can be shown that the requirement for spacing error attenuation always takes the form $\frac{c^2}{km} > C$, where C is a constant that increases with platoon size. Analysis has indicated that the minimum value of $\frac{c^2}{km}$ required for string stability increases without bound as vehicles are added to the platoon. Fig. 21 plots the required minimum value of $\frac{c^2}{km}$ as a function of platoon size. From (4.15) we see that $\frac{c^2}{km}$ is directly related to the damping coefficient ζ of the denominator of the transfer function $G_1(s)$:

$$\zeta = \frac{1}{\sqrt{2}}\sqrt{\frac{c^2}{km}}\,. \tag{4.19}$$

This implies that conditions of the form $\frac{c^2}{km} > C$ are in fact restrictions on the damping of the closed-loop system: Fig. 21 shows that the damping has to increase with the number of vehicles in the platoon.

Thus far, we have only considered the frequency-domain properties of this controller. To draw any conclusions about its string stability properties, we must also examine the sign of its impulse response.

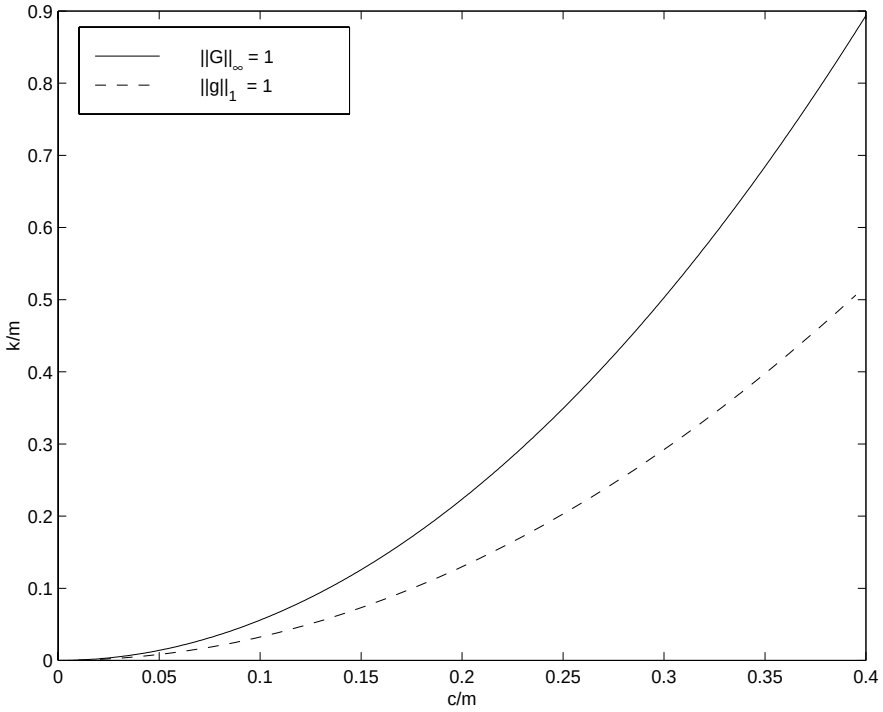

Figure 22: Regions of stability for a 3-vehicle bidirectional platoon with constant spacing.

In general, a necessary condition for achieving a positive impulse response is that the dominant pole of the transfer function is real and lies to the right of the dominant zero (Swaroop and Niemann 1996). In the transfer function $G_1(s)$, the poles cannot be moved relative to the zero in a way which satisfies this condition; the poles and zeros are coupled and cannot be placed independently. Hence, the impulse response of this system always crosses the zero axis in some finite positive time t, regardless of parameter choice. By moving the dominant pole (and zero) closer to the $j\omega$-axis, the magnitude of the undershoot of the impulse response can be made arbitrarily small. This improvement in platoon performance comes at the expense of individual vehicle performance, however, and thus some tradeoff must be made between the percentage of undershoot acceptable (if any) and controller performance. In most situations, allowing a small amount of vehicle overshoot *significantly* relaxes the constraints on the control gains.

Since the impulse response of this system is not positive, the analysis of the magnitude of $G_i(s)$ guarantees only L_2 stability. As stated previously, however, the equivalence of the norms implies that L_∞ stability can also be achieved. Fig. 22 provides a graphical comparison of the regions where the system achieves energy attenuation (L_2 stability) and spacing error attenuation (L_∞ stability). Noting that attenuation is achieved in the regions below the curves, we see that while the general curve characteristics are the same, the acceptable range of parameters is more restricted when L_∞ string stability is required.

Conclusion: The autonomous bidirectional constant spacing controller can achieve L_2 and L_∞ string stability when c/m and k/m are chosen as shown in Fig. 22, but it cannot achieve string stability without overshoot.

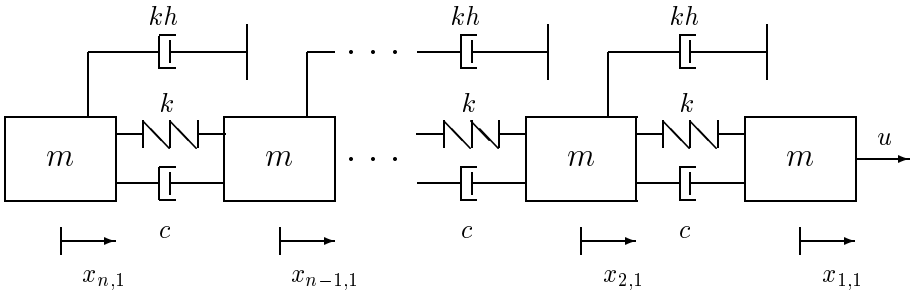

Figure 23: Representation of constant time headway in m-s-d system.

4.5.4 Unidirectional controller with speed-dependent spacing

We have shown that unidirectional controllers which try to maintain constant inter-vehicle spacing without using any form of communication do not result in string-stable platoons. One method of addressing this problem is to introduce speed-dependent spacing, also referred to as a time-headway spacing policy. The desired distance between the two vehicles varies based on how quickly the second vehicle is traveling—the faster it goes, the more space it leaves between itself and its predecessor. To avoid the bumper-to-bumper condition when the vehicles are stopped, a small constant distance is usually added to the time-headway term.

If a speed-dependent spacing policy is adopted, the desired inter-vehicle separation is proportional to the vehicle velocity, i.e., the spacing error for the i-th vehicle becomes $x_{i-1,1} - x_{i,1} - hx_{i,2}$ where h is the *time headway*. As shown in Fig. 23, the effect of using speed-dependent spacing is equivalent to introducing additional damping with respect to an absolute frame of reference (not with respect to any of the preceding or following vehicles). The equilibrium point of the mass-spring-damper system is now $x_{i,1} - x_{i+1,1} - hx_{i+1,2} = 0$.

Some explanation of the value of this additional damping constant, kh, is in order. Why, one may ask, does it include a *spring* constant term, k? The springs exert forces on the masses based on their displacement from the equilibrium position. Although the time headway is represented as a damper because of its dependence on the vehicle's velocity, its *effect* is to alter this equilibrium distance. As the velocity of the second vehicle increases, the equilibrium position changes such that the vehicles are "pushed" farther apart.

This configuration modifies the state space representation of the unidirectional controller in

spacing error coordinates (using $z_{i,1} = x_{i-1,1} - x_{i,1} - hx_{i,2}$) to

$$\begin{aligned}
\dot{z}_{1,1} &= z_{1,2} \\
\dot{z}_{1,2} &= -\frac{k}{m} z_{1,1} - \frac{c+kh}{m} z_{1,2} + \left(1 - \frac{ch}{m}\right) \frac{u}{m} \\
\dot{z}_{2,1} &= z_{2,2} \\
\dot{z}_{2,2} &= \frac{k}{m} z_{1,1} - \frac{k}{m} z_{2,1} + \frac{c}{m} z_{1,2} - \frac{c+kh}{m} z_{2,2} \\
&\vdots \\
\dot{z}_{n-2,1} &= z_{n-2,2} \\
\dot{z}_{n-2,2} &= \frac{k}{m} z_{n-3,1} - \frac{k}{m} z_{n-2,1} + \frac{c}{m} z_{n-3,2} - \frac{c+kh}{m} z_{n-2,2} \\
\dot{z}_{n-1,1} &= z_{n-1,2} \\
\dot{z}_{n-1,2} &= \frac{k}{m} z_{n-2,1} - \frac{k}{m} z_{n-1,1} + \frac{c}{m} z_{n-2,2} - \frac{c+kh}{m} z_{n-1,2} \,.
\end{aligned} \tag{4.20}$$

The spacing error transfer function is then

$$G(s) = \frac{z_i(s)}{z_{i-1}(s)} = \frac{\frac{c}{m}s + \frac{k}{m}}{s^2 + (\frac{c+kh}{m})s + \frac{k}{m}} \,. \tag{4.21}$$

The introduction of the time headway term in the denominator of $G(s)$ makes it possible to adjust the locations of the poles (by varying h) without moving the zero; it may now be possible to achieve a positive impulse response. Tedious but straightforward time-domain analysis shows (Eyre 1997) that the impulse response will be positive if the time headway h is chosen to satisfy the following condition:

$$h \geq \begin{cases} \dfrac{m}{c} & \text{for } \dfrac{c^2}{km} \geq 1 \\ -\dfrac{c}{k} + 2\sqrt{\dfrac{m}{k}} & \text{for } \dfrac{c^2}{km} < 1 \,. \end{cases} \tag{4.22}$$

We see that the term $\frac{c^2}{km}$ is important in this case, as it was in the case of bidirectional control with constant spacing. To connect the two cases, we note that in the case of unidirectional control, the damping coefficient ζ of the denominator of $G(s)$ is

$$\zeta = \frac{1}{2}\sqrt{\frac{c^2}{km}} \,. \tag{4.23}$$

This equation, which is the counterpart of (4.19), can be obtained by setting $h = 0$ in (4.21).

There is another method of analyzing this transfer function, however. The zero in the transfer function contributes to the impulse response undershoot; without it, the requirement for a positive impulse response would be simply that the poles must be real. The zero can be eliminated in two ways: by cancelation with one of the poles, as suggested by Shladover (1978), or by setting the damping constant c to zero.

Let us first consider pole-zero cancelation. If $h = \frac{m}{c}$, then the zero disappears and the one remaining pole is located at $-\frac{c}{m}$. This quantity is always negative and real, so the resulting system is stable and has a positive impulse response. Hence, this result agrees with the earlier time domain analysis.

The other method of eliminating the zero is to set $c = 0$, which corresponds to removing the damper connection between each vehicle and its predecessor. The controller, therefore, no longer has access to the velocity of the vehicle's predecessor but still uses relative position information. Although at first glance it may seem counterintuitive, ignoring the preceding vehicle's velocity improves the impulse response by removing the zero from the transfer function. Simulations of this controller using the full nonlinear longitudinal platoon model confirm that it results in a string-stable platoon. It should be noted, however, that the mass-spring-damper analysis framework is a simplified representation of a complex physical system, and while useful for qualitative analysis and comparison of control methods it may not illuminate all the possible disadvantages of ignoring the preceding vehicle's speed. In this case, the poles of the system are

$$s = -\frac{kh}{m} \pm \sqrt{\frac{kh}{m}^2 - 4\frac{k}{m}} \tag{4.24}$$

which are always negative. For the poles to be real, we need

$$h \geq 2\sqrt{\frac{m}{k}}\,, \tag{4.25}$$

which is the same condition as (4.22) when $c = 0$. To complete the string stability proof, we note that in general the magnitude of the transfer function $G(j\omega)$ is less than one when

$$\frac{c}{m} > \frac{2 - \frac{k}{m}h^2}{2h}\,; \tag{4.26}$$

when $c = 0$, this requirement is satisfied for

$$h \geq \sqrt{2\frac{m}{k}}\,. \tag{4.27}$$

Setting $c = 0$ may result in unrealistically large values for h, because of the requirement $h \geq 2\sqrt{\frac{m}{k}}$ given above.

The relationship between the input force and the first spacing error is

$$\frac{z_1(s)}{u(s)} = \frac{1 - \frac{ch}{m}}{m\left(s^2 + (\frac{c+kh}{m})s + \frac{k}{m}\right)}\,. \tag{4.28}$$

Note that (4.28) has the same poles as (4.21) and no zeros. If we choose $h = \frac{m}{c}$ then we satisfy the requirement for string stability (in the weak sense that $||G||_\infty = 1$) and we find that

$$\frac{z_1(s)}{u(s)} = 0\,. \tag{4.29}$$

In this case, the fact that the first spacing error is zero means that the spacing between the first two vehicles grows at exactly the rate needed to maintain the desired time headway. The fact that

the first spacing error is zero implies that, in the absence of disturbances, all subsequent spacing errors will also be zero. Therefore, once the platoon is in steady state, a control input applied to the lead vehicle will not generate spacing errors.

If we choose $h > \frac{m}{c}$ (i.e., choose a larger time headway), the system will still exhibit string stability, but now we have the problem of a strictly *negative* impulse response relating the input force to the first spacing error. In other words, no matter how benign the acceleration of the lead vehicle, the first spacing error will *always* be negative. This is not quite as bad as it sounds, however, because of the way we have defined $z_1(s)$: $z_1 = x_{1,1} - x_{2,1} - hx_{2,2}$. In this case, a negative spacing error does not necessarily imply that the vehicles are closer together than their minimum constant separation ($x_{1,1} = x_{2,1}$); it may simply mean that the large time headway requirement is not being satisfied during the transient state. Therefore, the negative spacing error is not as critical in this controller as it was in the constant spacing scenario.

This is an example of a case where string stability analysis alone does not reveal all the information of interest about the controller. The analysis of the first spacing error yields the additional information that a time headway policy of $h = \frac{m}{c}$ is the only possible value of h that generates zero spacing errors.

Conclusion: The autonomous unidirectional speed-dependent spacing controller can achieve string stability without overshoot (and thus also L_2 and L_∞ string stability). As we will see, this conclusion applies to all subsequent controllers in our analysis which use speed-dependent spacing.

4.5.5 Bidirectional controller with speed-dependent spacing

In the bidirectional scenario, speed-dependent spacing has several possible implementations. If a vehicle's desired separation from its predecessor varies as a function of its own velocity, the spacing error transfer function (again, starting from the end of the platoon) becomes the following:

$$\bar{G}_1(s) = \frac{z_{n-1}(s)}{z_{n-2}(s)} = \frac{\frac{c}{m}s + \frac{k}{m}}{s^2 + (\frac{2c+kh}{m})s + \frac{2k}{m}} \,. \tag{4.30}$$

The conditions conditions which guarantee a positive impulse response are similar to those derived for the previous case. The poles must be real, a condition satisfied when

$$h \geq \begin{cases} \dfrac{m}{c} & \text{for } \dfrac{c^2}{km} \geq \dfrac{1}{2} \\ -\dfrac{c}{k} + 2\sqrt{\dfrac{m}{k}} & \text{for } \dfrac{c^2}{km} < \dfrac{1}{2} \,. \end{cases} \tag{4.31}$$

Closed-form analysis of the magnitude of the transfer function is only possible for the case in which there are three vehicles in the platoon, when we obtain the following:

$$|\bar{G}_1(j\omega)| \; < \; 1 \,\forall\, \omega \text{ iff } \quad \frac{c}{m} > -\frac{2}{3}\frac{hk}{m} + \frac{1}{3}\sqrt{\left(\frac{hk}{m}\right)^2 + 1.608\frac{k}{m}} \,. \tag{4.32}$$

Fig. 24 illustrates the regions of L_2 and L_∞ stability for a 3-vehicle platoon employing a time headway of 0.8 second. Selection of parameters in the regions to the right of the curves result in energy or spacing error attenuation. It should be noted that the requirement for a positive impulse response, $\frac{c}{m} > 1.25$, is *much* more restrictive than is needed for either energy attenuation or spacing error attenuation.

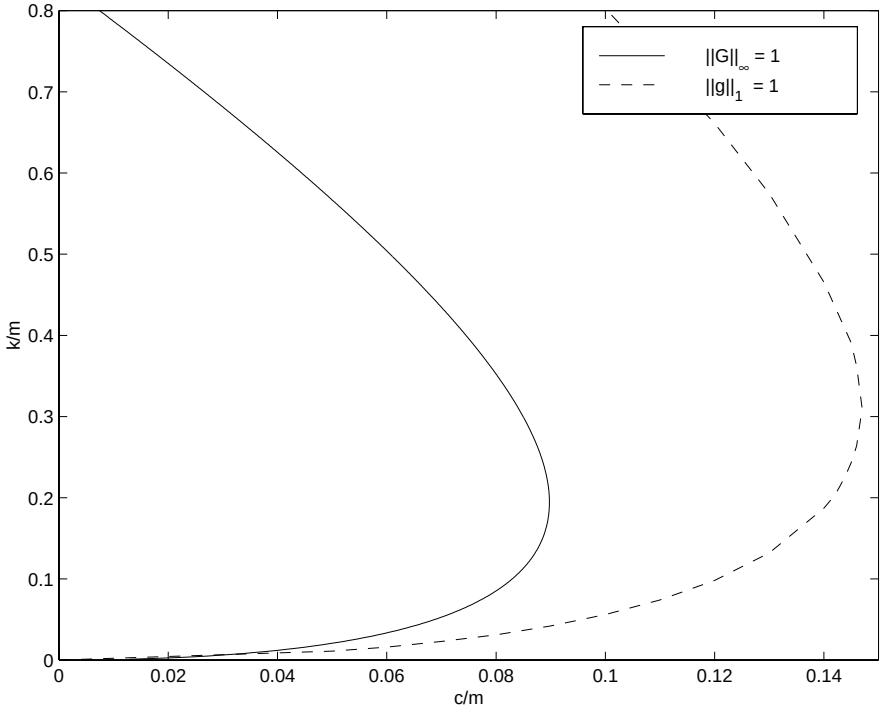

Figure 24: Regions of stability for 3-vehicle bidirectional platoon (using a .8-second time headway).

If $\frac{c^2}{km} > 0.179$ ($= \frac{1.608}{9}$ in equation (4.32) with $h = 0$), which is the condition derived for magnitude attenuation when a constant spacing policy is used, this requirement will be satisfied for any $h \geq 0$. In addition, for any choice of system parameters there exists an $h > 0$ for which this condition will be satisfied. The requirements for achieving error attenuation, therefore, are less restrictive than those derived for the bidirectional controller with constant inter-vehicle spacing. Fig. 25 illustrates the effect of increasing h on the region of string stability. It is clear that, as one would assume, increasing h expands the region of stability.

The iterative formula for this spacing policy is of the same form we have seen earlier:

$$\bar{G}_i(s) = \frac{\bar{G}_1(s)}{1 - \bar{G}_1(s)\bar{G}_{i-1}(s)} \; . \tag{4.33}$$

A second possible implementation of time headway in the bidirectional scenario is if, in addition to the forward-looking speed-dependent spacing term considered above, the vehicle's desired separation from its follower depends on the following vehicle's velocity. In essence, this spacing policy dictates that each vehicle should advance to the current position of its predecessor in h seconds, each vehicle should currently be where its follower *will* be in h seconds. The forward time headway depends on the vehicle's own speed, while the backward time headway depends on the speed

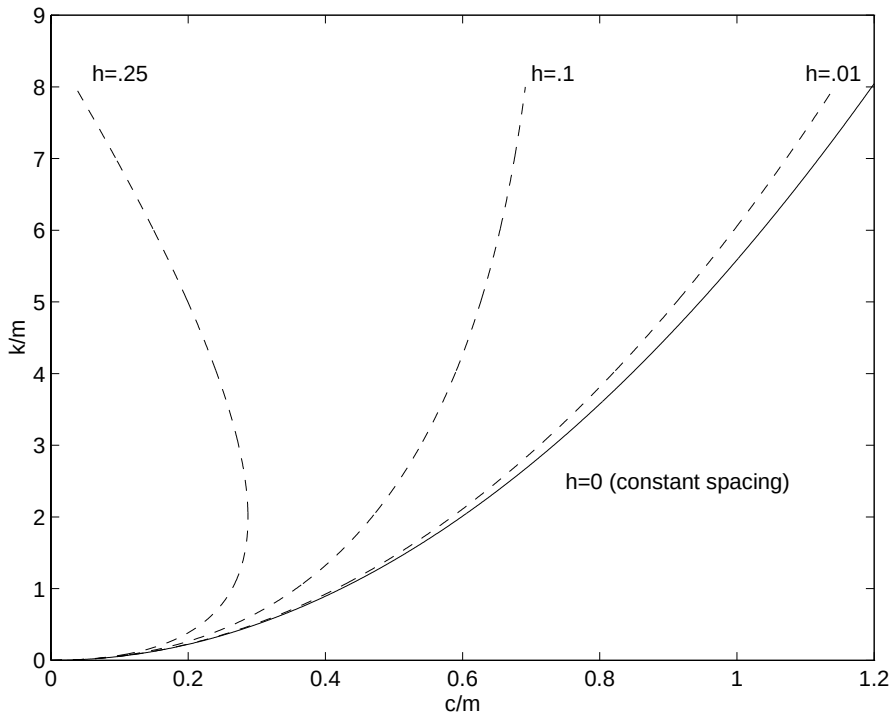

Figure 25: Effect of time headway on region of string stability.

of its follower. It can be shown that this spacing policy gives the same transfer function for G_1; i.e., $\hat{G}_1(s) = \bar{G}_1(s)$. The iterative formula, however, is no longer of the familiar form. It is modified to:

$$\hat{G}_i(s) = \frac{\hat{G}_1(s)}{1 - \left(\hat{G}_1(s) + \frac{\frac{kh}{m}s}{s^2 + \frac{2c+kh}{m}s + \frac{2k}{m}}\right)\hat{G}_{i-1}(s)} \,. \tag{4.34}$$

One may suspect, after comparing $\bar{G}_i$ to $\hat{G}_i$, that error attenuation is easier to achieve with the forward-looking only time headway approach. For $i > 1$, these transfer functions are not amenable to closed-form analysis, but we have been able to confirm the verity of our intuition for a 4-vehicle platoon using numerical analysis, and expect similar results for larger platoons. Fig. 26 shows the regions of error attenuation for 4-vehicle platoons using zero time headway, forward-only time headway, and forward and backward time headway. Again, choosing parameters in the area to the right of the curve results in transfer function magnitudes of less than unity. These curves were generated by varying the parameters $\frac{c}{m}$ and $\frac{k}{m}$ and evaluating the magnitude of the transfer function over the range of frequencies for which it is maximized. Points at which the magnitude became equal to one are plotted as small circles, with a curve interpolated between them. Adding backward time headway has made string stability more difficult to achieve.

A third possible speed-dependent spacing scheme is one in which the desired separation between the vehicle and its predecessor and the desired separation between the vehicle and its follower *both* depend on the vehicle's own speed. As it turns out, the speed-dependent terms for

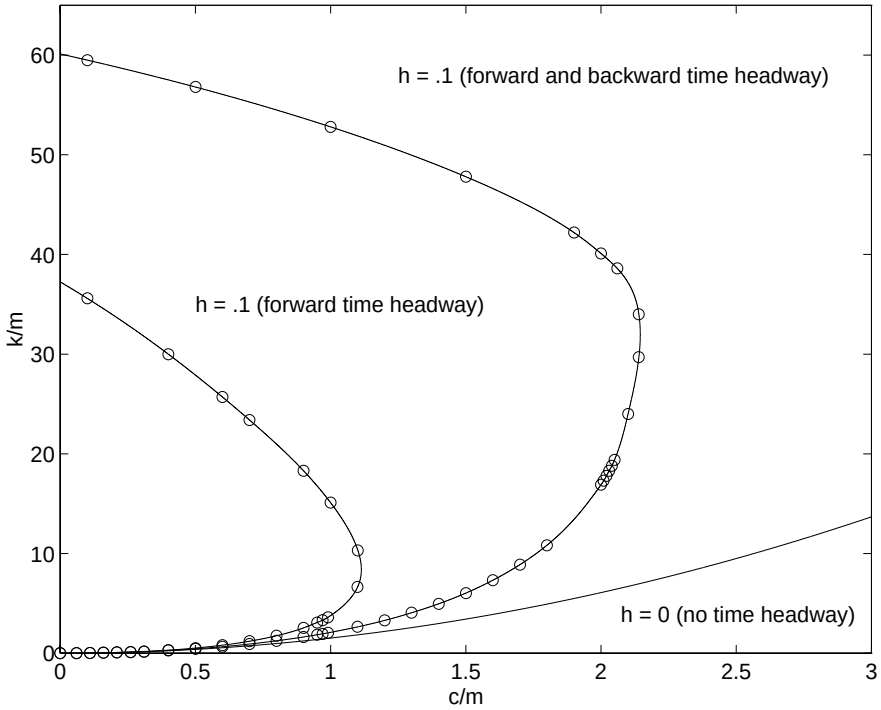

Figure 26: Regions of stability for 4-vehicle bidirectional platoon with time headway.

this controller cancel out in the state-space equations, leaving us with the simple constant spacing policy.

4.5.6 Variable time headway

The use of constant time headways may result in large spaces between vehicles, and thus decrease traffic throughput. A recently proposed spacing policy (Yanakiev and Kanellakopoulos 1996), overcomes this difficulty by allowing the time headway h to vary with the *relative* velocity. This time headway policy can be contrasted to the constant time-headway policy, which uses only the absolute velocity of each vehicle. The intuition used to develop this spacing policy is that if the car in front is traveling at a faster rate than its follower, the space between the two can safely be allowed to shrink. If the lead car is moving more slowly than its follower, however, it is appropriate to require more space between the two vehicles. In the steady state, the relative velocity term becomes zero and renders h constant at its nominal value $h_0 > 0$. The time headway now takes the following form:

$$h_i = h_0 - c_h(x_{i-1,2} - x_{i,2}) \tag{4.35}$$

where $c_h > 0$ is constant. The key here is that h_0 is much smaller than the constant h necessary to guarantee string stability. The inter-vehicle spacing during steady state is significantly reduced, thus increasing traffic throughput.

Let us consider again the unidirectional scenario and incorporate the variable time headway in

the error coordinates representation:

$$
\begin{aligned}
\dot{z}_{1,1} &= z_{1,2} \\
\dot{z}_{1,2} &= -\frac{k}{m}z_{1,1} - \frac{c}{m}z_{1,2} - \frac{kh_0}{m}z_{1,2} - \frac{kc_h}{m}x_{1,2}z_{1,2} + \frac{kc_h}{m}z_{1,2}^2 + \frac{u}{m} \\
\dot{z}_{2,1} &= z_{2,2} \\
\dot{z}_{2,2} &= \frac{k}{m}z_{1,1} - \frac{k}{m}z_{2,1} + \frac{c}{m}z_{1,2} - \frac{c}{m}z_{2,2} - \frac{kh_0}{m}z_{2,2} + \frac{kc_h}{m}(x_{1,2} - z_{1,2})(z_{1,2} - z_{2,2}) + \frac{kc_h}{m}z_{2,2}^2 \\
&\vdots \\
\dot{z}_{n-2,1} &= z_{n-2,2} \\
\dot{z}_{n-2,2} &= \frac{k}{m}z_{n-3,1} - \frac{k}{m}z_{n-2,1} + \frac{c}{m}z_{n-3,2} - \frac{c}{m}z_{n-2,2} \\
&\quad + \frac{kc_h}{m}(x_{1,2} - z_{1,2} - \cdots - z_{n-3,2})(z_{n-3,2} - z_{n-2,2}) - \frac{kh_0}{m}z_{n-2,2} + \frac{kc_h}{m}z_{n-2,2}^2 \\
\dot{z}_{n-1,1} &= z_{n-1,2} \\
\dot{z}_{n-1,2} &= \frac{k}{m}z_{n-2,1} - \frac{k}{m}z_{n-1,1} + \frac{c}{m}z_{n-2,2} - \frac{c}{m}z_{n-1,2} + \frac{kc_h}{m}(x_{1,2} - z_{1,2} - \cdots - z_{n-2,2}) \times \\
&\quad (z_{n-2,2} - z_{n-1,2}) - \frac{kh_0}{m}z_{n-1,2} + \frac{kc_h}{m}z_{n-1,2}^2 \,.
\end{aligned}
\tag{4.36}
$$

Linearizing around the nominal operating point $x_{1,2} = \cdots = x_{n,2} = v_{\mathrm{d}}$, $x_{i,1} = x_{i-1,1} - h_0 v_{\mathrm{d}}$, which corresponds to all vehicles moving at the desired platoon speed v_{d} and with the desired inter-vehicle spacing, we obtain:

$$
\begin{aligned}
\dot{z}_{1,1} &= z_{1,2} \\
\dot{z}_{1,2} &= -\frac{k}{m}z_{1,1} - \frac{c + kh_0 + kc_h v_{\mathrm{d}}}{m}z_{1,2} + u \\
\dot{z}_{2,1} &= z_{2,2} \\
\dot{z}_{2,2} &= \frac{k}{m}z_{1,1} - \frac{k}{m}z_{2,1} + \frac{c + kc_h v_{\mathrm{d}}}{m}z_{1,2} - \frac{c + kh_0 + kc_h v_{\mathrm{d}}}{m}z_{2,2} \\
&\vdots \\
\dot{z}_{n-2,1} &= z_{n-2,2} \\
\dot{z}_{n-2,2} &= \frac{k}{m}z_{n-3,1} - \frac{k}{m}z_{n-2,1} + \frac{c + kc_h v_{\mathrm{d}}}{m}z_{n-3,2} - \frac{c + kh_0 + kc_h v_{\mathrm{d}}}{m}z_{n-2,2} \\
\dot{z}_{n-1,1} &= z_{n-1,2} \\
\dot{z}_{n-1,2} &= \frac{k}{m}z_{n-2,1} - \frac{k}{m}z_{n-1,1} + \frac{c + kc_h v_{\mathrm{d}}}{m}z_{n-2,2} - \frac{c + kh_0 + kc_h v_{\mathrm{d}}}{m}z_{n-1,2} \,.
\end{aligned}
\tag{4.37}
$$

The magnitude of the transfer function becomes:

$$
\left|\frac{z_i(s)}{z_{i-1}(s)}\right| = \left|\frac{\frac{c+kc_h v_{\mathrm{d}}}{m}s + \frac{k}{m}}{s^2 + \frac{c+kh_0+kc_h v_{\mathrm{d}}}{m}s + \frac{k}{m}}\right| \begin{cases} = 1 & \text{if } \omega = 0 \\ < 1 & \forall\, \omega > 0 \text{ if } c > \frac{2m - kh_0^2 - 2kh_0 c_h v_{\mathrm{d}}}{2h_0} \,. \end{cases} \tag{4.38}
$$

Comparing the condition for string stability in the constant time headway case (4.21) and in the variable time headway case (4.38), we can conclude that for the same values of the system param-

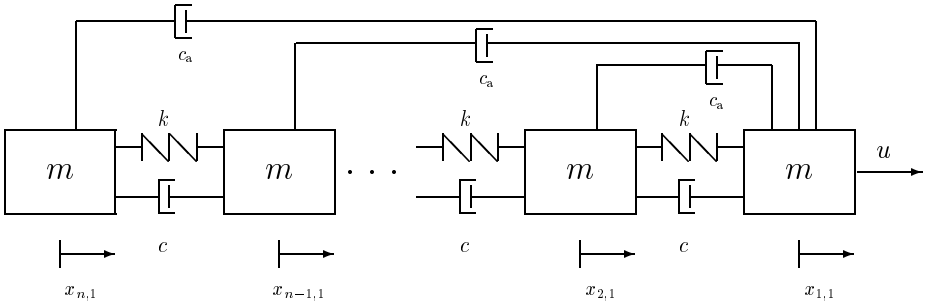

Figure 27: M-s-d system, leader broadcasts current velocity.

eters, i.e., c, k, m, string stability can be achieved for $h_0 < h$ due to the presence of the positive term $2kh_0c_hv_\mathrm{d}$ (the desired platoon speed v_d is always positive).

4.6 Non-autonomous controllers

Previously, we established the fact that unidirectional controllers which employ constant spacing and operate autonomously do not achieve string stability. We have examined one method of solving this problem; namely, by introducing speed-dependent spacing. If we do not restrict ourselves to autonomous controllers and allow the introduction of some form of inter-vehicle communication, then we can address the problem in another manner. For example, if the vehicle knows its position in the platoon and adjusts its controller gains accordingly, then a unidirectional constant spacing controller can achieve string stability (Swaroop et al. 1994). The string stability properties of controllers using several possible communication schemes will be examined here.

4.6.1 Communication of leader's current velocity

The first method considered is one in which the platoon leader broadcasts its current velocity to other platoon members. In the mass-spring-damper framework, this can be represented in Fig. 27 by connecting an additional unidirectional damper between each vehicle and the platoon leader. Following vehicles are able to use information about the position and velocity of their predecessor while also having access to information about the platoon leader's speed.

This controller results in the following state space representation:

$$\begin{aligned}
\dot{x}_{1,1} &= x_{1,2} \\
\dot{x}_{1,2} &= \frac{u}{m} \\
\dot{x}_{2,1} &= x_{2,2} \\
\dot{x}_{2,2} &= \frac{k}{m}x_{1,1} - \frac{k}{m}x_{2,1} + \frac{c}{m}x_{1,2} - \frac{c}{m}x_{2,2} + \frac{c_{\mathrm{a}}}{m}(x_{1,2} - x_{2,2}) \\
&\vdots \\
\dot{x}_{n-1,1} &= x_{n-1,2} \\
\dot{x}_{n-1,2} &= \frac{k}{m}x_{n-2,1} - \frac{k}{m}x_{n-1,1} + \frac{c}{m}x_{n-2,2} - \frac{c}{m}x_{n-1,2} + \frac{c_{\mathrm{a}}}{m}x_{1,2} - x_{n-1,2}) \\
\dot{x}_{n,1} &= x_{n,2} \\
\dot{x}_{n,2} &= \frac{k}{m}x_{n-1,1} - \frac{k}{m}x_{n,1} + \frac{c}{m}x_{n-1,2} - \frac{c}{m}x_{n,2} + \frac{c_{\mathrm{a}}}{m}(x_{1,2} - x_{n,2})\,.
\end{aligned} \tag{4.39}$$

This yields in error coordinates:

$$\begin{aligned}
\dot{z}_{1,1} &= z_{1,2} \\
\dot{z}_{1,2} &= -\frac{k}{m}z_{1,1} - \frac{c + c_{\mathrm{a}}}{m}z_{1,2} \\
\dot{z}_{2,1} &= z_{2,2} \\
\dot{z}_{2,2} &= \frac{k}{m}z_{1,1} - \frac{k}{m}z_{2,1} + \frac{c}{m}z_{1,2} - \frac{c + c_{\mathrm{a}}}{m}z_{2,2} \\
&\vdots \\
\dot{z}_{n-2,1} &= z_{n-2,2} \\
\dot{z}_{n-2,2} &= \frac{k}{m}z_{n-3,1} - \frac{k}{m}z_{n-2,1} + \frac{c}{m}z_{n-3,2} - \frac{c + c_{\mathrm{a}}}{m}z_{n-2,2} \\
\dot{z}_{n-1,1} &= z_{n-1,2} \\
\dot{z}_{n-1,2} &= \frac{k}{m}z_{n-2,1} - \frac{k}{m}z_{n-1,1} + \frac{c}{m}z_{n-2,2} - \frac{c + c_{\mathrm{a}}}{m}z_{n-1,2}\,.
\end{aligned} \tag{4.40}$$

This controller results in the spacing error transfer function

$$G(s) = \frac{z_i(s)}{z_{i-1}(s)} = \frac{\frac{c}{m}s + \frac{k}{m}}{s^2 + \frac{c+c_{\mathrm{a}}}{m}s + \frac{k}{m}}\,, \tag{4.41}$$

where c_{a} represents the additional damping with respect to the platoon leader. This transfer function is the same as that derived for the constant time headway controller, with kh replaced by c_{a}. Therefore, we obtain the same results for both the error attenuation and impulse response analysis. As in the unidirectional controller with constant time headway, it is possible to set $c = 0$ and maintain a stable system. This time, however, it is the damping with respect to the platoon leader (instead of the time headway) which must take on a minimum value for stability:

$$c_a \geq 2k\sqrt{\frac{m}{k}} = 2\sqrt{km}\,. \tag{4.42}$$

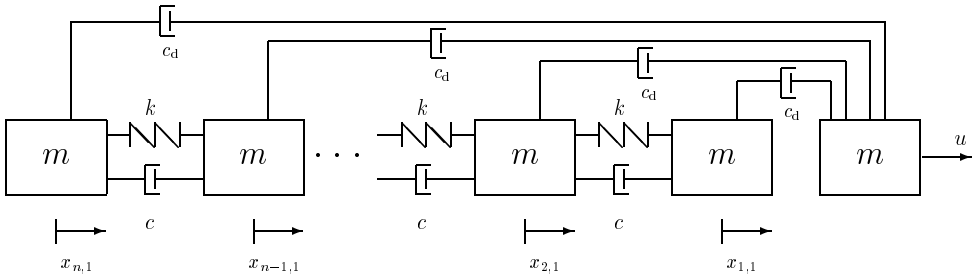

Figure 28: M-s-d system, leader broadcasts desired velocity.

This may be more practical to implement, as it does not require excessive intervehicle spacing.

The relationship between the input force and the initial spacing error is

$$\frac{z_1(s)}{u(s)} = \frac{\frac{1}{m}}{s^2 + \frac{c+c_{\rm a}}{m}s + \frac{k}{m}}\ , \tag{4.43}$$

which has the benefit of having no zeros and the same poles as (4.41). Therefore, the initial spacing error impulse response will be positive whenever $g(t) \geq 0$.

4.6.2 Communication of leader's desired velocity

An alternative communication scheme (Shladover 1978, Yanakiev and Kanellakopoulos 1996), is for the platoon leader to transmit its desired rather than actual velocity, which would presumably result in less frequent inter-vehicle transmissions and hence reduced bandwidth. Intuitively, it is expected that this controller will result in smoother transitions, because all vehicles in the platoon are given preview information about their desired velocity. This controller is represented in Fig. 28 with the addition of a "virtual" mass traveling in front of the platoon at the desired speed, to which every other mass (including the leader) is connected via a unidirectional damper. The state space representation of this communication scheme is

$$\begin{aligned}
\dot{v}_{\rm d} &= u \\
\dot{x}_{1,1} &= x_{1,2} \\
\dot{x}_{1,2} &= \frac{c_{\rm d}}{m}(v_{\rm d} - x_{1,2}) \\
\dot{x}_{2,1} &= x_{2,2} \\
\dot{x}_{2,2} &= \frac{k}{m}x_{1,1} - \frac{k}{m}x_{2,1} + \frac{c}{m}x_{1,2} - \frac{c}{m}x_{2,2} + \frac{c_{\rm d}}{m}(v_{\rm d} - x_{2,2}) \\
&\vdots \\
\dot{x}_{n-1,1} &= x_{n-1,2} \\
\dot{x}_{n-1,2} &= \frac{k}{m}x_{n-2,1} - \frac{k}{m}x_{n-1,1} + \frac{c}{m}x_{n-2,2} - \frac{c}{m}x_{n-1,2} + \frac{c_{\rm d}}{m}(v_{\rm d} - x_{n-1,2}) \\
\dot{x}_{n,1} &= x_{n,2} \\
\dot{x}_{n,2} &= \frac{k}{m}x_{n-1,1} - \frac{k}{m}x_{n,1} + \frac{c}{m}x_{n-1,2} - \frac{c}{m}x_{n,2} + \frac{c_{\rm d}}{m}(v_{\rm d} - x_{n,2})\,.
\end{aligned} \tag{4.44}$$

This yields in error coordinates ($z_{\mathrm{d},2} = x_{1,2} - v_{\mathrm{d}}$):

$$\begin{aligned}
\dot{z}_{\mathrm{d},2} &= -\frac{c_{\mathrm{d}}}{m} z_{\mathrm{d},2} + u \\
\dot{z}_{1,1} &= z_{1,2} \\
\dot{z}_{1,2} &= -\frac{k}{m} z_{1,1} - \frac{c + c_{\mathrm{d}}}{m} z_{1,2} \\
\dot{z}_{2,1} &= z_{2,2} \\
\dot{z}_{2,2} &= \frac{k}{m} z_{1,1} - \frac{k}{m} z_{2,1} + \frac{c}{m} z_{1,2} - \frac{c + c_{\mathrm{d}}}{m} z_{2,2} \\
&\vdots \\
\dot{z}_{n-2,1} &= z_{n-2,2} \\
\dot{z}_{n-2,2} &= \frac{k}{m} z_{n-3,1} - \frac{k}{m} z_{n-2,1} + \frac{c}{m} z_{n-3,2} - \frac{c + c_{\mathrm{d}}}{m} z_{n-2,2} \\
\dot{z}_{n-1,1} &= z_{n-1,2} \\
\dot{z}_{n-1,2} &= \frac{k}{m} z_{n-2,1} - \frac{k}{m} z_{n-1,1} + \frac{c}{m} z_{n-2,2} - \frac{c + c_{\mathrm{d}}}{m} z_{n-1,2} \, .
\end{aligned} \tag{4.45}$$

An interesting result of our analysis is that this control scheme yields spacing error transfer functions identical to those derived for the case in which the actual velocity of the platoon leader is transmitted:

$$G(s) = \frac{z_i(s)}{z_{i-1}(s)} = \frac{\frac{c}{m} s + \frac{k}{m}}{s^2 + \frac{c + c_{\mathrm{d}}}{m} s + \frac{k}{m}} \tag{4.46}$$

where c_{d} represents the additional damping with respect to the "virtual" mass. One would be tempted to conclude, then, that the benefits of transmitting the desired rather than actual velocity are minimal. However, analysis of the initial spacing error reveals an important advantage to the former method: the initial spacing error is always zero. This can be seen from (4.45), where the first equation is decoupled from the rest, thus yielding

$$\frac{z_1(s)}{u(s)} = 0 \tag{4.47}$$

regardless of the choice of input force, $u(s)$. In the case of the unidirectional controller with constant time headway, we found that if we chose a specific value of h, the result was a system that generated zero spacing errors. In the case of equation (4.47), however, we find that this result does not depend on the parameters of the system; we will not generate any spacing errors *regardless* of the parameters chosen. It should also be noted that the spacing errors will still be zero even when the effects of actuator and communications delays are included, assuming that these delays are identical for all vehicles.

4.7 Conclusions

It has been demonstrated that the mass-spring-damper platoon representation can be used to qualitatively compare the string stability properties of longitudinal vehicle controllers. From analysis

control	spacing policy	comm	$\|g\|_1 < 1$	$g(t) > 0$	comments
unidir	constant spacing				unstable
bidir	constant spacing		•		
unidir	constant h		•	•	z_1 may be zero
bidir	constant h (forward)		•	•	
bidir	constant h (forward, backward)		•	•	worse than forward-only
unidir	variable h		•	•	allows h to be smaller
unidir	constant spacing	actual veloc	•	•	
unidir	constant spacing	desired veloc	•	•	z_1 always zero

Table 1: Summary of string stability properties.

of both impulse and magnitude responses of various controllers, one can conclude that the introduction of time headway improves both responses, and that its exclusion eliminates the ability to avoid position overshoot in response to lead vehicle acceleration. It has also been shown that communication of desired velocity has an important benefit; namely, that the initial spacing error will be zero regardless of the control input applied to the lead vehicle. Somewhat surprisingly, analysis of the transfer functions resulting from the intervehicle communication methods considered here indicates that there may actually be an advantage to ignoring the immediately preceding vehicle's velocity, and instead referencing only the desired (or actual) velocity of the platoon leader. A summary of our findings is presented in Table 1.

5 Control with Significant Actuator Delays

5.1 Adaptive backstepping controller

The combination of the adaptive PIQ controller with the variable time headway and the variable separation error gain policies yields very good performance when the actuator delays are small, up to about 50 ms. However, when we consider vehicles without EBS, the delays become significantly larger, in the order of 200 ms. This makes the overall uncertainty (modeling errors and delays) too much for the above controller to handle. One possible approach to overcoming this problem would be to reduce the overall uncertainty by using a more accurate model for control design. For instance, we should account for the fact that the control input u is not immediately present in the dominant (vehicle velocity) equation. In Section 2, we used a first-order model which resulted from linearization around the trajectory defined by $v_{\rm r} + k\delta = 0$:

$$\dot{v}_{\rm f} = a(v_{\rm r} + k\delta) + bu + \bar{d}\,, \tag{5.1}$$

where $\bar{d}$ incorporates external disturbances and modeling errors, as well as the unknown nominal value of the control. Now we resort to a more elaborate model which is different from (5.1) in the following:

- it takes into consideration the presence of actuator dynamics; rather than assuming that the control input is directly present in (5.1), it recognizes the driving/braking torque T as the

input to (5.1) and adopts a first-order model to describe the actuator dynamics, i.e., the relationship between this torque and the actual control input u;

- it explicitly displays the aerodynamic drag in the vehicle velocity equation, rather than lumping it into the disturbance term $\bar{d}$; the aerodynamic drag term becomes significant at higher speeds and its inclusion in the control law yields better performance.

The new model then becomes:

$$\dot{v}_{\rm f} = a(v_{\rm r} + k\delta) + bT - \frac{C_{\rm a}}{m} v_{\rm f}^2 + d \tag{5.2}$$

$$\dot{T} = -a_1 T + a_1 u, \tag{5.3}$$

where $C_{\rm a}$ is the aerodynamic drag coefficient, m is the mass of the vehicle, and d is the new disturbances term, which now excludes the effect of the drag.

Now we proceed in the following steps:

- First consider only (5.2). Determine the desired torque $T_{\rm d}$ to regulate $v_{\rm r} + k\delta$ as if T were the actual control input in (5.2).

- Then, based on (5.3), we determine the actual control u so that the difference between the desired and the actual torque converges to zero, i.e., $T - T_{\rm d} \to 0$.

This procedure is based on the *backstepping technique* for nonlinear and adaptive control design, presented in detail in (Krstić et al. 1995).

We determine $T_{\rm d}$ starting with our original design based on a first-order linearized model. Since now we want to explicitly account for the effect of the aerodynamic drag term, the desired torque becomes

$$T_{\rm d} = u_{\rm orig} + \frac{C_{\rm a}}{bm} v_{\rm f}^2 \,, \tag{5.4}$$

where $u_{\rm orig} = u$ from (2.26). Then differentiating (5.4) and combining it with (5.3) yields:

$$\dot{T} - \dot{T}_{\rm d} = -a_1 T + a_1 u - \dot{u}_{\rm orig} - \frac{2C_{\rm a}}{bm} v_{\rm f} \dot{v}_{\rm f} \,. \tag{5.5}$$

To ensure $T - T_{\rm d} \to 0$, we augment the Lyapunov function that we use to derive the update laws for the adaptive controller parameters with the term $\frac{1}{2\gamma}(T - T_{\rm d})^2$

$$V_{\rm a} = V + \frac{1}{2\gamma}(T - T_{\rm d})^2 \,, \tag{5.6}$$

where $\gamma > 0$ is a design constant. The time derivative becomes

$$\dot{V}_{\rm a} = \dot{V} + \frac{1}{\gamma}(T - T_{\rm d})(\dot{T} - \dot{T}_{\rm d}) \,. \tag{5.7}$$

Let β be a positive design constant and define $c_1 = a_1\beta$. Adding and subtracting $c_1(T_{\rm d} - T)$ to the right hand side of (5.5) and regrouping terms, we obtain

$$\dot{T} - \dot{T}_{\rm d} = -c_1(T - T_{\rm d}) - a_1(1 - \beta)T + a_1 u - \dot{T}_{\rm d} - c_1 T_{\rm d}. \tag{5.8}$$

Then (5.7) becomes

$$\dot{V}_{\mathrm{a}} \;=\; \dot{V} - \frac{c_1}{\gamma}(T - T_{\mathrm{d}})^2 + \frac{1}{\gamma}(T - T_{\mathrm{d}})\left[-a_1(1-\beta)T + a_1 u - \dot{T}_{\mathrm{d}} - c_1 T_{\mathrm{d}}\right].$$

We should note that negative definiteness of $\dot{V}$ is no longer guaranteed, since T and T_{d} are different and an additional term appears in $\dot{V}$. Therefore, in order to guarantee negative definiteness of $\dot{V}_{\mathrm{a}}$, hence asymptotic convergence of $T - T_{\mathrm{d}}$ to zero, we need to choose γ very small and we need the last term of (5.9) to vanish. The latter can be achieved with the control law

$$u = (1-\beta)T + \frac{1}{a_1}\dot{T}_{\mathrm{d}} + \beta T_{\mathrm{d}}\,, \tag{5.9}$$

or

$$u \;=\; (1-\beta)T + \frac{1}{a_1}\left(\dot{u}_{\mathrm{orig}} + \frac{2C_{\mathrm{a}}}{bm} v_{\mathrm{f}} \dot{v}_{\mathrm{f}}\right) + \beta\left(u_{\mathrm{orig}} + \frac{C_{\mathrm{a}}}{bm} v_{\mathrm{f}}^2\right).$$

This control law uses some quantities which were not needed in our previous designs. In particular, the acceleration of the current vehicle $\dot{v}_{\mathrm{f}}$ is assumed to be measured, while the term $\dot{u}_{\mathrm{orig}}$ contains the derivative of the error $\frac{d}{dt}(v_{\mathrm{r}} + k\delta)$:

$$\dot{u}_{\mathrm{orig}} \;=\; k_{\mathrm{p}}\frac{d}{dt}(v_{\mathrm{r}} + k\delta) + \gamma_{\mathrm{i}}(v_{\mathrm{r}} + k\delta) + k_{\mathrm{p}}\frac{d}{dt}(v_{\mathrm{r}} + k\delta)\,|v_{\mathrm{r}} + k\delta|\,.$$

Of course, this derivative cannot be measured, since in autonomous operation we have no way of measuring the acceleration of the vehicle ahead. Here, we evaluate it using a so-called "dirty derivative", that is, an implementable approximation of the derivative operator, given by $\frac{s}{s\tau_{\mathrm{d}}+1}$, where τ_{d} is small (as $\tau_{\mathrm{d}} \to 0$, this operator becomes a pure derivative).

Tuning the design parameter to achieve good performance in our simulations, we realized that β should be chosen small. Therefore, the complexity of the controller can be reduced by exclusion of the negligible terms and using the control law

$$u_{\mathrm{s}} = T + \frac{1}{a_1}\left(\dot{u}_{\mathrm{orig}} + \frac{2C_{\mathrm{a}}}{bm} v_{\mathrm{f}} \dot{v}_{\mathrm{f}}\right) \tag{5.10}$$

instead of the one in (5.10).

5.2 Predictor design

A widely used approach for systems with known constant delays is to include a *predictor* in the control loop as shown in Fig. 29. One of the classic predictor structures is the *Smith predictor* (Smith 1957) shown in Fig. 30. The Smith predictor assumes that a compensator K_0 has already been designed for the plant P_0 to give a desired command response in the delay-free case. Then the compensator

$$K_{\mathrm{s}} = \frac{K_0}{1 + (1 - e^{-s\tau})P_0 K_0} \tag{5.11}$$

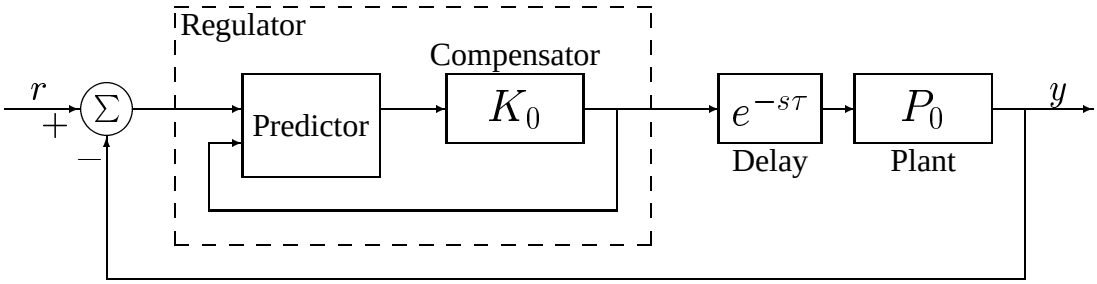

Figure 29: General predictor diagram.

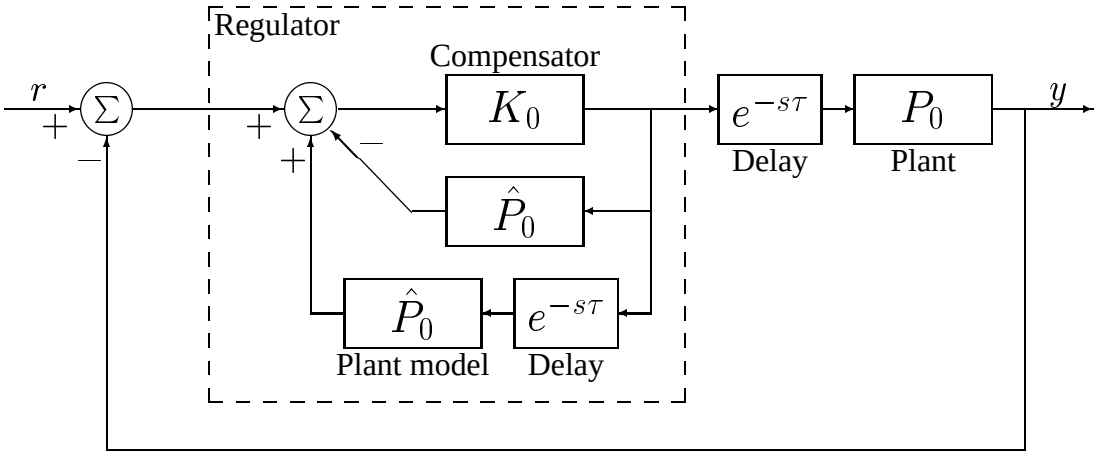

Figure 30: Smith predictor.

applied to the plant with the delay gives the same command response but with a delay of τ seconds. The main difficulty in our case is that we need to control a formation of several vehicles rather than just one individual truck, and we want to do this using a completely decentralized controller structure, with each vehicle depending only on its own measurements of the preceding vehicle's behavior. Therefore, delays in individual vehicle responses accumulate as they propagate upstream through the whole platoon. As a result, the stabilizing effect of the Smith predictor is limited only to the individual trucks and does not help much with the string stability of the whole platoon, since it cannot prevent the spacing and velocity errors from growing upstream. As expected, the Smith predictor applied to the original PIQ design based on the first-order linearized model could not achieve acceptable performance. Even when applied to the new control design presented in the previous section, the Smith predictor resulted in only slightly improved control smoothness. The latter is essential in automotive applications, where fuel consumption and passenger comfort and safety are important issues.

The fact that the Smith predictor does not fit our needs, however, does not mean that we should abandon the idea of using a predictor to compensate for delays. We have to look for a scheme which does not result in a delayed, albeit stable, response, but is truly predictive. The following reasoning was a starting point for our design. Suppose there is a delay of τ seconds from the issuing a control command until it is actually applied to the plant. If we were able to predict the state of the plant in τ s, we could issue a control command based on that estimate, $\hat{x}(t+\tau)$, rather than based on the current state of the plant, $x(t)$, which would no longer be appropriate when this control command reaches the plant in τ s. A first-order linear model is used to approximate the vehicle dynamics and to predict the spacing and velocity errors, δ and v_{r}, respectively. A discrete representation with sampling period Δ is adopted for the implementation of the predictor. Let $\tau = l\Delta$, where l is an integer. Hence, the state space representation of the above described predictor is

$$\begin{aligned} e_{i+l} &= a_{\mathrm{d}} e_{i+l-1} + b_{\mathrm{d}} u_{i-1} \\ e_{i+l-1} &= a_{\mathrm{d}} e_{i+l-2} + b_{\mathrm{d}} u_{i-2} \\ &\vdots \\ e_{i+1} &= a_{\mathrm{d}} e_i + b_{\mathrm{d}} u_{i-l} \end{aligned} \tag{5.12}$$

where e stands for "error" and represents either v_{r} or δ, and a_{d} and b_{d} are the discretized parameters a and b of the linear model $\frac{\delta v}{\delta u} = \frac{b}{s+a}$. This yields the predictor equation

$$e_{i+l} = a_{\mathrm{d}}^{l} e_i + a_{\mathrm{d}}^{l-1} b_{\mathrm{d}} u_{i-l} + a_{\mathrm{d}}^{l-2} b_{\mathrm{d}} u_{i-l+1} + \cdots + b_{\mathrm{d}} u_{i-1} \,. \tag{5.13}$$

The diagram in Fig. 31 illustrates the implementation of this scheme. Values of the control command from $u(t-\tau)$ to $u(t-\Delta)$ are stored in order to compute $\delta(t+\tau)$ and $v_{\mathrm{r}}(t+\tau)$ and based on them $u(t)$.

To investigate the stability properties of this scheme, we represent the whole system in discrete form, i.e., the delay $e^{-s\tau}$ becomes z^{-l}. The plant is denoted by $P_0 = \frac{\bar{b}_{\mathrm{d}}}{z-\bar{a}_{\mathrm{d}}}$, where the bars indicate that the model used in this predictor is not assumed to be accurate as in the case of the Smith predictor. Consider first the simplest case when $l = 1$ and the controller is just a proportional gain K_0. The transfer function of the regulator in Fig. 31 is

$$K_{\mathrm{r}} = \frac{K_0 a_{\mathrm{d}} z}{z - K_0 b_{\mathrm{d}}} \,. \tag{5.14}$$

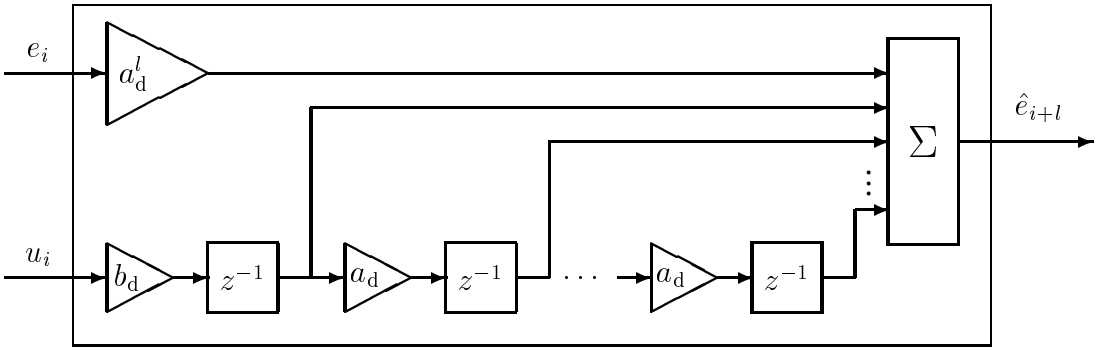

Figure 31: An alternative predictor with true predictive action.

The open-loop transfer function then becomes

$$H_{\rm ol}(z) = K_{\rm r} z^{-1} P_0 = \frac{K_0 a_{\rm d} \bar{b}_{\rm d}}{z^2 - (K_0 b_{\rm d} + \bar{a}_{\rm d}) z + K_0 b_{\rm d} \bar{a}_{\rm d}} \,, \tag{5.15}$$

and the closed-loop transfer function of the system is

$$H_{\rm cl}(z) = \frac{\frac{K_0 a_{\rm d} \bar{b}_{\rm d}}{z(z-\bar{a}_{\rm d})}}{1 + K_0(-b_{\rm d}) \frac{z - (\bar{b}_{\rm d} a_{\rm d}/b_{\rm d} + \bar{a}_{\rm d})}{z(z-\bar{a}_{\rm d})}} \,. \tag{5.16}$$

The closed-loop poles are

$$z_{1,2} = \frac{(K_0 b_{\rm d} + \bar{a}_{\rm d}) \pm \left[(K_0 b_{\rm d} + \bar{a}_{\rm d})^2 - 4 K_0 (b_{\rm d} \bar{a}_{\rm d} + \bar{b}_{\rm d} a_{\rm d}) \right]^{\frac{1}{2}}}{2}. \tag{5.17}$$

Since $a_{\rm d} \approx \bar{a}_{\rm d}$ and $b_{\rm d} \approx \bar{b}_{\rm d}$, we can determine approximately the conditions for the closed-loop poles of the system to be inside the unit disk. It turns out that for $|z_{1,2}| < 1$ we need $0 < K_0 \bar{b}_{\rm d} < \frac{1}{2\bar{a}_{\rm d}}$. Since $\bar{a}_{\rm d} \approx 1$ in our case, $K_0 \bar{b}_{\rm d} < 0.5$ would guarantee stability of this scheme. However, if $b_{\rm d}$ is negative in (5.16) and $b_{\rm d} \approx -\bar{b}_{\rm d}$, then $K_0(b_{\rm d}\bar{a}_{\rm d} + \bar{a}_{\rm d} b_{\rm d})$ cancels. Hence, one of the poles becomes approximately zero and the condition for the other one to be inside the unit disk is approximately $0 < K_0 \bar{b}_{\rm d} < 2$, which is achievable for a wide range of K_0's, since $\bar{b}_{\rm d}$ is very small in our case.

Now consider the case when $l = 2$ and the controller is still just a proportional gain K_0. The transfer function of the regulator in Fig. 31 becomes

$$K_{\rm r} = \frac{K_0 a_{\rm d}^2 z^2}{z^2 - K_0 b_{\rm d} z - K_0 a_{\rm d} b_{\rm d}} \,. \tag{5.18}$$

Hence, the closed-loop transfer function of the system is

$$H_{\rm cl}(z) = \frac{\frac{K_0 a_{\rm d}^2 \bar{b}_{\rm d}}{z^2(z-\bar{a}_{\rm d})}}{1 + K_0(-b_{\rm d}) \frac{z^2 + (a_{\rm d} - \bar{a}_{\rm d}) z - a_{\rm d}(\bar{b}_{\rm d} a_{\rm d}/b_{\rm d} + \bar{a}_{\rm d})}{z^2(z-\bar{a}_{\rm d})}} \,. \tag{5.19}$$

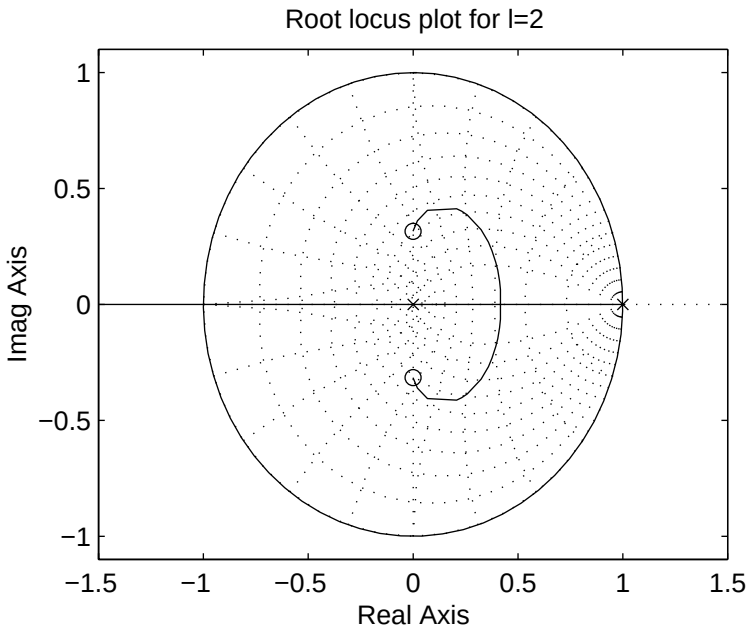

Figure 32: Root locus for $(-b_{\rm d})\frac{z^2+(a_{\rm d}-\bar{a}_{\rm d})z-a_{\rm d}(\bar{b}_{\rm d}a_{\rm d}/b_{\rm d}+\bar{a}_{\rm d})}{z^2(z-\bar{a}_{\rm d})}$.

Now we can plot the root locus of the open-loop transfer function which multiplies K_0 in the denominator of (5.19) and conclude that stability can be guaranteed for the same values of K_0 as in the $l = 1$ case. The root locus is shown in Fig. 32. It is worth noting that $b_{\rm d} < 0$ again.

A more general result can be reached if we perform the calculations for an arbitrary value of l. Using the predictor equation (5.13), we obtain for the transfer function of the regulator in Fig. 31

$$K_{\rm r} = \frac{K_0 a_{\rm d}^l z^l}{z^l - K_0 b_{\rm d} z^{l-1} - \cdots - K_0 a_{\rm d}^{l-2} b_{\rm d} z - K_0 a_{\rm d}^{l-1} b_{\rm d}} \,. \tag{5.20}$$

The closed-loop transfer function of the system is

$$\frac{\frac{K_0 a_{\rm d}^l \bar{b}_{\rm d}}{z^l(z-\bar{a}_{\rm d})}}{1+K_0(-b_{\rm d})\frac{z^l+(a_{\rm d}-\bar{a}_{\rm d})z^{l-1}+\cdots+a_{\rm d}^{l-2}(a_{\rm d}-\bar{a}_{\rm d})z-a_{\rm d}^{l-1}(\bar{b}_{\rm d}a_{\rm d}/b_{\rm d}+\bar{a}_{\rm d})}{z^l(z-\bar{a}_{\rm d})}} \,. \tag{5.21}$$

If the plant is modeled accurately, i.e., $a_{\rm d} = \bar{a}_{\rm d}$ and $b_{\rm d} = -\bar{b}_{\rm d}$, cancelation of terms will reduce the denominators of the transfer functions in (5.16), (5.19), and (5.21) to only

$$1 + K_0 \frac{\bar{b}_{\rm d}}{z - \bar{a}_{\rm d}} = 1 + K_0 P_0 \,. \tag{5.22}$$

Hence, the stability of the system with this predictor will be independent of the sampling, provided that the linear model used is an accurate representation of the plant.

5.3 Comparative simulations

To illustrate the capability of our control design to cope with the actuator delays, we use simulations of a platoon comprising seven (7) tractor-semitrailer combination vehicles. Both fuel and

brake actuator have a pure time delay $\tau = 0.2\,\text{s}$ each. The platoon starts out at an initial speed of 12 m/s. At $t = 10\,\text{s}$ the platoon leader is given a command to accelerate at $0.2\,\text{m/s}^2$ for 10 s. Then at $t = 35\,\text{s}$ a command for deceleration at $3\,\text{m/s}^2$ is issued for 3 s. The minimum desired separation between vehicles is $s_0 = 3\,\text{m}$. This demanding scenario is representative of the difficulties the system might have maintaining stable platoon behavior when trying to meet a challenging acceleration/deceleration objective. In all our simulation plots, different vehicles are represented by lines of different thickness: Vehicle 1 is shown with a thick solid line, while lines corresponding to the following vehicles become thinner as the vehicle's number in the platoon increases. The desired velocity profile is given in a dash-dotted line.

The original PIQ controller together with both nonlinear spacing policies, variable time headway $h = 0.1 - 0.2v_\text{r}\,\text{s}$ and variable separation error gain $k = 0.1 + (1 - 0.1)e^{-0.1\delta^2}$ cannot yield acceptable performance because its gains have to be reduced in order to maintain stability in the presence of delays. Multiple crashes are observed in the "vehicle separation" plot of Fig. 33 due to the abrupt deceleration maneuver commanded from $t = 35\,\text{s}$ to $t = 38\,\text{s}$. The backstepping controller with the same nonlinear spacing policies achieves dramatic reduction of errors as it can be seen by comparing the plots of Fig. 35 to the ones of Fig. 33. The fact that the variable h and k still achieve superior performance is illustrated in Figs. 34 and 35, where the same backstepping controller is being used with constant and variable h and k respectively. However, the minor difference between Figs. 36 and 37 indicates that the role of these nonlinear spacing policies for performance enhancement is considerably diminished when the backstepping controller is used in the absence of significant actuator delays. Of course, when the original PIQ controller is used, variable h and k are necessary for acceptable performance even in the absence of delays as seen in Fig. 38. It is worth noting that while incapable to yield acceptable performance in the presence of significant delays, the PIQ design is tolerant to small actuator delays as seen in Fig. 39.

We also investigated the possibilities to achieve smoother control by adding a predictor to the control design. The results with the Smith predictor are shown in Fig. 40. The platoon performance is improved when the other predictor discussed in this section is used. The latter yields reduced separation errors and smoother control as shown in Fig. 41. The backstepping design demonstrates reasonable robustness with respect to the value of the delay as seen in Figs. 42 and 43, where the value of the delay is increased to $\tau = 0.3\,\text{s}$. Comparison between these figures confirms the role of the alternative predictor as a smoothing factor for the control effort.

5.4 PID controller

As mentioned earlier, reducing controller complexity is essential for automotive applications where cost and simplicity of implementation are crucial. After reaching a solution to our longitudinal control problem in the absence of intervehicle communication, we would like to determine the key factor that renders the new design superior to the original one. Moreover, we can use that as a starting point to finding a simpler controller, which still provides the robustness with respect to actuator delays.

Originally we avoided the ubiquitous PID scheme because measurements of the derivative of the error are not available. Recall that only the relative distance and velocity with respect of the preceding vehicle, as well as the current vehicle velocity, are used by the controller. While it is realistic to obtain accurate measurements of the acceleration of the vehicle with nowadays tech-

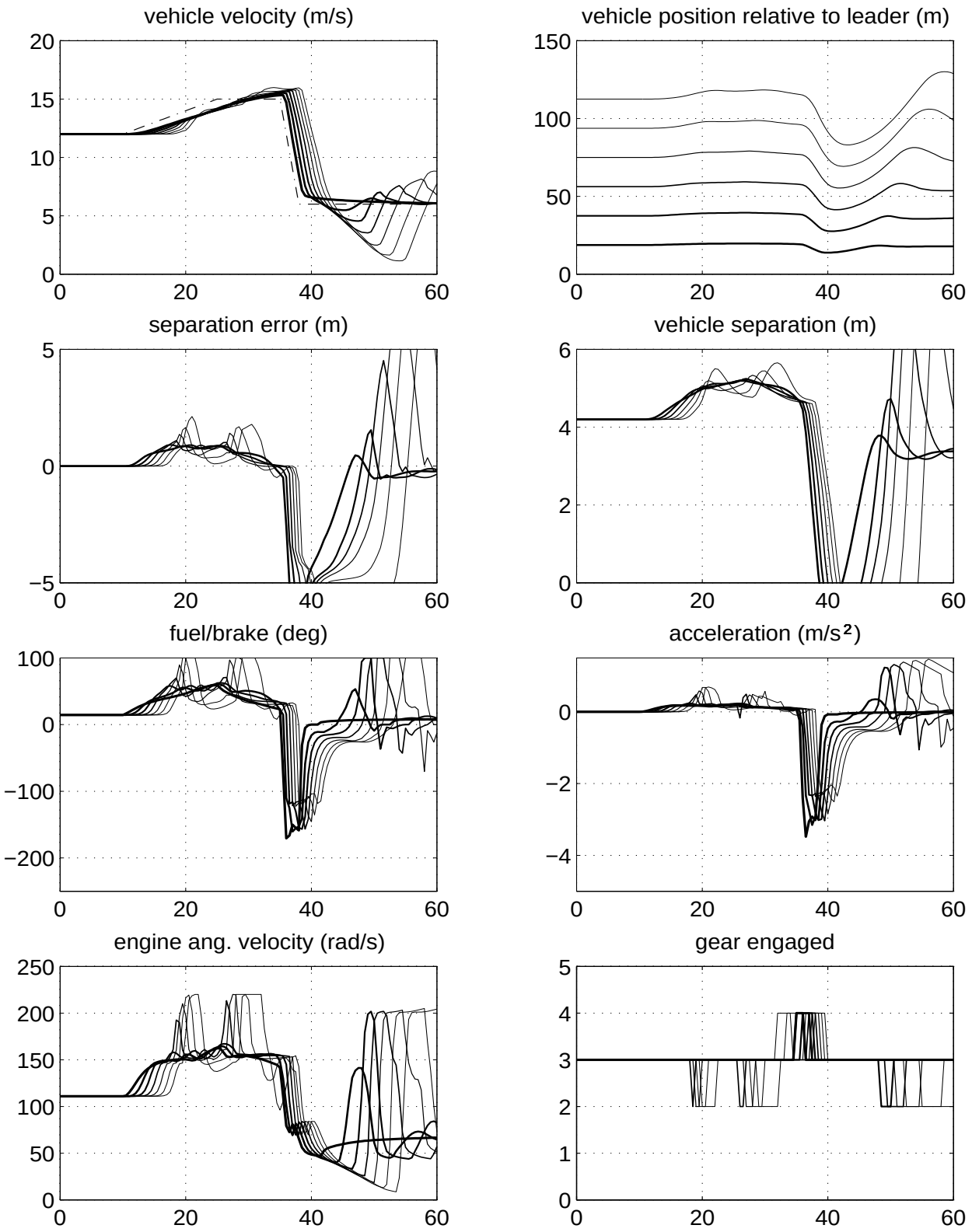

Figure 33: Actuator delay $\tau = 0.2$ s, original PIQ controller with variable time headway $h = 0.1 - 0.2v_{\mathrm{r}}$ s and variable separation error gain $k = 0.1 + (1 - 0.1)e^{-0.1\delta^2}$.

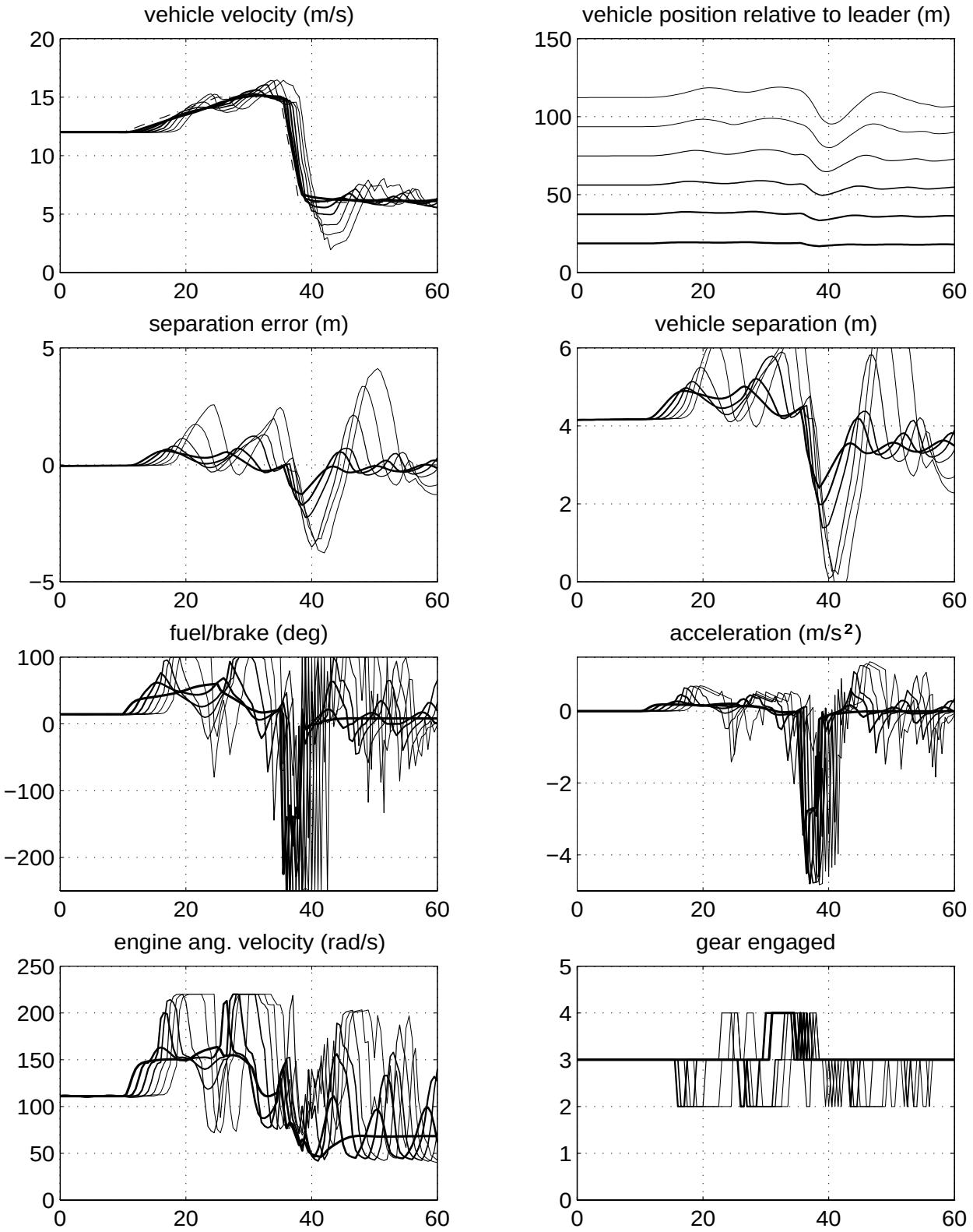

Figure 34: Actuator delay $\tau = 0.2\,\mathrm{s}$, backstepping controller with constant time headway $h = 0.1\,\mathrm{s}$ and constant separation error gain $k = 1$.

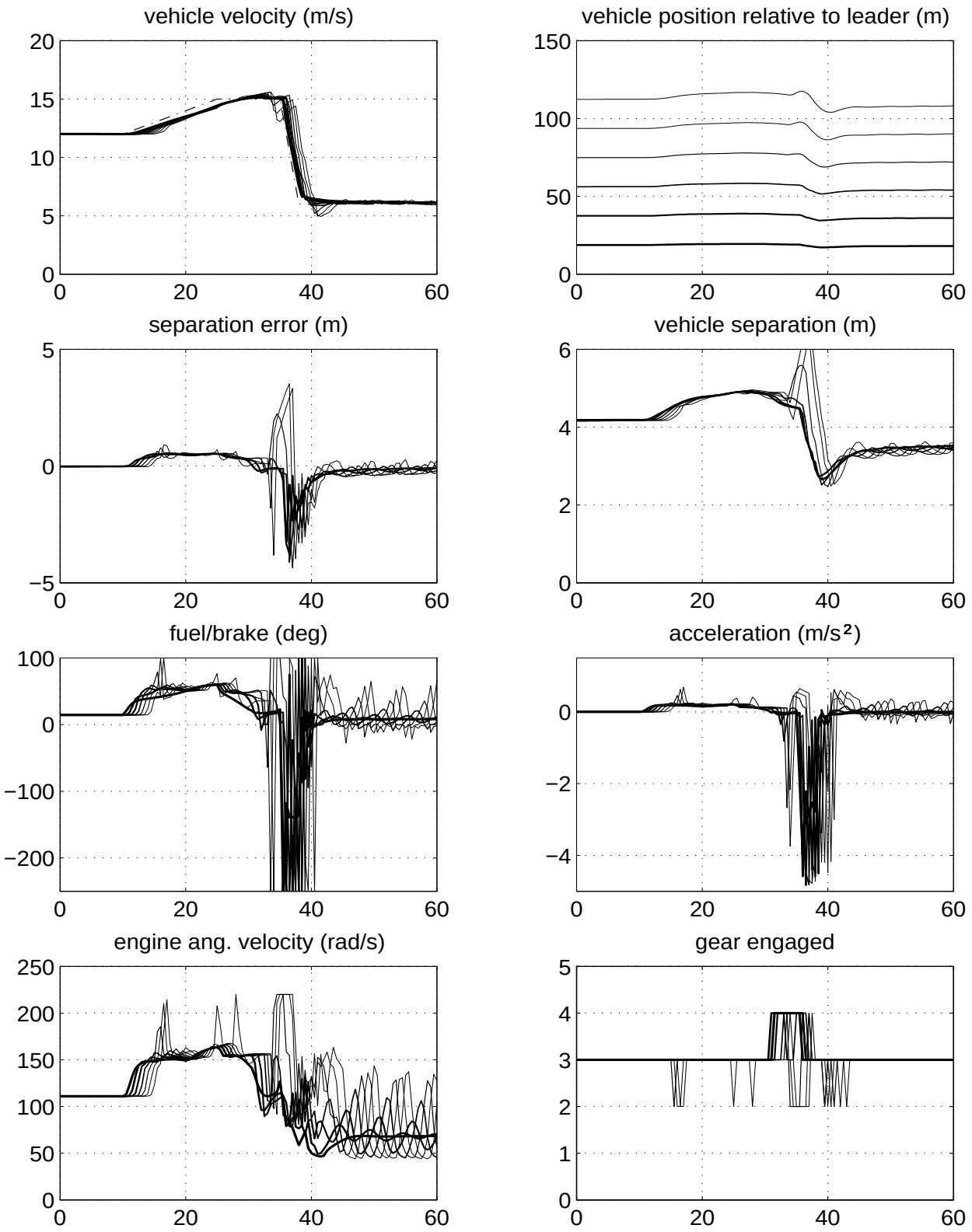

Figure 35: Actuator delay $\tau = 0.2$ s, backstepping controller with variable time headway $h = 0.1 - 0.2v_{\mathrm{r}}$ s and variable separation error gain $k = 0.1 + (1 - 0.1)e^{-0.1\delta^2}$.

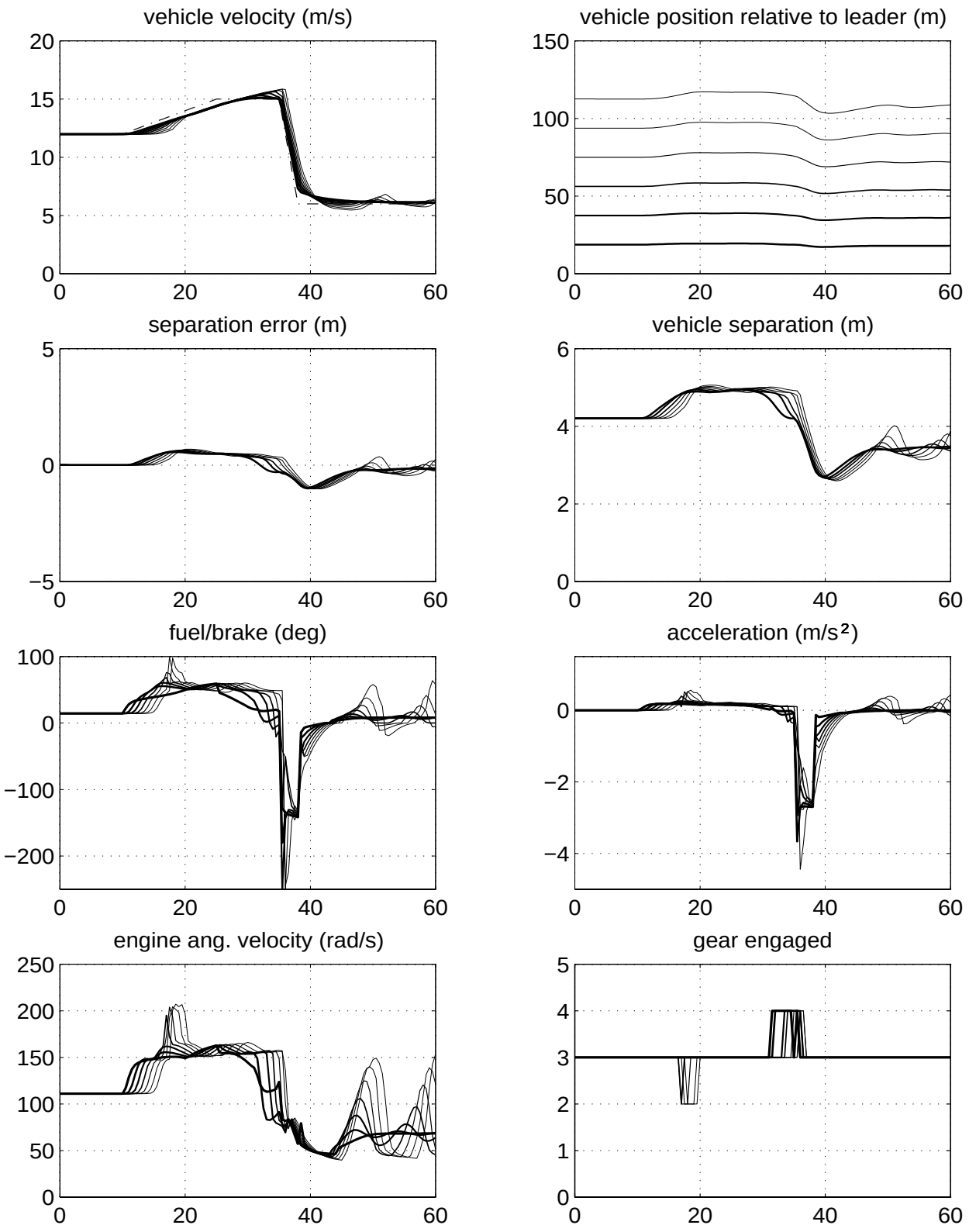

Figure 36: No delay, backstepping controller with constant time headway $h = 0.1$ s and constant separation error gain $k = 1$.

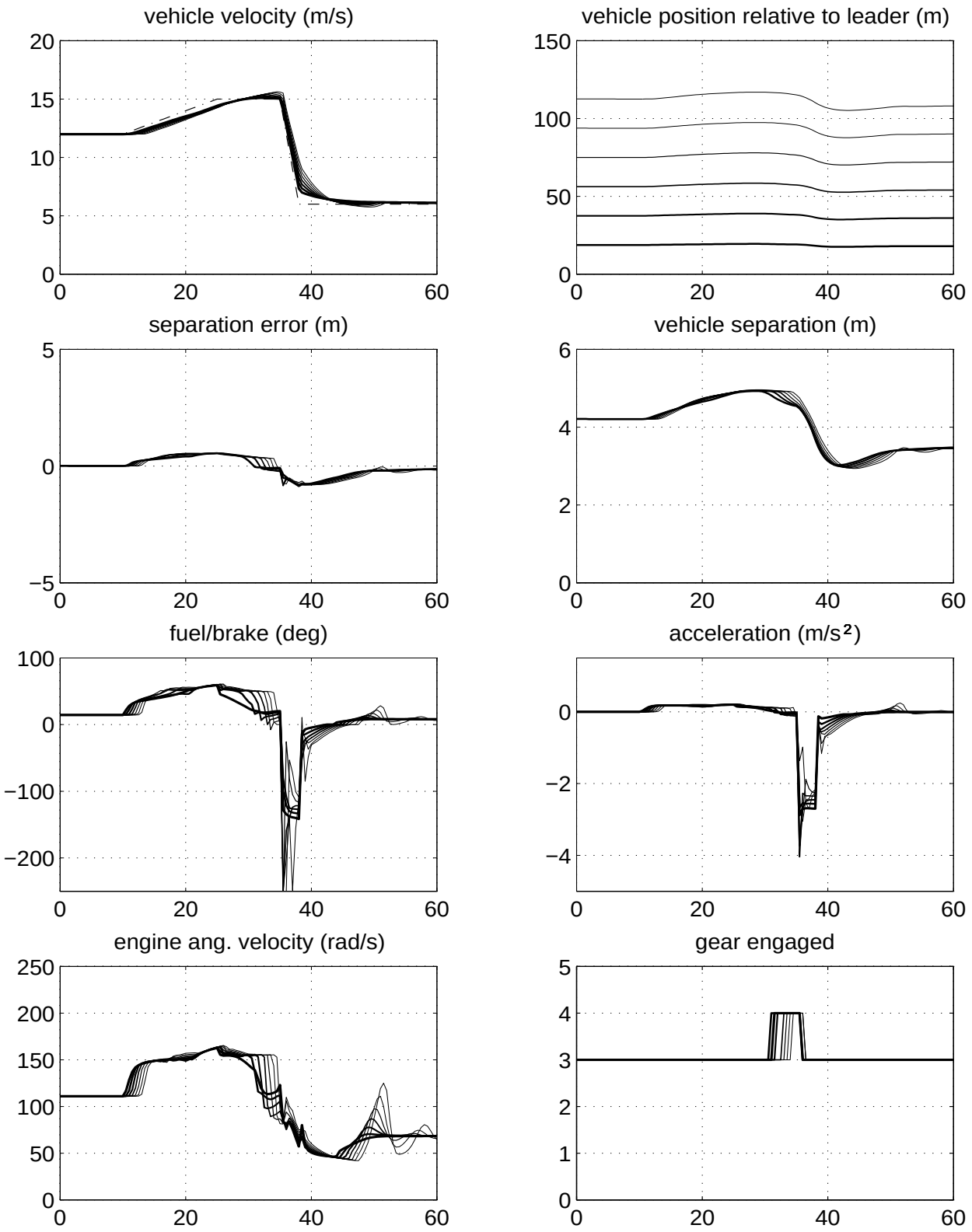

Figure 37: No delay, backstepping controller with variable time headway $h = 0.1 - 0.2v_{\mathrm{r}}$ s and variable separation error gain $k = 0.1 + (1 - 0.1)e^{-0.1\delta^2}$.

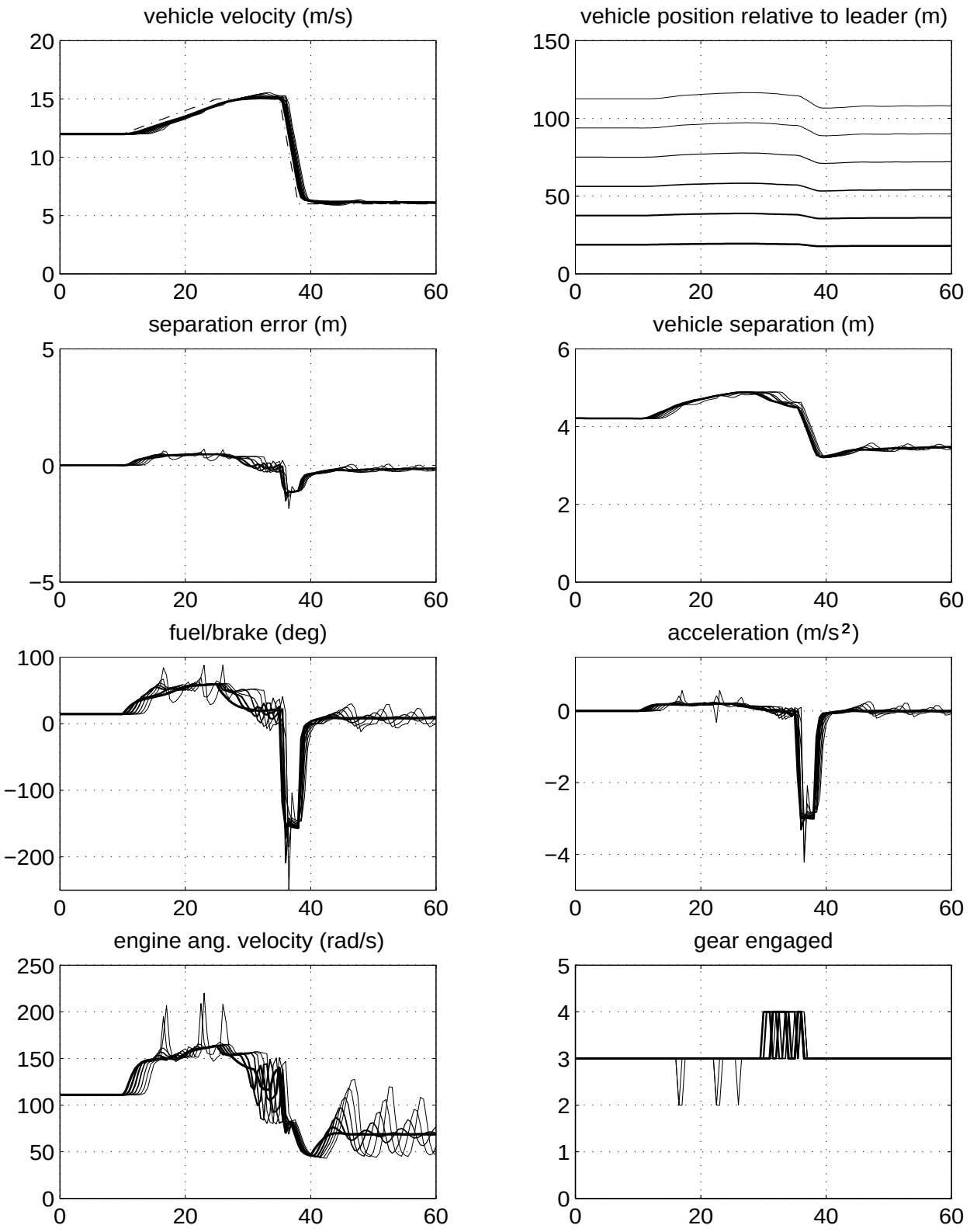

Figure 38: No delay, original PIQ controller with variable time headway $h = 0.1 - 0.2v_{\mathrm{r}}$ s and variable separation error gain $k = 0.1 + (1 - 0.1)e^{-0.1\delta^2}$.

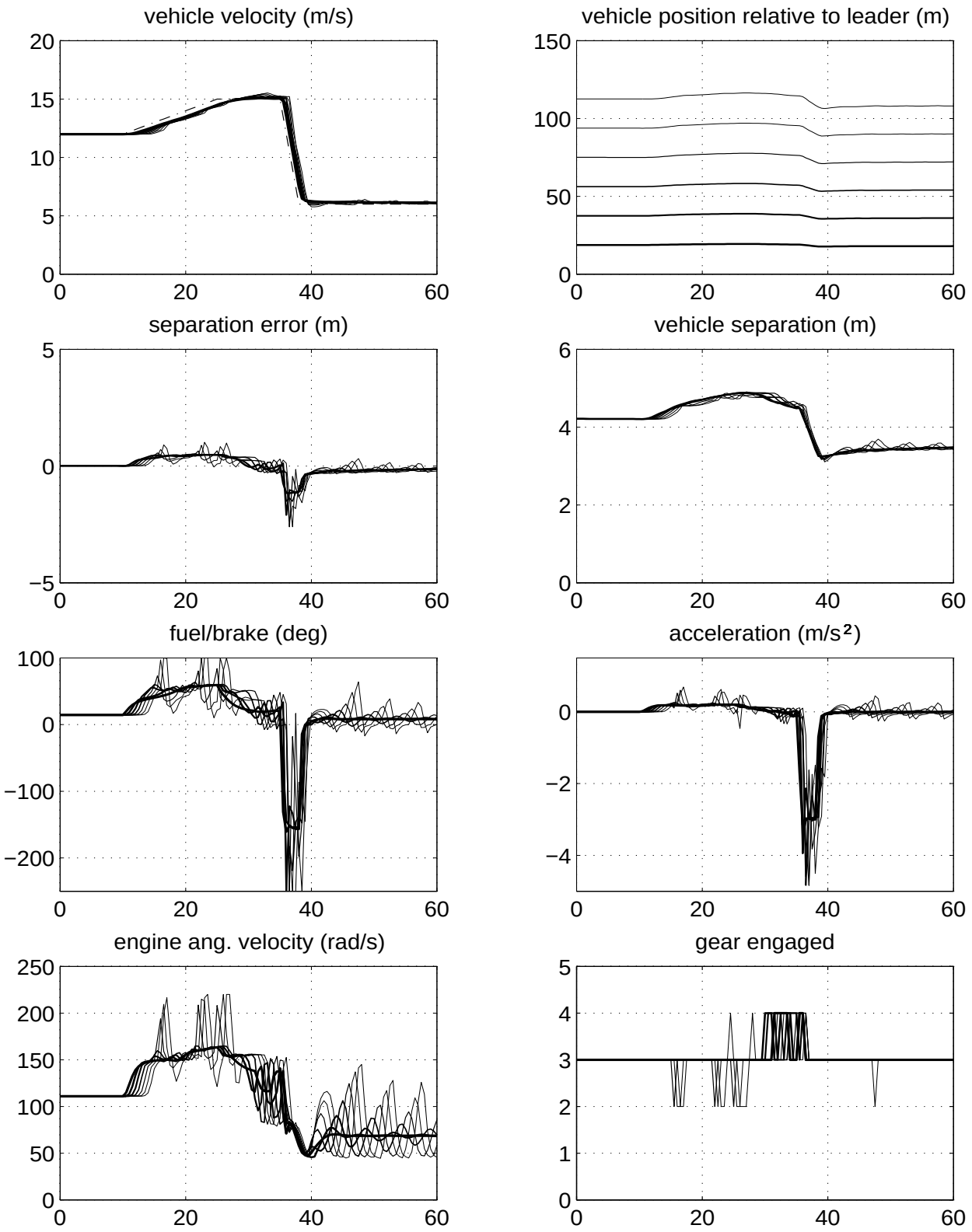

Figure 39: Actuator delay $\tau = 0.05$ s, original PIQ controller with variable time headway $h = 0.1 - 0.2v_{\mathrm{r}}$ s and variable separation error gain $k = 0.1 + (1 - 0.1)e^{-0.1\delta^2}$.

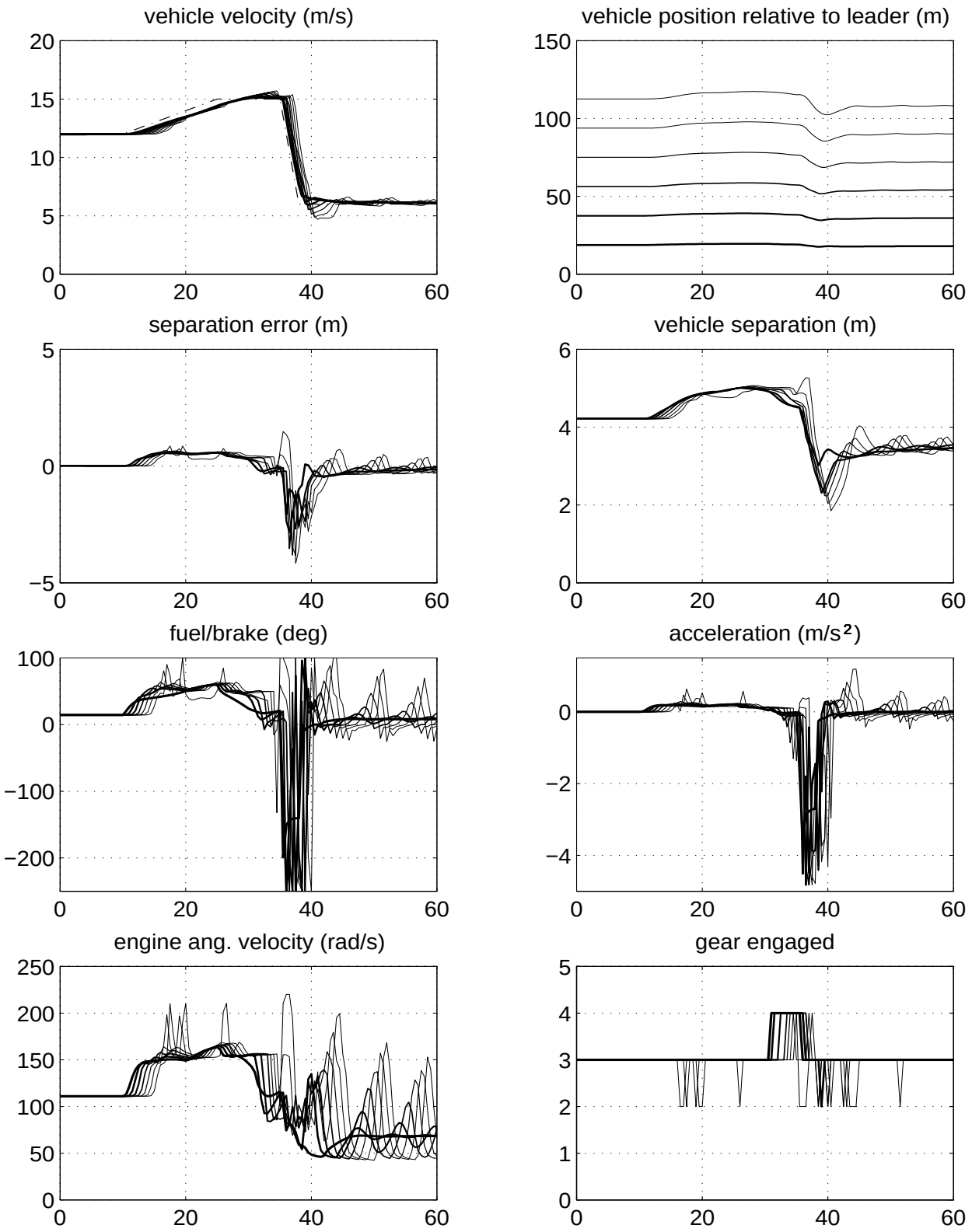

Figure 40: Actuator delay $\tau = 0.2\,\mathrm{s}$, backstepping controller with Smith predictor variable time headway $h = 0.1 - 0.2v_\mathrm{r}\,\mathrm{s}$, and variable separation error gain $k = 0.1 + (1 - 0.1)e^{-0.1\delta^2}$.

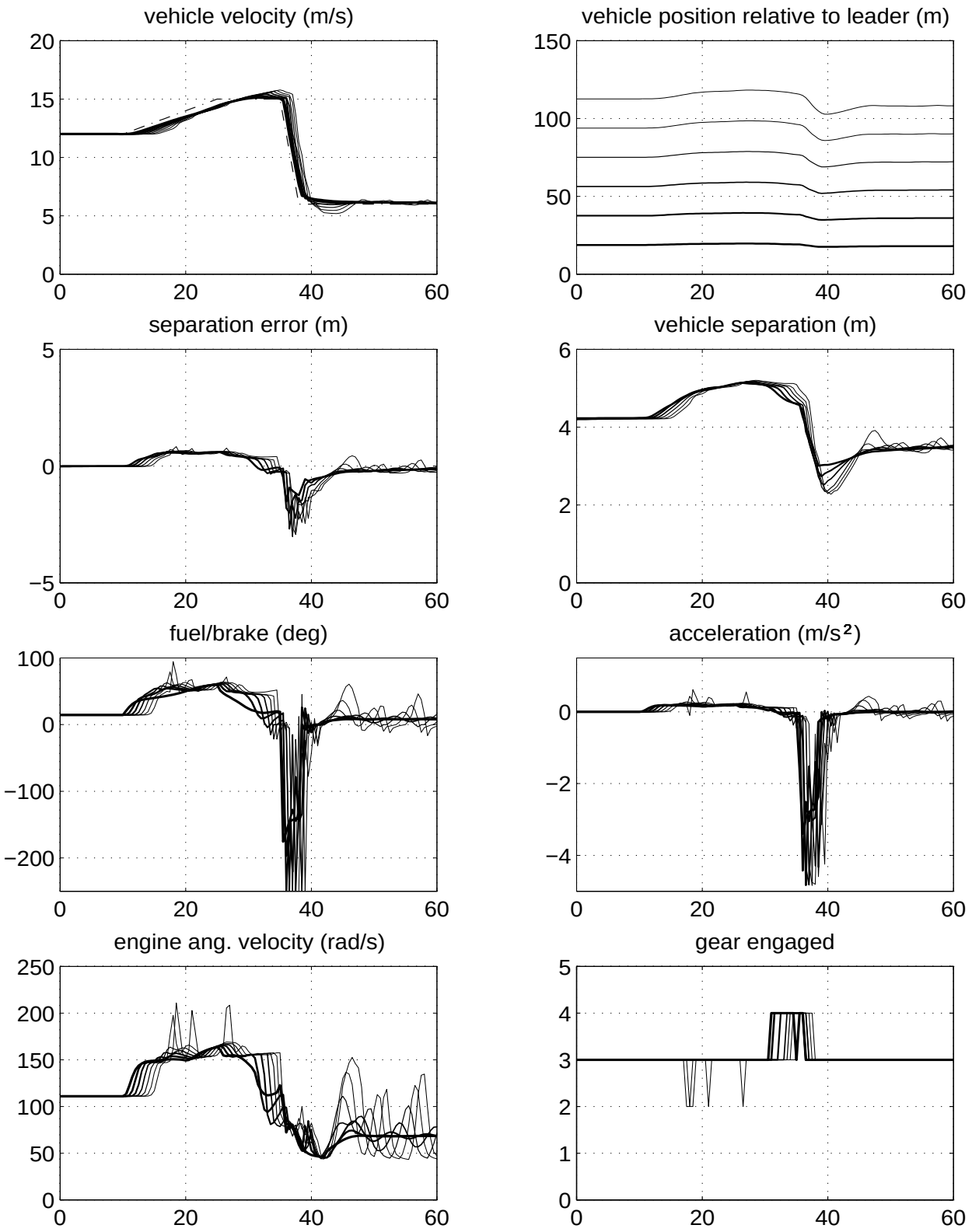

Figure 41: Actuator delay $\tau = 0.2$ s, backstepping controller with alternative predictor, $l = 5$, $\Delta = 0.04s$, variable time headway $h = 0.1 - 0.2v_{\mathrm{r}}$ s, and variable separation error gain $k = 0.1 + (1 - 0.1)e^{-0.1\delta^2}$.

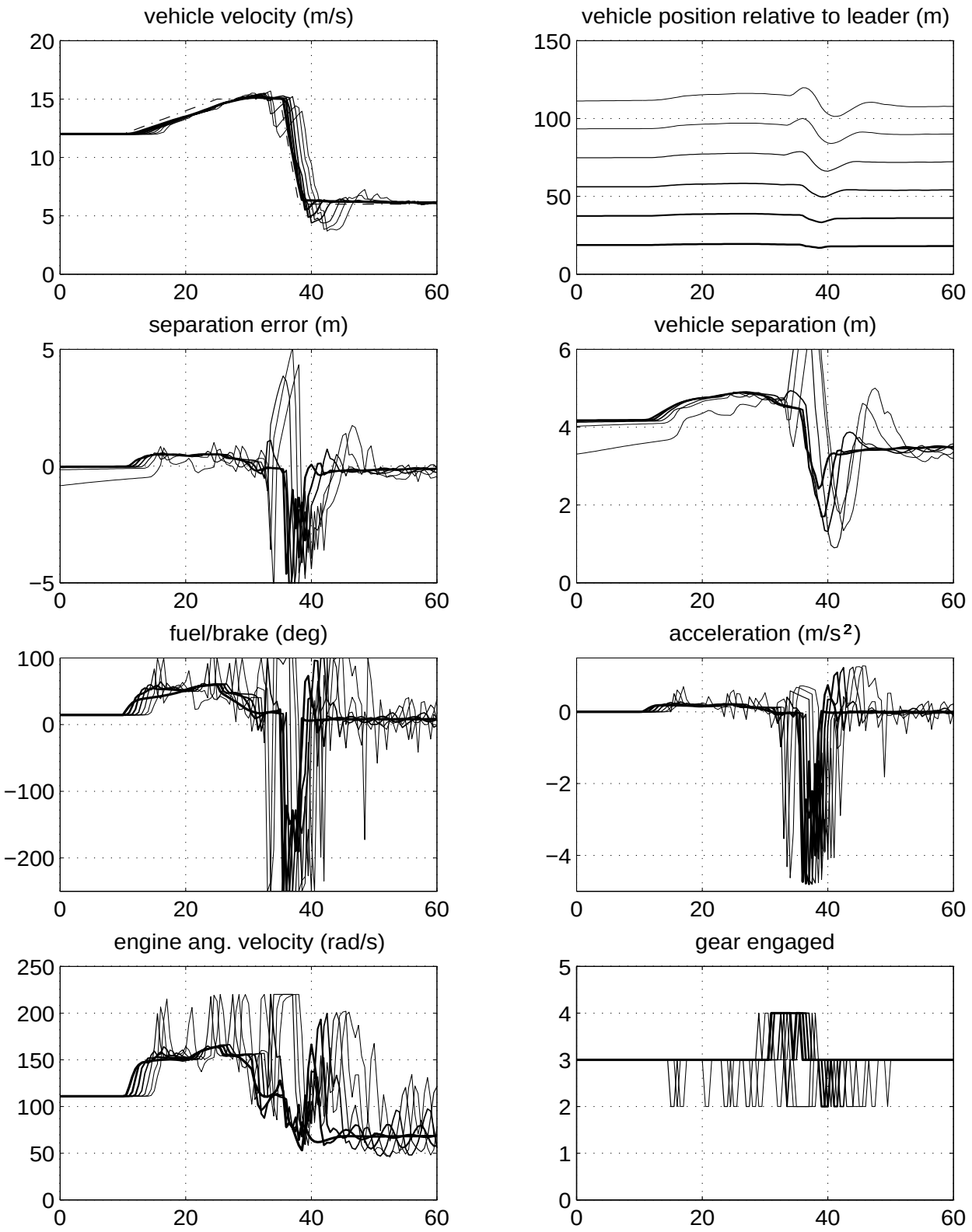

Figure 42: Actuator delay $\tau = 0.3$ s, backstepping controller, variable time headway $h = 0.1 - 0.2v_{\mathrm{r}}$ s, and variable separation error gain $k = 0.1 + (1 - 0.1)e^{-0.1\delta^2}$.

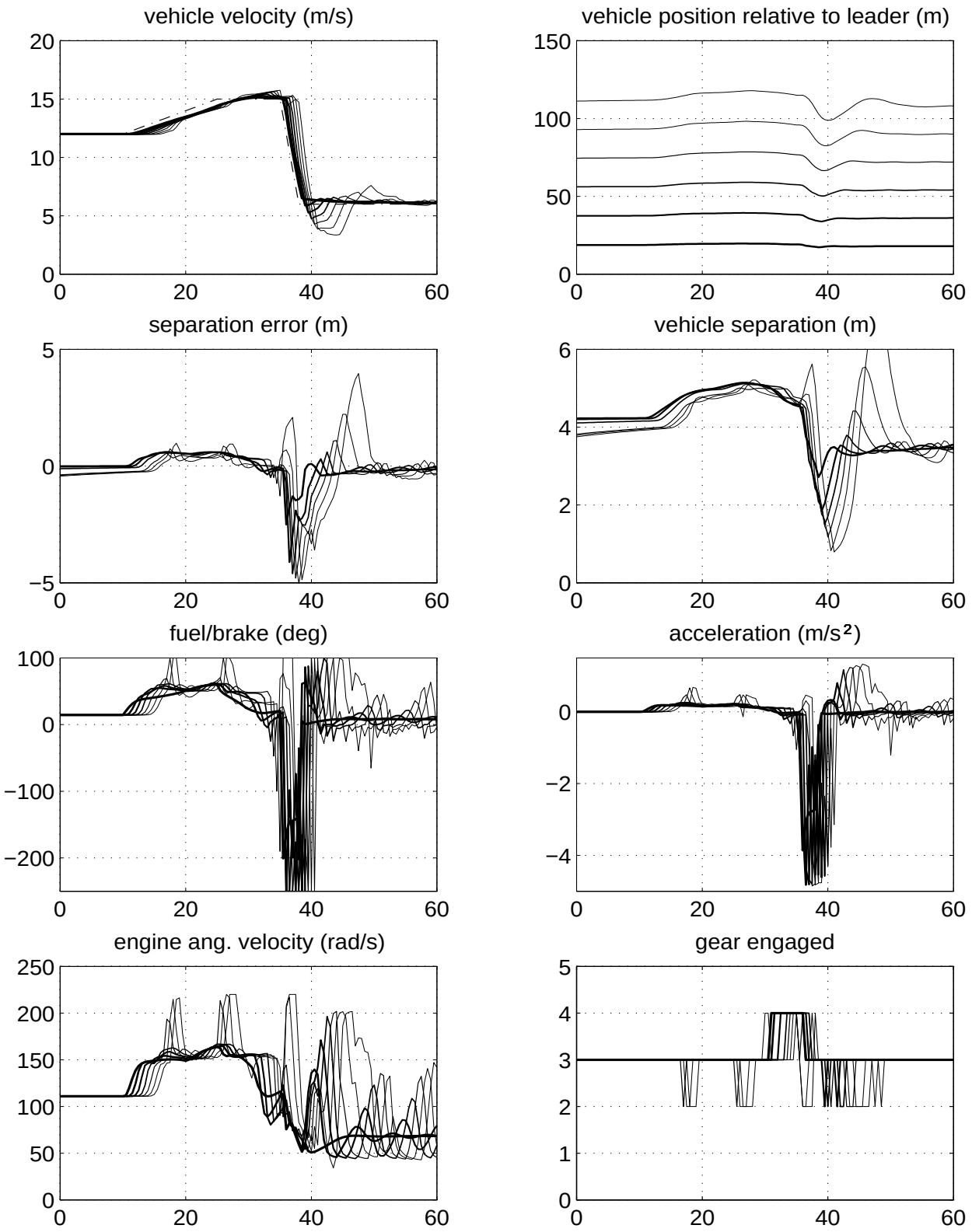

Figure 43: Actuator delay $\tau = 0.3$ s, backstepping controller with alternative predictor, $l = 5$, $\Delta = 0.06s$, variable time headway $h = 0.1 - 0.2v_{\mathrm{r}}$ s, and variable separation error gain $k = 0.1 + (1 - 0.1)e^{-0.1\delta^2}$.

nology, the preceding vehicle's acceleration cannot be measured directly. Therefore, a derivative term would not be physically implementable.

However, the backstepping design of section 5.2 results in a control law which also requires knowledge of the derivative of the error $\frac{d}{dt}(v_{\mathrm{r}} + k\delta)$. There we substituted the derivative operator with its realizable approximation $\frac{s}{s\tau_{\mathrm{d}}+1}$. Evaluation of the terms comprising the control law of (5.10) via computer simulations lead to the expected conclusion that the derivative action is crucial for achieving robustness with respect to delays. We can use the same approximation of the derivative term in the classical PID controller and obtain

$$u = k_{\mathrm{p}}(v_{\mathrm{r}} + k\delta) + k_{\mathrm{i}}\frac{1}{s}(v_{\mathrm{r}} + k\delta) + k_{\mathrm{d}}\frac{s}{s\tau_{\mathrm{d}} + 1}(v_{\mathrm{r}} + k\delta) \tag{5.23}$$

Under these circumstances, it is only natural to compare the performance of a PID controller to the controller in (5.10) and determine whether the complexity of the latter is justified by its performance. It turns out that without the nonlinear modifications of the control objective proposed in section 5.2, i.e., variable time headway, h, and variable separation error gain, k, the PID controller is incapable of achieving acceptable performance in the presence of actuator delays. However, if variable h and k are used, the performance of the PID scheme is similar and even better in certain aspects than the nonlinear design of section 5.1. One can verify this by comparing the PID controller results plotted in Fig. 44 to the backstepping scheme in Fig. 35 and even its version with the alternative predictor scheme in Fig. 41. Not only does the PID controller result in spacing errors of similar magnitude during the transient phase, but it also yields faster convergence of the errors to zero. One should keep in mind that the negative spacing errors are the most undesirable in the vehicle following scenario because they can result in collisions. Moreover, the PID scheme also demonstrates reasonable robustness with respect to the value of the delay. This is can be observed in Figs. 46 and 47 where $\tau = 0.3$ s. The alternative predictor still improves control smoothness as seen by comparing Fig. 45 to Fig. 44 and Fig. 47 to Fig. 46.

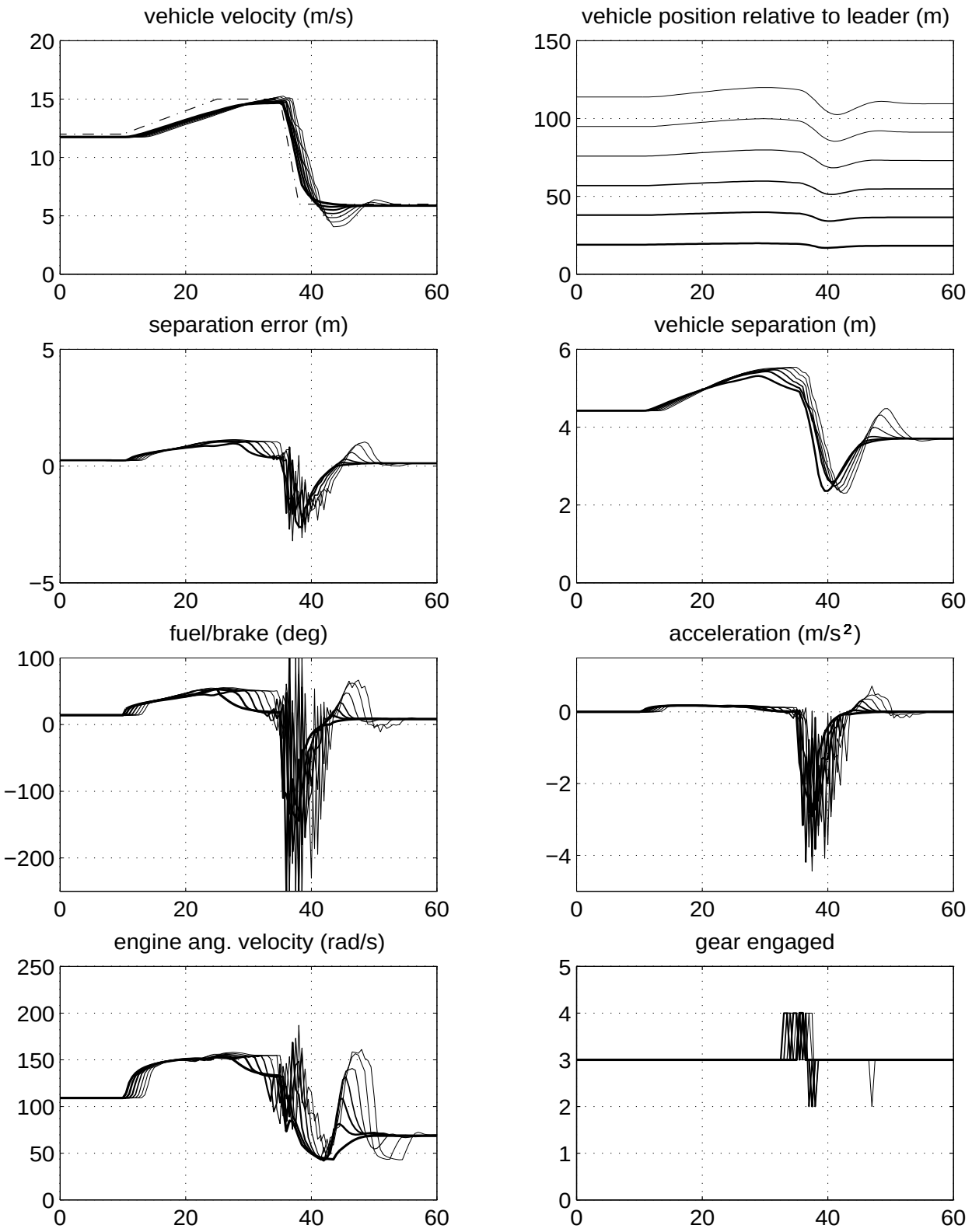

Figure 44: Actuator delay $\tau = 0.2$ s, PID controller, variable time headway $h = 0.1 - 0.2v_{\mathrm{r}}$ s, and variable separation error gain $k = 0.1 + (1 - 0.1)e^{-0.1\delta^2}$.

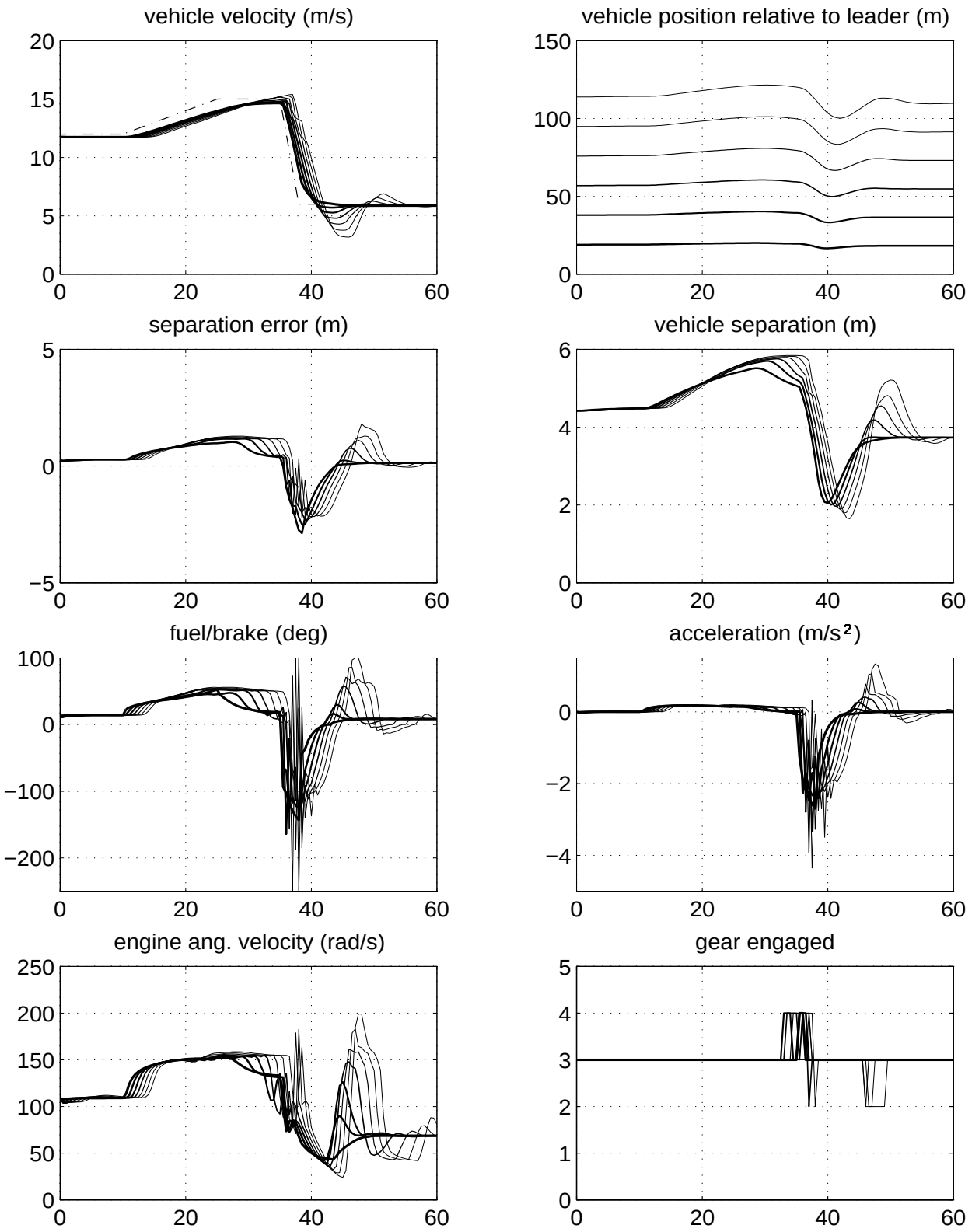

Figure 45: Actuator delay $\tau = 0.2$ s, PID controller with alternative predictor, $l = 5$, $\Delta = 0.04s$, variable time headway $h = 0.1 - 0.2v_{\mathrm{r}}$ s, and variable separation error gain $k = 0.1 + (1 - 0.1)e^{-0.1\delta^2}$.

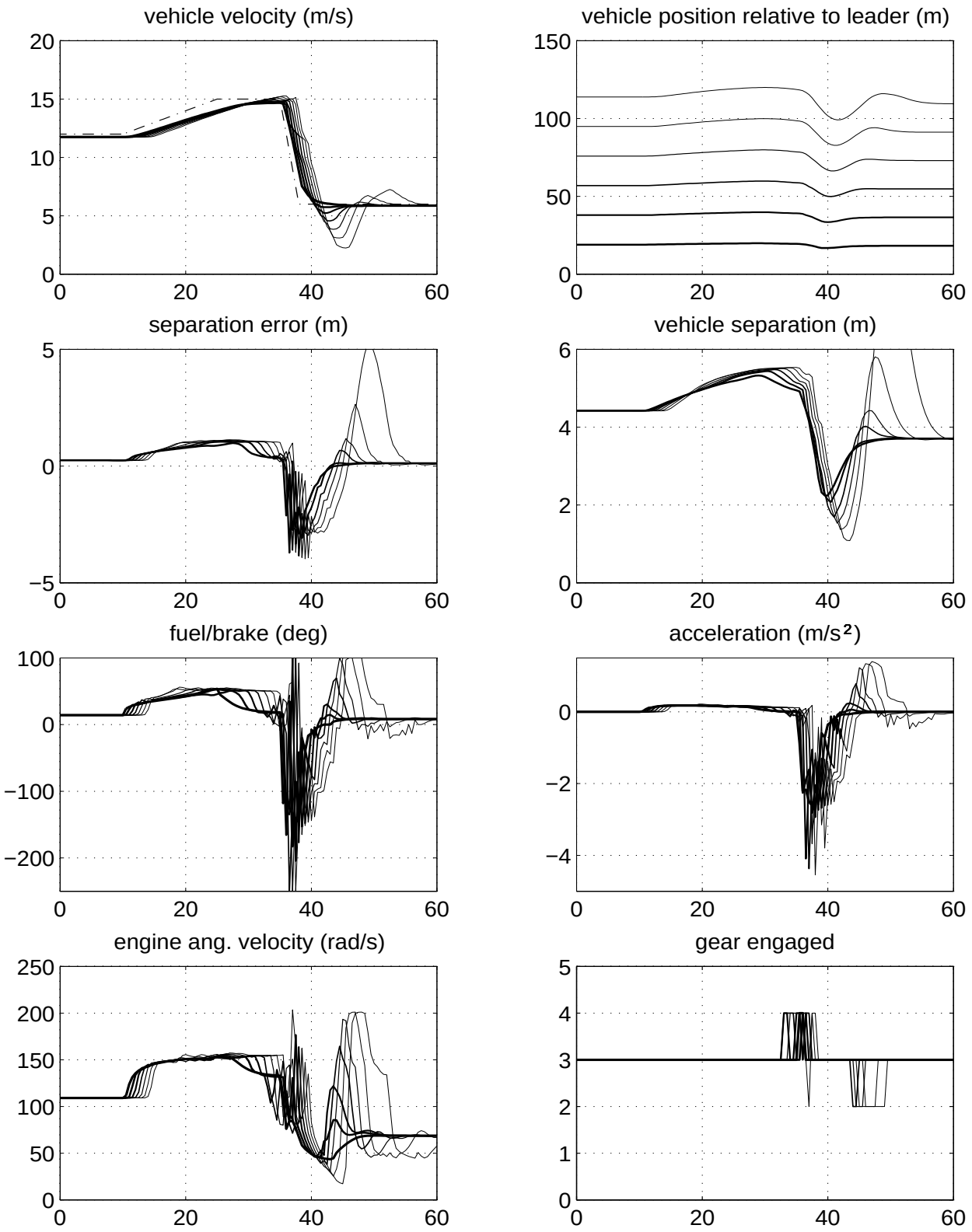

Figure 46: Actuator delay $\tau = 0.3$ s, PID controller, variable time headway $h = 0.1 - 0.2v_{\mathrm{r}}$ s, and variable separation error gain $k = 0.1 + (1 - 0.1)e^{-0.1\delta^2}$.

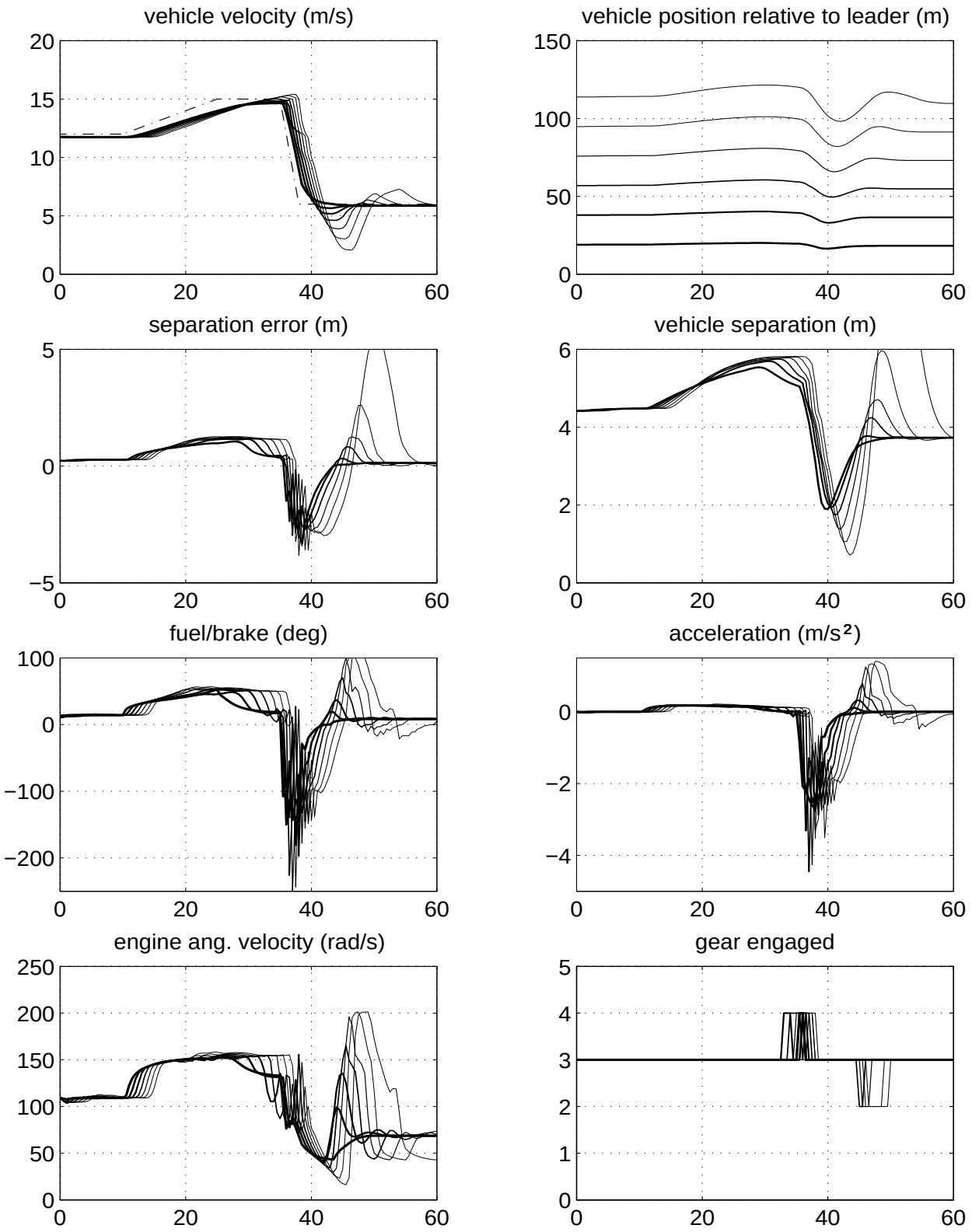

Figure 47: Actuator delay $\tau = 0.3$ s, PID controller with alternative predictor, $l = 5$, $\Delta = 0.06s$, variable time headway $h = 0.1 - 0.2v_{\mathrm{r}}$ s, and variable separation error gain $k = 0.1 + (1 - 0.1)e^{-0.1\delta^2}$.

5.5 Qualitative comparison

Considering the importance of implementation cost when dealing with AHS applications, we give a graphical qualitative comparison of the new control schemes, which not only summarizes the results presented in the former sections, but also allows designers to better negotiate the trade-offs between platoon performance, control smoothness, robustness, and controller complexity in the choice of a scheme which best fits the needs of a particular implementation. First of all, we combine *robustness with respect to maneuvers* and *robustness with respect to actuator delays* into one criterion called *robustness*. This not only allows us to represent things graphically, but also gives the designer a "one-shot" picture of the available options. The robustness with respect to maneuvers is evaluated in the same way as by Yanakiev and Kanellakopoulos (1998), where two additional types of maneuvers were considered: (a) a challenging "merge" maneuver, in which two platoons of 5 trucks each merge from an initial spacing of 83 m to a final spacing of only 3 m, and (b) an even more challenging "merge/brake" maneuver, in which 5 s after the merge maneuver described in (a) has commenced, the front platoon brakes hard from 22 m/s to 12 m/s. Based on these simulation results we draw the 3D comparison diagram in Fig. 48.

As expected, the schemes discussed in this section offer improved platoon performance, control smoothness and, undoubtedly, are more robust with respect to actuator delays. The only thing that may seem surprising, is the worse overall robustness of schemes with predictor compared to the ones without. This is due to the fact that the schemes with predictor perform poorer in extremely challenging maneuvers as the merge/brake considered here. This makes sense intuitively: The predictor attempts to "figure out" ahead of time what is going to happen in τ s and when something totally unexpected happens, the predictor is misleading rather than helping.

Our results show that the cumulative effect of actuator delays in platoons of automated vehicles without intervehicle communication is not an insurmountable obstacle. If design simplicity, cost of implementation and computational requirements are not primary concerns, then one can nearly recover the original "delay-free" performance by using the more complex nonlinear control scheme of section 3.2 with the predictor of Fig. 31; this is seen by comparing Fig. 38 to Fig. 41. On the other hand, if simplicity and ease of implementation are more important, one can still achieve acceptable performance by using the simpler PID-based nonlinear scheme of section 3.5.

It is important to note that we do not assume perfect knowledge of the plant model; our results incorporate a great deal of modeling uncertainty due to the fact that the models we use for control design are only crude approximations of our complex simulation models. The only parameter which is assumed to be very well known is the actuator delay used in the design of our predictor. However, further simulations have indicated that the performance is not affected by small errors in this assumed value. Nevertheless, in real applications it is nearly impossible to measure this value with high accuracy, primarily because these delays change significantly with temperature and operating conditions. Hence, if the performance requirements dictate that these delays be fairly well known, it may be necessary to install torque sensors on the wheels in order to perform on-line measurements of the time it takes for a fuel or brake command to affect vehicle acceleration.

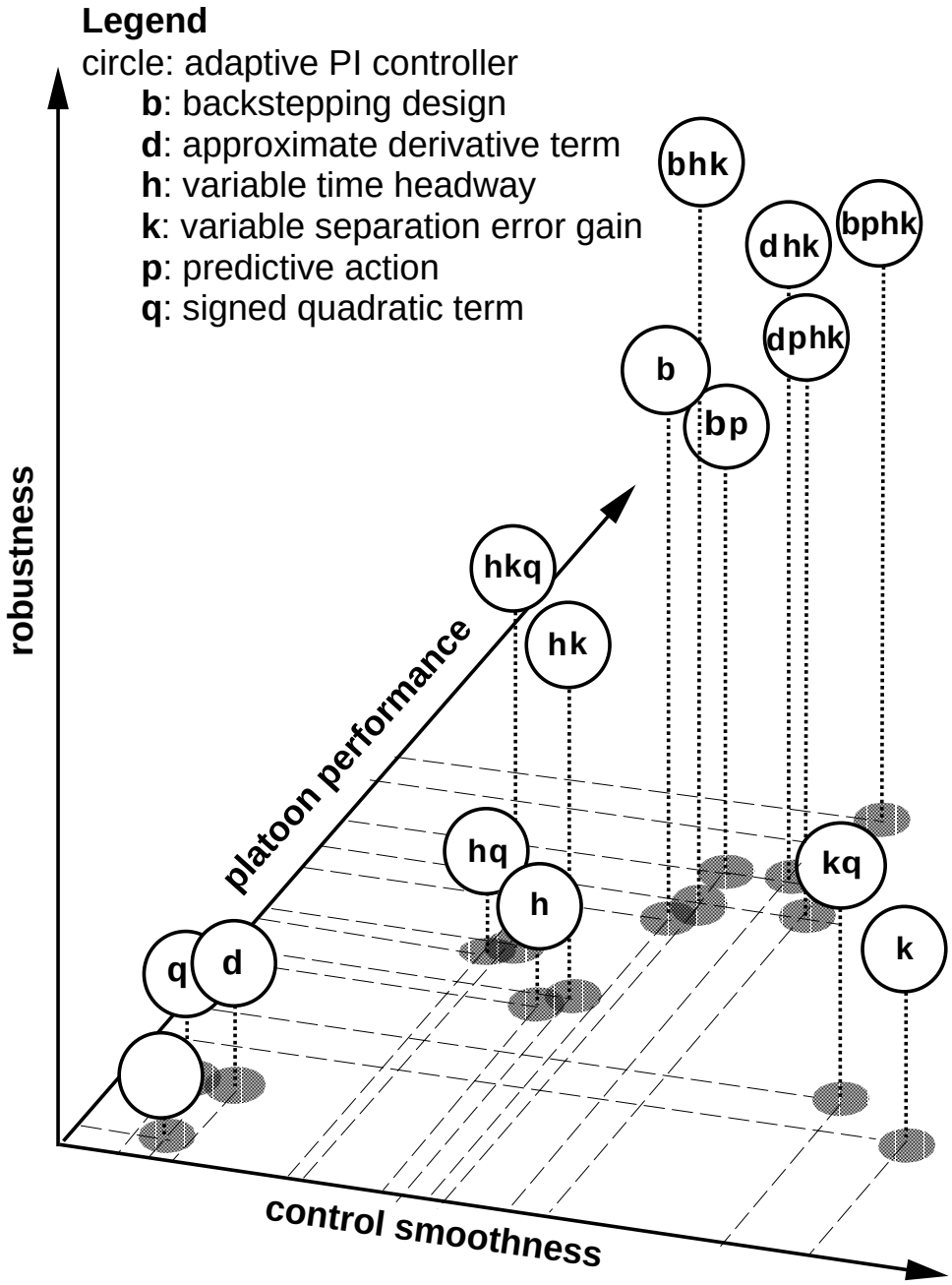

Figure 48: Qualitative comparison diagram.

6 Software

6.1 Platoon Builder toolbox

Platoon Builder is a MATLAB/SIMULINK based graphical user interface program. Through the graphical interface, the user can select platoon parameters such as the number of vehicles in the platoon, the control algorithm, and the vehicle and controller parameters (mass, delays, gains). Then, at the click of a button, the program automatically generates a SIMULINK model of the platoon with the user-selected parameters.

System requirements: The basic requirements are MATLAB 4.X and SIMULINK 1.X (on workstations, PCs or Macs). However, since some S-function files are written in C, in order to generate new simulation results you must have an appropriate C-compiler on your machine to generate the correct `.mex` files.

Installation: The software is available for downloading from http://ansl.ee.ucla.edu/software in a single compressed file. Download, uncompress, and copy all the files into a directory.

Running Platoon Builder: In the Matlab command window, type `plbuild`. A window named *Platoon Builder'* will come up (of course, you either have to be in the directory that contains the file `plbuild.m`, or you have to add that directory to your Matlab path). Out of the four function modules, only *Build a truck platoon* is actually implemented in the current version. Pressing the *Build a truck platoon'* button takes you to the *Truck Platoon Builder'*window. In this window you can set up the simulation parameters, such as vehicle mass, brake and fuel delays and choose different control algorithms and their corresponding parameters.

There are five sub-functions in the window, each of them corresponding to a button on the left side of window.

Build platoon: creates a SIMULINK platoon module which can be used for simulation.

Start simulation: this function only can be executed after a SIMULINK platoon module has been built. It starts the platoon simulation.

Load data from file: this function allows the user to load existing simulation results for the purposes of display and animation.

Plot data: plots the velocity, acceleration, separation and separation error of each vehicle in the platoon.

Animate data: translates the data into the necessary format for TruckVis, and runs TruckVis to animate the simulation results.

6.2 TruckVis: Truck Visualization software

TruckVis is a package that allows the animation of longitudinal and lateral control simulations of automated heavy-duty vehicles. Its origins are in the *Dynavis* package developed at the Center for Advanced Transportation Technologies of the University of Southern California. TruckVis is written in C++ and uses the OPENGL library. It currently runs on SILICON GRAPHICS machines using

the IRIX 6.X operating system, but it can be ported to other platforms which support C++,. X11, and OPENGL, using the source code which is included in the distribution. TruckVis animations provide many useful visual features such as displaying the vehicle's speed in digital form (measured in meters per second), and two color-coded moving bars displaying vehicle acceleration (in m/s^2) and vehicle jerk (in m/s^3). The bars become red whenever the value of acceleration or jerk becomes larger than $+1$ or smaller than -1 in the corresponding units. The user can also animate in real time, detect vehicle collisions, produce "snapshots" of the animation where the animation moves step by step, zoom, pause, etc. Clicking the left mouse button on any of the color-coded tractors causes the animation window to be re-centered with this tractor as the center point; this feature is useful for zooming into a specific vehicle to study its individual behavior during the animation.

System requirements: You need to have a SILICON GRAPHICS C++ compiler, running under the IRIX 6.X operating system, and OPENGL libraries. The OPENGL graphics system is a software interface to graphics hardware. (The GL stands for Graphics Library.) It allows you to create interactive programs that produce color images of moving three-dimensional objects. With OPENGL, you can control computer-graphics technology to produce realistic pictures.

Installation: The software is available for downloading from http://ansl.ee.ucla.edu/software in a single compressed file. Download and uncompress. Copy the source files into a sudirectory, and then run `make`. The executable `truckvis` will be created.

Running TruckVis: TruckVis needs a datafile and a parameter file to run. The command to run TruckVis is:

```
truckvis [datafile] [parameterfile]
```

You can create parameter and data files with the Platoon Builder, but you can also modify files into TruckVis format. The format for the **data file** is the following:

A. Single-lane data: The following data vectors are required to generate the animation data file:

`t:` simulation sampling times.

`RelPos:` relative distance between each vehicle and the reference position.

`RefPos:` reference position to set up the coordinates for drawing all the trucks. Normally it is set to zero.

`velx:` velocity of each truck in the platoon.

`accel:` acceleration of each truck in the platoon.

`jerk:` derivative of the acceleration of each truck in the platoon.

The TruckVis data file is an ASCII file. The data structure is as follows:

- the first line starts with the first sampling time (usually it is zero because we start our simulation at t=0); then comes the data for the first truck: relative distance of the first truck with respect to the reference position, reference position (normally zero), velocity. acceleration and jerk of the first truck;

- then comes the data for the second truck: relative distance of the second truck with respect to the reference position, reference position (normally zero), and so on for the second truck and for the third etc.;
- the second line starts with the second sampling time, then all the data for the trucks at the second sampling time which are in the same format as the first line.

B. Two and Three lane data: A two- or three-lane dataset is the combination of two or three single-lane datasets; the only difference is that for the second lane and the third lane, all the data concerning the sampling time and the first truck are discarded, which means that the animation is based on the assumption that the first truck in each of the three lanes has the same data and all three lanes are sampled at the same time interval. More specifically, each line of a three-lane data file contains all the data for one sampling instant: it starts with the sampling time, followed by the corresponding (to this sampling time) data for all the trucks in the first lane, then the data for truck 2 to truck N in the second lane, and then the data for truck 2 to truck N in the third lane.

Parameter files are also ASCII files which provide the necessary parameters for the animation. The format for the **parameter file** is the following:

`Lanes number:` the number of lanes to be animated; can take values from 1 to 3. This value must match the number of lanes in the corresponding data file.

`Truck number:` the number of the trucks in the platoon. It also must match the number of trucks in the data file.

`TimHdwyL1:` the nominal time headway (in seconds) for the trucks in the first lane.

`TimHdwyL2:` the nominal time headway (s) for the trucks in the second lane. If there is only one animated lane, this value does not affect the animation.

`TimHdwyL3:` the nominal time headway (s) for the trucks in the third lane. If there are only one or two animated lanes, this value does not affect the animation.

`FixHdwyL1:` The fixed intervehicle spacing (added to the time headway for safety and measured in meters) for the trucks in the first lane.

`FixHdwyL2:` The fixed intervehicle spacing for the second lane. If there is only one animated lane, this value does not affect the animation.

`FixHdwyL3:` The fixed intervehicle spacing for the third lane. If there are only one or two animated lanes, this value does not affect the animation.

`Time Headway given:` set this to 0.

`RelPosition X:` If the data file contains absolute longitudinal position data, set this to 1 in order to have TruckVis compute the relative position during animation. Usually, the data file already contains relative position data, so this parameter should be set to 0.

`RelPosition Y:` Same as above, but for lateral position data.

`Velocity X:` a value of 1 means the data file has the data for velocity in the longitudinal direction.

`Velocity Y:` if the data file includes lateral motion data, set this to 1, otherwise to 0.

`Accel avail:` if the data file includes acceleration data, set this to 1, otherwise to 0.

`Jerk avail:` if the data file includes jerk data, set this to 1, otherwise to 0.

`Estimate Acceleration:` set this to 0.

`Estimate Jerk:` set this to 0.

The graphical user interface of TruckVis has the following menus:

1. Commands:
    1a. `Pause-Continue`
    1b. `Step:` with step, you can have snapshots of the simulation, where the simulation moves one time step, each time you press the “single step” button. If you press the “Done” button, the simulation continues.
2. Options
    2a. `Real Time:` by choosing “real time” you have real time simulation, which means that some frames may be dropped or new frames may be added (through interpolation) if the actual hardware performance is respectively slower or faster than real time.
    2b. `Detect Collision:` by choosing “detect collision”, the user will hear a beep for each collision occurrence.

References

Barbieri, E. 1993. Stability analysis of a class of interconnected systems. *Transactions of the ASME, Journal of Dynamic Systems, Measurement, and Control*, vol. 115, pp. 546–551.

Bottiger, F., H. D. Chemnitz, J. Doorman, U. Franke, T. Zimmermann, and Z. Zomotor. 1995. Commercial vehicle and transit AHS analysis. *Precursor Systems Analyses of Automated Highway Systems*, Final Report, vol. 6, Federal Highway Administration, Report FHWA-RD-95-XXX.

Chien, C., and P. Ioannou. 1992. Automatic vehicle following. Proceedings, American Control Conference, Chicago, IL, pp. 1748–1752.

Chien, C., Y. Zhang and C. Y. Cheng. 1995. Autonomous intelligent cruise control using both front and back information for tight vehicle following maneuvers. Proceedings, American Control Conference, Seattle, WA, pp. 3091–3095.

Cho, D., and J. K. Hedrick. 1989. Automotive power train modeling for control. *Transactions of the ASME, Journal of Dynamic Systems, Measurement, and Control*, vol. 111, pp. 568–576.

Chu, K. C. 1974. Decentralized control of high-speed vehicular strings. *Transportation Science*, vol. 8, pp. 361–384.

Cogan, H. F. 1983. A simple method for the estimation of air brake systems actuation times. *Braking of Road Vehicles*.

Eyre, J. T., D. Yanakiev, and I. Kanellakopoulos, 1997. String stability properties of AHS longitudinal vehicle controllers. Proceedings, 8th IFAC/IFIP/IFORS Symposium on Transportation Systems, Chania, Greece, pp. 69–74.

Fancher, P., Z. Bareket, and G. Johnson. 1993. Predictive analyses of the performance of a highway control system for heavy commercial vehicles. Proceedings, 13th IAVSD Symposium, Supplement to *Vehicle System Dynamics*, vol. 23, pp.128–141.

Garrard, W. L., R. J. Caudill, A. L. Kornhauser, D. MacKinnon, and S. J. Brown. 1978. State-of-the-art of longitudinal control of automated guideway transit vehicles. *High Speed Ground Transportation Journal*, vol. 12, pp. 35–68.

Hedrick, J. K., D. H. McMahon, V. K. Narendran, and D. Swaroop. 1991. Longitudinal vehicle controller design for IVHS systems. Proceedings, American Control Conference, Boston, MA, pp. 3107–3112.

Hendricks, E. 1989. Mean value modeling of large turbocharged two-stroke diesel engine. *SAE Transactions*, paper no. 890564.

Heusser, R. B. 1991. Heavy truck deceleration rates as a function of brake adjustment. *SAE Transactions*, paper no. 910126.

Horlock, J. H., and D. E. Winterbone. 1986. *The Thermodynamics and Gas Dynamics of Internal Combustion Engines*. Claredon Press, Oxford.

Hurtig, J. K., S. Yurkovich, K. M. Passino, and D. Littlejohn. 1994. Torque regulation with the General Motors ABS VI electric brake system. Proceedings, American Control Conference, pp. 1210–1211.

Ioannou, P., and Z. Xu. 1994. Throttle and brake control systems for automatic vehicle following. *IVHS Journal*, vol. 1, pp. 345–377.

Jennings, M. J., P. N. Blumberg, and R. W. Amann. 1986. A dynamic simulation of Detroit diesel electronic control system in heavy duty truck powertrains. *SAE Transactions*, paper no. 861959.

Jensen, J. P., A. F. Kristensen, S. C. Sorenson, and E. Hendricks. 1991. Mean value modeling of a small turbocharged diesel engine. *SAE Transactions*, paper no. 910070.

Kao, M., and J. J. Moskwa. 1993. Turbocharged diesel engine modeling for nonlinear engine control and state estimation. Proceedings, ASME Winter Annual Meeting. DSC-vol. 52, Symposium on Advanced Automotive Technologies: Advanced Engine Control Systems, New Orleans, LA.

Kotwicki, A. J. 1982. Dynamic models for torque converter equipped vehicles. *SAE Transactions*, paper no. 820393.

Krstić, M., I. Kanellakopoulos, and P. Kokotović. 1995. *Nonlinear and Adaptive Control Design*. New York, NY: Wiley Interscience.

Leasure, W. A., and S. F. Williams. 1989. Antilock systems for air-braked vehicles. *SAE Transactions*, paper no. 890113.

Ledger, J. D., R. S. Benson, and N. D. Whitehouse. 1971. Dynamic modeling of a turbocharged diesel engine. *SAE Transactions*, paper no. 710177.

McMahon, D. H., J. K. Hedrick, and S. E. Shladover. 1990. Vehicle modeling and control for automated highway system. Proceedings, American Control Conference, San Diego, CA, pp. 297–303.

Peppard, L. E.. 1974. String stability of relative-motion PID vehicle control systems. *IEEE Transactions on Automatic Control*, vol. 19, pp. 579–581.

Post, T., P. Fancher, and J. Bernard. 1975. Torque characteristics of commercial vehicles. *SAE Transactions*, paper no. 750210.

Radlinski, R. W., and M. A. Flick. 1986. Tractor and trailer brake system compatibility. *SAE Transactions*, paper no. 861942.

Sheikholeslam, S., and C. A. Desoer. 1990. Longitudinal control of a platoon of vehicles. Proceedings, American Control Conference, San Diego, CA, pp. 291–297.

Shladover, S. E. 1978. Longitudinal control of automated guideway transit vehicles within platoons. *Transactions of the ASME, Journal of Dynamic Systems, Measurement, and Control*, vol. 100, pp. 302–310.

Shladover, S. E. 1995. Review of the state of development of advanced vehicle control systems (AVCS). *Vehicle System Dynamics*, vol. 24, pp. 551–595.

Smith, O. J. M. 1957. Closer control of loops with dead time. *Chemical Engineering Progress*, vol. 53, pp. 217-219.

Swaroop, D. 1997. String stability of interconnected systems—an application to platooning in AHS, California PATH Research Report UCB-ITS-PRR-97-14.

Swaroop, D., J. K. Hedrick, C. C. Chien, and P. Ioannou. 1994. A comparison of spacing and headway control laws for automatically controlled vehicles. *Vehicle System Dynamics*, vol. 23, pp. 597–625.

Swaroop, D., and J. K. Hedrick. 1996. String stability of interconnected systems. *IEEE Transactions on Automatic Control*, vol. 41, pp. 349–357.

Swaroop, D., and D. Niemann. 1996. Some new results on the oscillatory nature of impulse and step responses for linear time-invariant systems. Proceedings, 35th IEEE Conference on Decision and Control, Kobe, Japan, pp. 2511–2512.

University of Michigan, seminar on Brakes and Brake Actuation Systems.

Varaiya, P. 1993. Smart cars on smart roads: problems of control. *IEEE Transactions on Automatic Control*, vol. 38, pp. 195–207.

Winterbone, D. E., C. Thiruarooran, and P. E. Wellstead. 1977. A wholly dynamic model of turbocharged diesel engine for transfer function evaluation. *SAE Transactions*, paper no. 770124.

Xu, Z., and P. Ioannou. 1994. Adaptive throttle control for speed tracking. *Vehicle System Dynamics*, vol. 23, pp. 293–306.

Yanakiev, D., and I. Kanellakopoulos. 1995. Variable time headway for string stability of automated heavy-duty vehicles. Proceedings, 34th IEEE Conference on Decision and Control, New Orleans, LA, pp. 4077–4081.

Yanakiev, D., and I. Kanellakopoulos. 1995. Engine and transmission modeling for heavy-duty vehicles. University of California, Los Angeles, *California PATH Program*, PATH Technical Note 95-6.

Yanakiev, D., and I. Kanellakopoulos. 1996. A simplified framework for string stability analysis in AHS. Preprints, 13th IFAC World Congress, vol. Q, pp. 177–182.

Yanakiev, D., and I. Kanellakopoulos. 1996. Speed tracking and vehicle follower control design for heavy-duty vehicles. *Vehicle System Dynamics*, vol. 25, pp. 251–276.

Yanakiev, D., and I. Kanellakopoulos. 1998. Nonlinear spacing policies for automated heavy-duty vehicles. *IEEE Transactions on Vehicular Technology*, vol. 47, to appear.

Yang, Y. T., and B. H. Tongue. 1996. A new control approach for platoon operations during vehicle exit/entry, *Vehicle System Dynamics*, vol. 25, pp. 305–319.